

2-DIMENSIONAL SEISMIC REFRACTION MAPPING STUDY OF THE
CRETACEOUS-PALEOGENE BOUNDARY COMPLEX FROM THE BRAZOS,
TEXAS SECTION

A Thesis

by

JOSHUA SMITH GOWAN

Submitted to the Office of Graduate Studies of
Texas A&M University
in partial fulfillment of the requirements for the degree of

MASTER OF SCIENCE

May 2012

Major Subject: Geophysics

2-Dimensional Seismic Refraction Mapping Study of the Cretaceous-Paleogene
Boundary Complex from the Brazos, Texas Section
Copyright 2012 Joshua Smith Gowan

2-DIMENSIONAL SEISMIC REFRACTION MAPPING STUDY OF THE
CRETACEOUS-PALEOGENE BOUNDARY COMPLEX FROM THE BRAZOS,
TEXAS SECTION

A Thesis

by

JOSHUA SMITH GOWAN

Submitted to the Office of Graduate Studies of
Texas A&M University
in partial fulfillment of the requirements for the degree of

MASTER OF SCIENCE

Approved by:

Co-Chairs of Committee,	Mark Everett
	Christopher Mathewson
Committee Members,	Thomas Yancey
	Bruce Dickson
Head of Department,	Rick Giardino

May 2012

Major Subject: Geophysics

ABSTRACT

2-Dimensional Seismic Refraction Mapping Study of the Cretaceous-Paleogene Boundary Complex from the Brazos, Texas Section. (May 2012)

Joshua Smith Gowan, B.A., Bates College

Co-Chairs of Advisory Committee, Dr. Mark Everett
Dr. Christopher Mathewson

Many scientific studies have been conducted on the Cretaceous-Paleogene boundary (KTB) in the Gulf coast region and, in particular, the Brazos River section in Falls County, Texas. Despite this, there remains much to be learned about the KTB and its depositional environment. Study of the KTB has been multidisciplinary, primarily in the fields of sedimentology and paleontology. Some researchers in these disciplines have questioned the consensus view of the placement of the KTB and subsequent interpretation of the timing of depositional events and mass extinction events.

Geophysical methods have potential to provide additional understanding of the physical properties of the KTB. To date, study of the KTB has relied on point data and borehole information to create cross sections of the complex. Seismic refraction surveys can provide spatially continuous information on subsurface horizons located adjacent to the KTB. In this study, seismic first-arrival traveltimes are processed with a tomographic modeling program to map the top of the hummocky cross-bedded sandstone (HCS), which is a key indicator of the deposition environment at the time of KTB boundary complex placement.

The survey area is located at Cottonmouth Creek, a tributary of the Brazos River. Three seismic lines were surveyed, one across Cottonmouth Creek, and two parallel to the creek on either side. The data from the two parallel lines were processed using the 2-D seismic refraction tomography algorithm of Zelt and Smith. The reconstructed depth to the HCS in the survey area is approximately 6 m, with layer seismic velocities of 364, 1800, and 2200 m/s, respectively. Seismic tomography successfully mapped the HCS layer and reveals approximately 1 m amplitude undulations vertically and undulations on the order of several m horizontally. These variations are consistent with exposed surfaces of the HCS in the creek bed. Seismic refraction has been utilized successfully herein to map a key buried indicator, namely the top of the HCS layer, associated with the KTB complex. A detailed 3-D seismic refraction survey at this site is recommended to generate a high-resolution 2-D terrain map of the top of the HCS layer.

DEDICATION

To my parents Samuel and Karen Gowan
and my wife Samantha

ACKNOWLEDGEMENTS

I would like to thank my committee co-chairs, Dr. Mark Everett, Dr. Christopher Mathewson, and my committee members, Dr. Thomas Yancey, and Dr. Bruce Dickson, for their guidance and support throughout the course of this research.

Thanks also to the Mullinax family, who allowed access to the field survey area. I would like to express gratitude to all of my friends who provided field support, especially Dax Soule and Doug Sassen. I thank all of my friends and family who have provided inspiration and support which gave me the ability to complete this project.

Finally, thanks to my mother and father for their encouragement and to my wife for her patience and love.

TABLE OF CONTENTS

	Page
ABSTRACT	iii
DEDICATION	v
ACKNOWLEDGEMENTS	vi
TABLE OF CONTENTS	vii
LIST OF FIGURES.....	ix
INTRODUCTION AND OBJECTIVE.....	1
Introduction	1
Objective	11
NEAR-SURFACE SEISMIC REFRACTION	13
Basic Theory and Concepts.....	14
Acquisition	16
Seismic Tomography.....	22
Model Input Files	25
Data Analysis	30
RESULTS AND INTERPRETATION.....	42
Topography	42
Seismic Survey	44
Tomographic Model.....	46
CONCLUSION AND RECOMMENDATIONS.....	52
REFERENCES.....	54
APPENDIX A	57
APPENDIX B	90
APPENDIX C	131

	Page
APPENDIX D	134
VITA	139

LIST OF FIGURES

FIGURE	Page
1 Brazos Site Location Relative to the Chicxulub Impact and Other Exposed KTB Locations	5
2 Map Taken from Adatte et al. (2011) Showing Cretaceous-Paleogene Boundary Outcrops and Borings Drilled Along the Brazos River, Cottonmouth Creek, and Darting Minnow Creek of Falls County, TX.....	7
3 Stratigraphic Sections of the KTB Complex at Four Locations in the Brazos Riverbed at the Site	10
4 Approximate Locations of Survey Lines	16
5 An Outcrop of the HCS Sandstone to the East of Line 1	17
6 Outcrops of the HCS Sandstone Downstream to the East of Line 1	18
7 Schematic of a Seismic Refraction Survey	19
8 A Representative Seismogram Showing First-Arrival Picks	21
9 Simplified Depiction of the Initial Model Structure	27
10 Section of v.IN Describing the Starting h_1 of Line 2	28
11 An Example d.IN Input File Used in Tomography of Line 3	30
12 Line 3 Convergence Graphs for the Damping Factor Trials	34
13 Roughness Versus Misfit Trade-Off Graph of Convergence Points from Figure 12 for Line 3	37
14 Line 2 Convergence Graphs for the Damping Factor Trials	38
15 Roughness Versus Misfit Trade-Off Graph of Convergence Points from Figure 14 for Line 2	41
16 Graphs that Represent the Topography of Lines 1 through 3	43

	Page
17 A View Facing North of the HCS Exposure in Line 1.....	44
18 A Representative Seismogram Taken During the Brazos K-T Boundary Study.....	45
19 Final Tomographic Model of $h(x)$ from the Line 3 Data Set	47
20 Final Tomographic Model of $h(x)$ from the Line 2 Data Set	48
21 Combined $h(x)$ Plot for the Spectrum of D for Line 3	50
22 Combined $h(x)$ Plot for the Spectrum of D for Line 2	50
23 A View of the Top of the HCS Layer Down-Stream of Line 1	51

INTRODUCTION AND OBJECTIVE

Introduction

The great biological diversity observed on Earth today is due in large part to past mass extinctions and subsequent radiations. During the Phanerozoic, five mass extinction events and roughly two dozen smaller extinction events, with associated evolutionary radiations, have been documented (Sepkoski, 1986). Mass extinctions may be defined as global events that dramatically alter the environments in which large numbers of species live.

Extraterrestrial impacts can be sufficiently energetic to affect planetary surfaces and trigger mass extinction events (Kring, 2007). One of the most famous mass extinctions occurs at the Cretaceous-Paleogene (KT) transition and has been associated with an extraterrestrial meteorite impact. According to Alvarez et al. (1980), an asteroid of 10 ± 4 km diameter struck the Earth, triggering a number of catastrophic consequences including dispersal of dust into the stratosphere that hindered photosynthesis for several years. This dust would have disrupted photosynthesis for multitudes of plant species and caused the collapse of food chains. The resulting mass extinction wiped out roughly

This thesis follows the style of Geophysics.

70% of all species on Earth at the time (Sole and Newman, 2002)

The search for an impact crater large enough to generate the KT mass extinction event culminated with the discovery of an impact origin for the previously known Chicxulub subsurface geological structure located in the Yucatan Peninsula, Mexico (Kring, 2007).

The discovery that the end of the Cretaceous Period occurred simultaneously with a major meteoroid impact on the surface of the Earth (Alvarez et al., 1980) is one of the great geological discoveries of the last 30 years. This collision, which produced a crater approximately 180 km in diameter, greatly affected Earth surface environment and processes (Kring, 2007). The environmental effects of an impact this large include: sulfur vapor injection into the stratosphere after impact with anhydrite, causing acid rain; wildfires, as evidenced from the recovery of fusinite, soot, and carbonized plant debris; and dust from the direct impact event (Kring, 2007; Heymann et al., 1998). These effects combined to block sunlight and degrade water quality, which resulted in disaster for all life relying on photosynthesis and fresh water. The influence of this impact is recorded in a complex of KT boundary (KTB) sedimentary deposits that can be recognized in numerous regions around the Earth.

Oil exploration surveys in the 1940's drew attention to the Yucatan Peninsula as a possible location for an impact of the necessary magnitude to cause the KT mass extinction. Three exploratory borings were drilled into the Chicxulub structure. The resulting discovery of shocked quartz and altered impact melt demonstrated that the

structure is of impact origin (Kring, 2007). The shallow borings also indicated large density and magnetization contrasts between identifiable crater-related lithologies and the surrounding formations. The density and magnetization contrasts allowed for further identification of the impact structure through gravity and magnetic geophysical imaging (Pilkington and Hildebrand, 2000). Chemical analysis and age dating confirmed that the timing of the Chicxulub impact event occurs at the end of the Cretaceous period. The KTB is exposed in many areas throughout the world, the stratotype being located at El Kef, Tunisia. The site at El Kef was chosen for a number of reasons including the continuity of sedimentation, completeness of exposure, thickness of sediments, abundance and diversity of well-preserved fossils, and lack of unconformities (Molina et al., 2006).

The occurrence of the impact at Chicxulub, Mexico has caused re-analysis of the criteria that have traditionally defined the KTB in sedimentary deposits. This process of re-analysis has generated controversy about the best method to describe the environmental conditions that prevailed immediately post-impact and are now preserved in KTB complexes at different sites (Keller et al., 2007). Alternative indicators to describe the KTB include the observations of the extinction and/or origin of fossil species, and the use of physical evidence of an impact. There is potential for near-surface geophysical methods to provide additional information to aid in the description the KTB.

Paleontological and physical disturbance evidence typically occurs at different levels

within the same geological exposure; consequently, conflict has arisen regarding the interpretation of the KTB record. The use of fossils to pinpoint a sudden cataclysmic event in Earth's history has fundamental uncertainties, to some extent, because the remains of the extinct organisms can be transported in sediments for a long time after the event before they are finally deposited, while the newly evolving organisms will take some time to establish themselves before they make their first appearance in the fossil record. This KTB controversy is most acute in exposed KTB locations close to the impact site (up to 1000 km from the crater, as shown in Figure 1), where the KTB deposits are best developed. At some of these sites, for example, environmental disturbances produced mass wasting that created large debris flows and slump deposits (Yancey, 1996). These most complete and thickest records of the KTB section are proximal to Chicxulub and display the event disturbances in the highest resolution. In more distant areas, the KTB deposits are usually thin with insufficient material to advance significantly our understanding of the boundary depositional history. In the proximal areas, e.g. around the Gulf of Mexico, the KTB complex is often several meters thick.

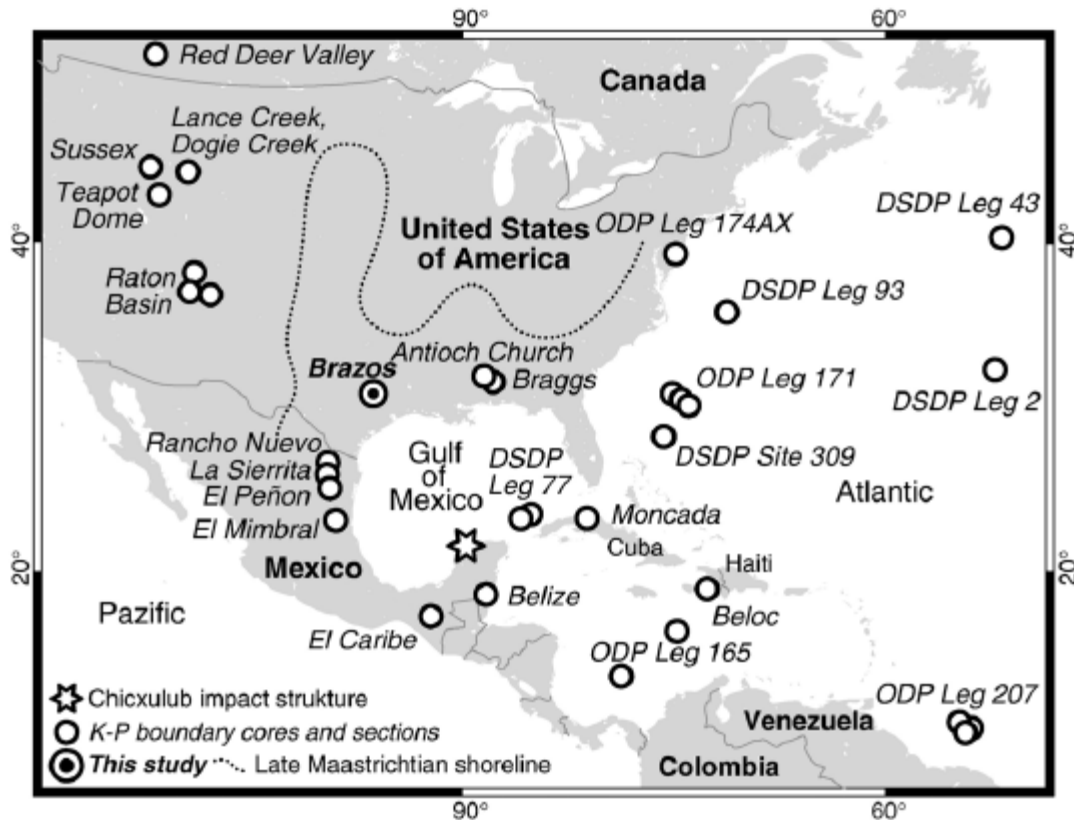


Figure 1. Brazos site location relative to the Chicxulub impact (star) and other exposed KTB locations (circles); after Schulte et al. (2006).

The relationship between the Chicxulub impact event and the paleontologically defined boundary between the Cretaceous and the Paleogene is a hotly debated subject. The debate centers on the disputed timing of events contributing to the mass extinction and is magnified by inconsistencies in the paleontological record across the KTB complex. The KTB has commonly been placed at the Chicxulub event, which is below the paleontologically defined mass extinction of the upper Maastrichtian (end of Cretaceous) planktic foraminifera and first appearance of Danian species as defined at the Brazos section by Keller et al. (2011).

An opportunity for further study is available at an exposure of the KTB located along the Brazos River in Falls County, TX. This exposure, which consists of the KTB complex capped by mudstone and sandstone beds, is an excellent study location for several reasons: it is the most complete section of the complex preserved along the Texas segment of the Gulf Coast (Yancey, 1996); it is close (~1000 km) to the impact crater; the microfossils deposited subsequent to the deposition of the KTB are well-preserved as the result of tectonically undisturbed sedimentary sequences; and the sandstone complex, which is also known as the “event deposit”, is exposed at this location (Keller et al., 2007). The sandstone complex is important to the discussion because there are competing theories about its depositional origin. The debate centers on whether the sandstone was deposited as a result of a tsunami or through multiple high-energy storm events (Yancey, 1996). The opposing views have resulted in a lack of consensus among researchers regarding a complete description of the event history.

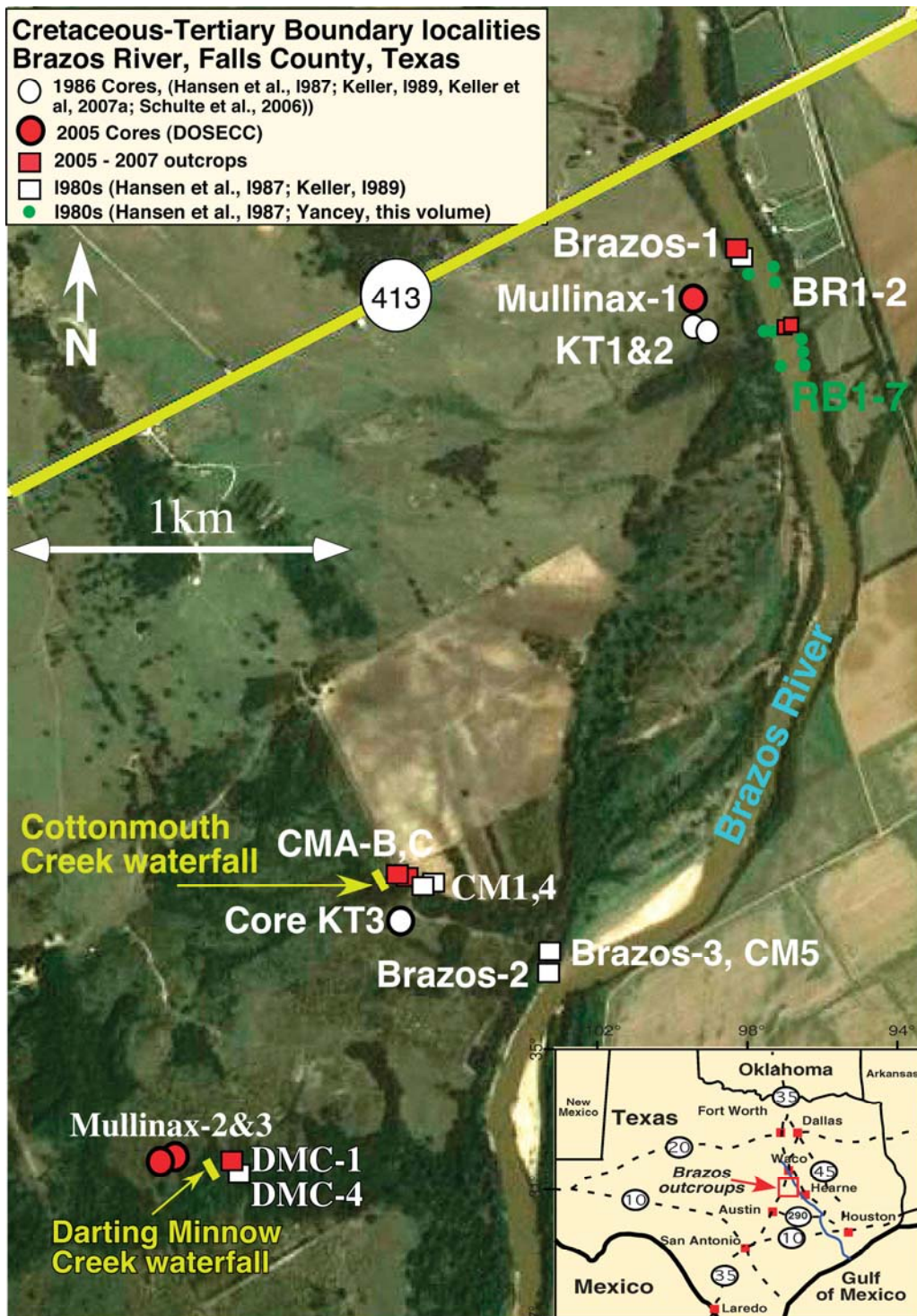


Figure 2. Map taken from Adatte et al. (2011) showing Cretaceous-Paleogene boundary outcrops and borings drilled along the Brazos River, Cottonmouth Creek, and Darting Minnow Creek of Falls County, TX.

The KTB deposits at Brazos River, Texas (Figure 2) play a central role because they appear as a complete section at this location. The Brazos section was the first in which disagreement on KTB placement was identified (Yancey, 1996). The Brazos section has been examined and described in many reports, making it one of the most documented KTB sections in the world. Despite the extensive study of the Brazos section, some important questions remain unanswered, such as determining the lateral continuity of the described section. While geologic time is determined by studying the stratigraphy and paleontology of geologic cross sections, geophysics is a complementary tool often under-utilized by stratigraphers and paleontologists. This project is a feasibility study on the ability of the non-invasive seismic refraction method to accurately map the lateral continuity of subsurface lithological interfaces within the KTB section at the Brazos site. This geophysical method can provide continuous areal coverage of the boundary complex, albeit based on indirect subsurface information that requires interpretation. Traditional stratigraphic information, by contrast, relies on fortuitous outcrops and invasive drilling.

To date, approximately 20 outcrops and cores displaying the KTB complex have been documented in the Brazos area (Schulte et al., 2006). In Yancey (1996), traditional geological observations were extracted from outcrops and borings to construct a cross section approximately 80 m long of the boundary complex. This cross-section however is not spatially continuous; consequently, to gain a contiguous lateral map of the boundary complex there is a need to interpolate between the point observations. By

contrast, spatially continuous subsurface information can be provided inexpensively and non-invasively by the use of geophysical methods such as seismic refraction.

Keller et al. (2011) provides descriptions of cross-sections of KTB complex exposures at a number of locations covering a 3 km stretch along the Brazos River and two of its tributaries. Schulte et al. (2006) present a complete description of the boundary complex based on two cores in close proximity; in this case, very little information is revealed about the lateral continuity of the subsurface geology. In general, no complete 2-D examination of the boundary complex exists across the site area. Understanding the lateral continuity of the sandstone is important because it can shed light on the types of energy that were necessary for deposition.

The Brazos “event deposit”, shown in Figure 3, consists of basal conglomeratic beds deposited by cohesive plastic flows overlain by sandstones and capped by calcareous mudstone. These upper layers were deposited by turbulent flow of sediment carried in suspension (Yancey, 1996). The specific layer studied in this thesis is the hummocky cross-bedded sandstone (HCS) that is a significant component of the upper section of the “event deposit”.

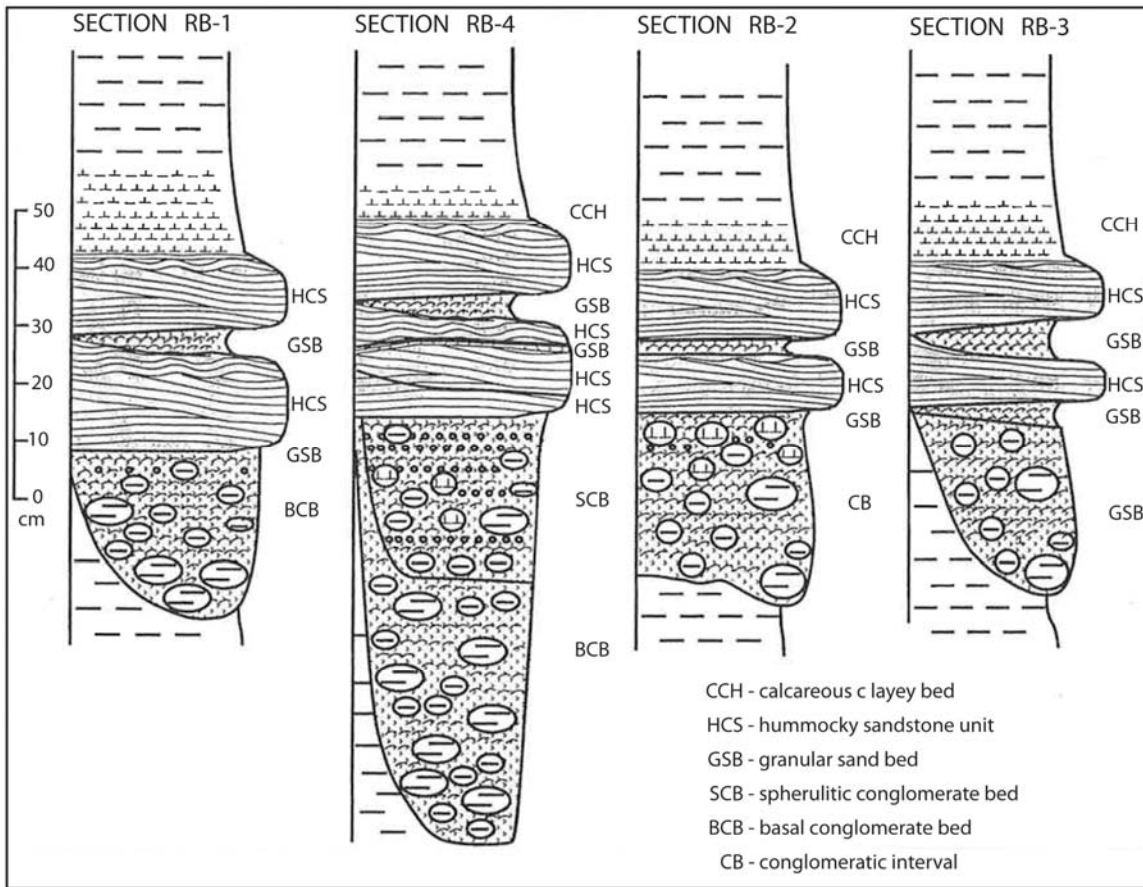


Figure 3. Stratigraphic sections of the KTB complex at four locations in the Brazos riverbed at the site (modified from Yancey, 1996). HCS is the layer of concern to this study.

The HCS unit lies within the Littig member of the Kincaid formation (Yancey, 1996) and is observed in cores to be approximately 10 cm thick, consisting of alternating layers of light gray, silty, and calcareous sands. The unit contains spherules, rusty concretions and burrow features. In the lower part of the HCS unit, planar laminations and low-amplitude, wavy bedding is exhibited, while, in the upper part, there are prominent asymmetric current ripples (Schulte et al., 2006). The low amplitude undulations are associated with post-depositional deformation. On a regional scale, sediments dip to the

southeast towards the Gulf of Mexico coast, but locally the sediments may be regarded as a horizontal stack (Yancey, 1996). This site was chosen for the nearby availability of outcrops of the boundary complex and the presence of minimal vegetation cover, which facilitated respectively the interpretation and acquisition of the seismic data. The HCS is the focus of this study because of its contrasting hardness with overlying subsurface material.

The seismic refraction method is an ideal geophysical technique to detect subsurface interfaces that exhibit strong contrasts in hardness, or resistance to elastic deformation. Hardness is described by bulk modulus, which is a measure of the resistance of a material to an applied mechanical force, which in turn affects seismic velocity. Seismic velocity is the principal physical property that is directly sensed using seismic refraction (Knight and Andres, 2005).

Objective

The objective of this study is to determine whether the seismic refraction method is an appropriate means of gathering non-invasive information that can contribute to debates about geological interpretation of the Brazos KTB complex. The focus of my thesis research is to construct a spatially continuous map of the top of the HCS sandstone layer. The sandstone should have a seismic velocity significantly higher than those of the overlying sediments; consequently, the top of sandstone should figure prominently in seismic refraction tomograms. Seismic refraction tomography will be used to map key

characteristics of the sandstone layer such as undulations and lateral continuity. The seismic tomographic results will be interpreted in terms of the overall geological interpretation of the KTB.

NEAR-SURFACE SEISMIC REFRACTION

Seismic refraction is one of the oldest of the applied geophysical methods commonly used for mapping the geometry of shallow geologic interfaces (Pelton, 2005). The seismic refraction method was chosen for use at the Brazos site because the HCS is presumed to exhibit distinct elastic properties compared to other layers in the shallow subsurface and the intention is to map its undulating upper surface. The HCS is likely to present a stronger elastic contrast to the overlying bed than the corresponding electrical, dielectric, magnetic, or density contrasts; therefore seismic refraction was chosen instead of electromagnetics, resistivity, ground penetrating radar, magnetics, or gravity as the primary geophysical tool.

First arrival times extracted from field seismograms are easily observed, informative, and straightforward to interpret in seismic refraction analysis. The first arrivals are used herein to map the top of the uppermost refractor. Identification of the first arrival energy is important because it is almost always the primary refraction, i.e. seismic energy traveling along the top of the uppermost refractor. Later arriving seismic phases can be used to map deeper refracting layers because refractions are generated when seismic waves propagate downward and encounter faster layers. The refraction method requires overlying sediments to have a lower seismic velocity than underlying material. This condition is typically satisfied near the surface because the top layer is aerated and hence seismic waves travel slowly through it, while underlying layers are compacted and hence

the seismic waves travel faster. Beyond a certain distance from the source, the head, or refracted, wave is the first arrival; while at shorter source-receiver distances the first arrival is usually a direct body wave propagating in the slower surficial layer. Identification of these different seismic phases in field seismograms is described in the following sections.

Basic Theory and Concepts

Refraction of seismic waves occurs when energy travels from the shot-point down to an interface and then propagates along the interface before traveling back to the surface (Satti, 2000). In a simple two layer model, Snell's law states that a head wave is generated when the angle of refraction into the underlying medium reaches a critical value of 90° . This condition is achieved if the ratio of velocities is related to the incident angle i by (Sharma, 1997):

$$\sin i = V_1/V_2 , \quad (1)$$

where V_1 is the velocity of the overlying layer 1 and V_2 is the velocity of layer 2 beneath.

Refracted first arrivals are observed only at a source-receiver offset x that exceeds a certain critical distance. Specifically, the refracted waves must “overtake” the direct wave and appear as the first arrival. This occurs beyond the cross-over distance, x_{co} . At this distance, the direct wave and refracted arrival travel-times are equal. Expressing

these travel times in terms of distance and velocity and equating them yields (Sharma, 1997, equation 4.29):

$$\frac{x_{co}}{V_1} = \frac{x_{co}}{V_2} + \frac{2h_1\sqrt{(V_2^2 - V_1^2)}}{V_2 V_1}. \quad (2)$$

Solving equation (2) for x_{co} gives:

$$x_{co} = 2h_1\sqrt{(V_2 + V_1)/\sqrt{(V_2 - V_1)}}, \quad (3)$$

where h_1 is the depth from the surface to the interface. Beyond the cross-over distance, $x > x_{co}$, the refracted energy appears as the first arrival in seismic records. At smaller source-receiver offsets, the direct body wave is the first arrival.

The seismic compressional (P-wave) velocity of a material scales with its bulk modulus, which is a measure of the resistance of the material to an applied mechanical force. If the material strongly resists an applied mechanical force (high bulk modulus) then it generally has a high P-wave velocity (Sharma, 1997). In this study, shear waves are not considered because they are more difficult to generate with appreciable amplitude using a sledgehammer source as described in the following section.

Acquisition

The first step in the constructing a 2-D seismic tomographic image is to plan and execute a near-surface seismic survey. At the Brazos site, three lines were chosen for seismic data acquisition. Their locations are based on proximity to outcrops of the sandstone and easy accessibility. The locations of the survey lines are shown in Figure 4.



Figure 4. Approximate locations of survey lines. Site location is shown in Figure 2. For scale, Line 3 is ~144 m in length. North is oriented towards the top of the page. Cottonmouth Creek flows to the southeast.

Line 1 is roughly centered on and aligned perpendicular to Cottonmouth Creek, extending approximately 70 m on either side, and is aligned generally north to south. Cottonmouth Creek is important to this study because it exposes the HCS. This allows for ground-truthing of the tomograms in terms of the depth to the HCS observed in outcrop. The HCS, being a relatively hard layer, is more resistant to erosion than surrounding, softer beds, as shown in Figures 5 and 6.



Figure 5. An outcrop of the HCS sandstone to the east of Line 1.



Figure 6. Outcrops of the HCS sandstone downstream to the east of Line 1.

Line 2 extends from the northern end of Line 1 toward the SE and is 128 m in length. This line is located in a pasture, does not cross any streams or major ditches, and its elevation is above that of the HCS layer for the entire transect. Line 3 is also perpendicular to Line 1 and lies approximately 23 m beyond its SW termination, oriented in a NW-SE direction, and is 144 m long. The elevation of Line 3 is also above that of the HCS layer and this line has less relief than the others.

The topography of each line must be determined because seismic refraction data are affected by the distance between the ground surface and the top of the underlying high-velocity layer. Topographic data were collected for this purpose using a Topcon® total

station. Each geophone and shotpoint location was surveyed, recording vertical and horizontal positions with respect to an arbitrary local coordinate system. There was no need to geo-reference the seismic survey lines to achieve the objectives of the study.

The seismic data were acquired using a 36-channel Geometrics Strataview™ seismograph with a Geostuff rollalong switchbox (RS 120/48). Geophones were placed 2 m apart, firmly coupled to the ground, and attached to a 24-station cable. A schematic of the survey setup is shown in Figure 7. For each line, three cables were connected in series, but because of environmental constraints, such as cattle fences and a large ditch, Line 2 used only 18 geophones on the third cable. As a result, Lines 1 and 3 are a full 144 m in ground length while Line 2 is 128 m in length.

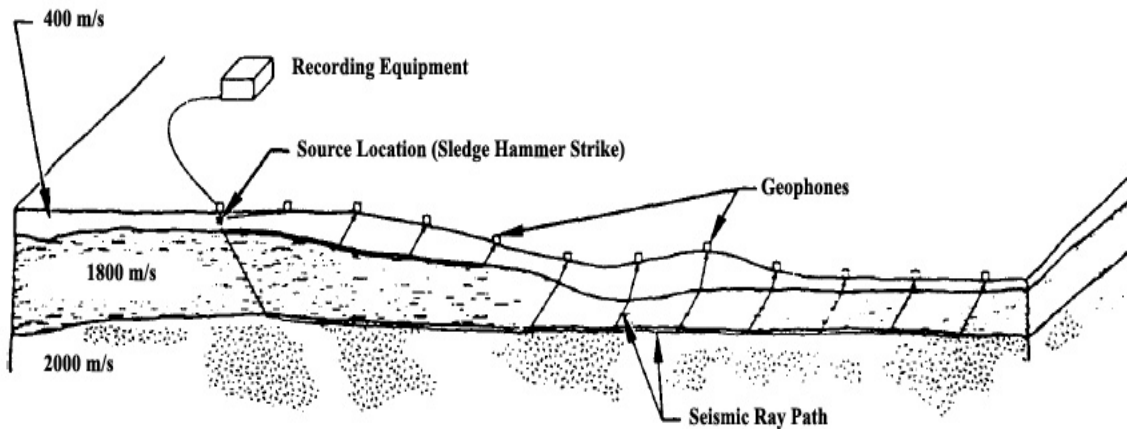


Figure 7. Schematic of a seismic refraction survey (modified from Redpath, 1973). Velocities are approximately correct for the Bazos Site.

A rollalong switch selects the group of geophones that are activated by the seismograph, which can record up to 36 geophone responses for each shot. Without this important device, to perform a common-mid-point (CMP) reflection profile, the selected group of geophones would have to be manually picked up and moved by one station interval each time a shot is taken (Geostuff, 2008). A CMP profile is a configuration of source-receiver pairs placed symmetrically on either side of a midpoint (Pelton, 2005). We used the CMP acquisition protocol despite this being a refraction survey so that the data could also be later processed as a CMP reflection survey, if desired. This gives us flexibility to perform future analyses. It should be noted that large source-receiver offsets, as is typical in refraction studies, were not required because the HCS layer is closer to the surface than one cable length. This survey began with the rollalong switch in position 1 and geophones 1-24 connected to the seismograph. After the first shot was taken, the switch was rotated one position, disconnecting geophone 1 and adding geophone 25 for the next shot. This process was continued until geophones 24-47 were connected to the seismograph through the rollalong switch. Once the cable length was exhausted, the seismograph was moved, or “rolled along”, and the cable at the start of the line was moved to the end of the previous line.

The seismic source is a 4.5 kg hammer striking a small metal plate. The resulting seismic records (seismograms) are processed by manually picking the first arrival travel times for each shot location, as shown by the circles plotted on the representative seismogram in Figure 8. The x -axis of the seismogram is the geophone number

(separated by 2 m in this survey) and the *y*-axis is the two-way travel-time in seconds, increasing downwards. Channel 8 does not show a proper signature because of a malfunction in the instrumentation. Channel 1 is connected to the source and used for triggering the acquisition. A break in the slope of the first-arriving energy is clearly shown in the seismogram at channel 6. This is the cross-over distance at which the refracted wave energy appears as the first arrival before the direct-wave energy. The break in slope confirms our ability to recover refracted arrivals at this site. Additional representative seismograms are included in Appendix A. A CD of the complete set of seismograms is available from the author on request.

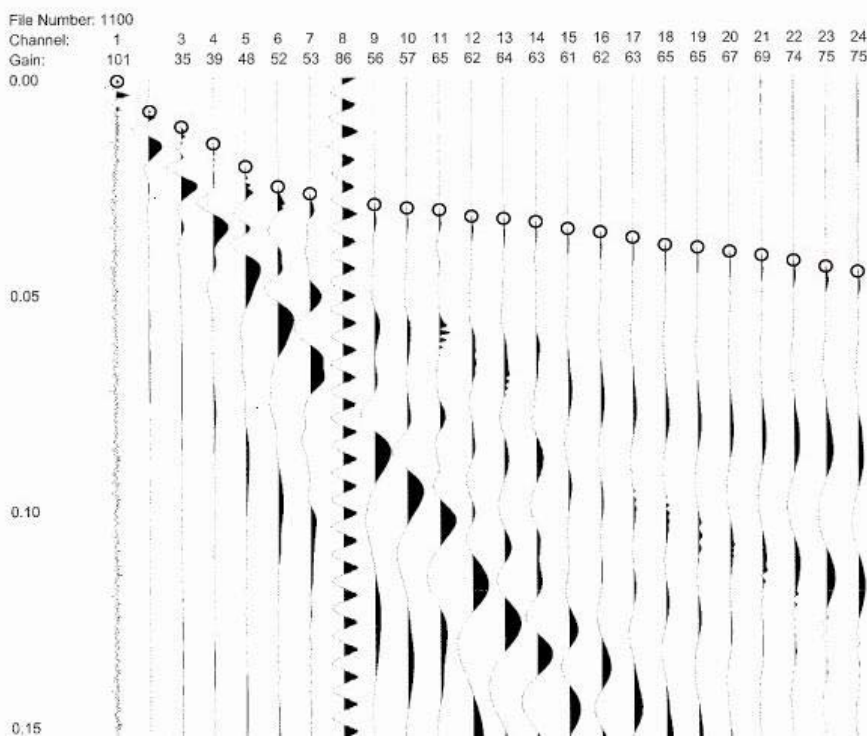


Figure 8. A representative seismogram showing first-arrival picks (circles).

Two distinct slopes in the first arrival times are evident if a pair of line segments is drawn connecting the circles in Figure 8, one before and one after channel 6. The slopes of these curves are $1/V_1$ and $1/V_2$ respectively, or the inverse of the velocities of layers 1 and 2. The velocity V_1 is calculated from the slope of the line to be approximately 385 m/s and similarly the velocity V_2 is roughly 2000 m/s. Expected P-wave velocities for unconsolidated sediment and sandstone are in the range of 300-600 and 1800-4000 m/s respectively (Jakosky, 1957). The long-wavelength energy arriving later than the first arrivals represents ground roll, possibly with low-amplitude, high-frequency reflected waves embedded. The only arrivals used for this study are those from refracted waves, which appear as the first arrivals.

A seismic interpretation program developed by Zelt and Smith (1992) is used to create a 2-D tomographic image of the seismic velocity structure of the subsurface. The tomography is based on inversion of the first arrival times. Graphs showing the depth to the HCS layer relative to the topography are extracted from the tomograms for each line. These graphs show a continuous representation of the top of the HCS layer, which is the sought-after parameter of this study.

Seismic Tomography

Seismic tomography is used to construct an image of the subsurface velocity distribution of a geologic formation based on the travel times of seismic waves typically measured at locations on the ground or within a borehole (Sharma, 1997). A slightly adapted version

of the seismic travel-time tomography algorithm developed by Zelt and Smith (1992) is used for this study. This program was originally developed for crustal-scale geologic mapping. The program was modified to be applicable to near-surface, low-velocity geological media and fast travel-times, as required for the current application. The essential approach in either case is based on a subsurface discretization method in which the slowness (reciprocal of velocity, $1/V$) values of discrete cells are constant and seismic energy propagates as straight rays through each cell.

Travel-time, as calculated by Zelt and Smith's (1992) program, is a linear combination of slowness (the reciprocal of velocity) and distance traveled by a given ray i :

$$T_i = \sum_{j=1}^m d_{ij} P_j , \quad (4)$$

where d_{ij} is the distance that ray i travels in cell j , $P_j = 1/V_j$ is the slowness in cell j , and m is the number of cells through which ray i passes (Sharma, 1997). Slowness P is used instead of velocity V so that travel-time T_i becomes a linear function of the material property.

Zelt and Smith's (1992) tomographic construction algorithm is based on a forward ray-tracing module combined with an iterative inversion technique. The input is a set of observed first-arrival travel-times, along with a 2-D discretization of the subsurface

characterized by a user-specified number of cells. The program is capable of tracing all refracted and all reflected rays but in this study, for simplicity, only the first-arriving head wave paths are used and all later arrivals are neglected. Only large source-receiver offsets (beyond $x \sim 14$ m) were considered so that all of the first-arriving direct rays were ignored. The direct-wave arrival times do not provide essential information about the undulation of the uppermost refractor in the sense that the directed rays do not interact with it. The implementation details outlined in Zelt and Smith (1992) were followed. A first estimate of the depth to the underlying fast layer is made, taking into account the presence of topographic variations. With these input data, a grid of slowness cells is constructed. The program then traces ray paths that describe the energy propagating to each receiver location from each transmitter location. Because rays are traced of all types of energy, including reflection and refraction, a numeric code is assigned to enable separate tracking of each phase (e.g. the first arrival ray code = 1.3, in our case). The first arrival time data that are input by the user is compared to the travel-time predictions for rays traced within the model. A misfit χ^2 is then calculated between the observed travel-times and the model-predicted travel-times based on the following equation:

$$\chi^2 = \sum_{i=1}^N (T_i - T_i^p)^2, \quad (5)$$

where T_i is the observed travel-time and T_i^p is the model-predicted travel-time, and N is the number of transmitter to receiver pairs.

Based on the value of the misfit and the sensitivity of travel-times to small changes in cell velocities, the velocity in each cell is adjusted and the model is run again and the misfit is reevaluated. The sensitivity S_{ij} is the ratio of the change in travel-time ΔT_i resulting from a change $1/\Delta V_i$ in slowness of cell j :

$$S_{ij} = \Delta T_i / \Delta V_i \quad (6)$$

A higher (lower) sensitivity value indicates that the cell slowness value must be adjusted by a larger (smaller) amount. After the model adjustment is complete and the forward code run again, the misfit is re-computed. This process is iterated several times until the misfit is lowered to a satisfactory level.

Model Input Files

Four input files are required to run the tomographic software: r.IN, tx.IN, v.IN, and d.IN. Each input file was tailored to the specific data set collected for the individual survey lines. Initial input files for Line 2 and Line 3 are included in Appendix B.

Individualized for each line, the r.IN file specifies important quantities such as shot locations and ray tracing parameters.

Travel-time data picked from the field collected seismograms are used by the tomographic imaging software. These data are input as a tx.IN file. Data from every other shot location were used in this study. Travel-times were input only from receivers located further than 16 m from the shot location to ensure that the first arrival travel-times used were from refracted energy rather than reflected or, more likely, direct-arriving energy.

The v.IN file specifies the structure of the model subsurface in terms of topography, seismic velocities, depth to the uppermost refractor, and grid geometry. The latter describes the cell geometric structure of the modeled subsurface. The shot locations are used to create vertical cell boundaries as shown in Figure 9.

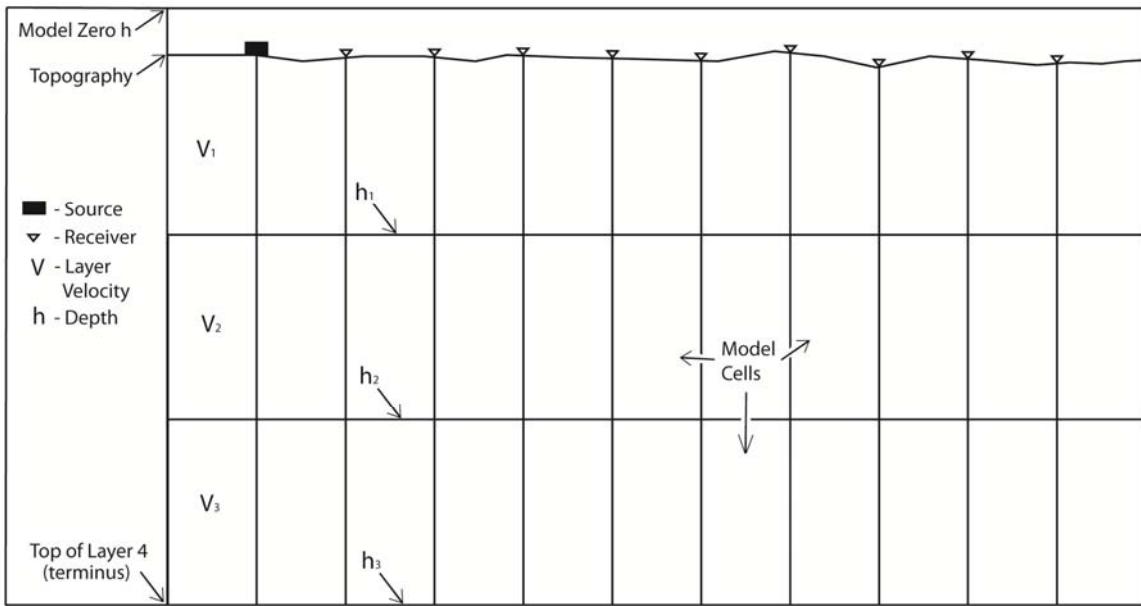


Figure 9. Simplified depiction of the initial model structure.

The v.IN file instructs the software which of the model parameters, i.e. cell boundaries and slowness values, are to be adjusted at each iterative step. To specify that a parameter in the v.IN file should be adjusted, a 1 is placed under it, as shown in Figure 10.

2	.00000	.00193	.00392	.00602	.00796	.00995	.01193	.01392	.01588
.01791									
1	.00600	.00600	.00600	.00600	.00600	.00600	.00600	.00600	.00600
.00600									
1	1	1	1	1	1	1	1	1	1
1									
2	.01991	.02193	.02393	.02588	.02787	.02993	.03190	.03393	.03593
.03787									
1	.00600	.00600	.00600	.00600	.00600	.00600	.00600	.00600	.00600
.00600									
1	1	1	1	1	1	1	1	1	1
1									
2	.03990	.04189	.04393	.04589	.04788	.04988	.05182	.05384	.05585
.05781									
1	.00600	.00600	.00600	.00600	.00600	.00600	.00600	.00600	.00600
.00600									
1	1	1	1	1	1	1	1	1	1
1									
2	.05981	.06177	.06384	.06579	.06785	.06979	.07180	.07378	.07575
.07776									
1	.00600	.00600	.00600	.00600	.00600	.00600	.00600	.00600	.00600
.00600									
1	1	1	1	1	1	1	1	1	1
1									
2	.07982	.08174	.08378	.08574	.08774	.08975	.09173	.09374	.09570
.09772									
1	.00600	.00600	.00600	.00600	.00600	.00600	.00600	.00600	.00600
.00600									
1	1	1	1	1	1	1	1	1	1
1									
2	.09970	.10171	.10366	.10567	.10761	.10964	.11165	.11362	.11556
.11761									
1	.00600	.00600	.00600	.00600	.00600	.00600	.00600	.00600	.00600
.00600									
1	1	1	1	1	1	1	1	1	1
1									
2	.11957	.12160	.12355	.12553	.12752				
0	.00600	.00600	.00600	.00600	.00600				
1	1	1	1	1	1				

Figure 10. Section of v.IN describing the starting h_1 of Line 2. The first row is x location of the line, the second row is the h_1 value, and the third row enables the sensitivity calculation for the model parameter in the row directly above it.

Layers with linear velocity variations are allowed in the Zelt and Smith (1992) program.

However, constant-velocity cells are used here because this study assumes a laterally homogeneous velocity structure within each layer in the subsurface. The upper and lower boundaries of a layer are allowed to vary laterally. Initial velocities could have

been chosen based on typical P-wave velocity ranges found in Knight and Andres (2005), (e.g. 180-450 m/s for unconsolidated material, 1450-1650 m/s for sandstone, and 2200-4000 m/s for shale). However, site-specific data were used to generate seismic velocities by simply calculating the slopes of the average first arrival travel times for the entire Line 3. This produced velocities of approximately 382 m/s for V_1 , 1920 m/s for V_2 , and 1975 m/s for V_3 . These velocities were plugged into the tomographic software and were run through several iterations with the velocity layers turned on in order to lower the misfit. The layer interfaces were kept flat during the velocity determination phase. The inversion converged to velocities of 364 m/s for V_1 , 1800 m/s for V_2 , and 2200 m/s for V_3 . These velocities were also applied to the processing of Line 2.

Initial layer-depths, or h , values, were estimated based primarily on measuring the elevation of the exposure of the HCS in Line 1, with additional input from previous descriptions of local outcrops and bore-holes (Yancey, 1996; Adatte et al., 2011; Keller et al., 2011). The parameter h_1 represents the top of the HCS layer, h_2 represents the bottom of the HCS, and h_3 is the model terminus and was chosen arbitrarily. The initial h values were 6 m, 7 m, and 12 m for h_1 , h_2 , and h_3 , respectively and are defined as the distance from the $z=0$ datum.

The fourth input file specifies the damping factor used by the tomographic inversion. The damping factor acts to stabilize the model parameter adjustments, or to constrain the ability for the program to modify them in a volatile or haphazard manner (Zelt and

Smith, 1992). The presence of the damping factor causes the program to minimize the misfit in small increments. A lower damping factor allows the program to make larger model adjustments during an iteration in an attempt to lower the misfit. Entered into the program as a d.IN file, shown in Figure 11, the damping factor is always less than unity.

```
0.14192      ! xmax
0.050        ! damping factor
0.001        ! velocity uncertainty [km/s]
0.00001      ! depth-to-boundary uncertainty [km]
```

Figure 11. An example d.IN input file used in tomography of Line 3.

Data Analysis

Recall that the primary objective of the data analysis is to estimate the depth to the top of the undulating HCS layer; in other words, to determine a function $h(x)$ that best describes the undulations of the HCS layer surface along each of the surveyed seismic lines. Roughness R is a parameter that characterizes lateral variations of the function $h(x)$ along a survey line. It is defined by the sum of the square of differences between adjacent h values, that is

$$R = \sum_i [h(x_i + \Delta x) - h(x_i)]^2, \quad (7)$$

where the sum runs over the pairs of adjacent horizontal cells in the slowness model; in our case, this is the same as the number of pairs of adjacent geophone locations on the surveyed seismic line. The parameter Δx is the spacing between adjacent geophones. A

rough model of $h(x)$ is characterized by a relatively large value of R while a smooth model of $h(x)$ is one for which the roughness value R is relatively small.

It is well known in seismic tomography (e.g. Zelt and Smith, 1992), as in other kinds of geophysical ill-posed problems, that there exists a trade-off between the roughness of a reconstructed model and its data misfit. Specifically, an implausibly rough model can always be found that fits the data better than a smooth model. An implausibly rough model of $h(x)$ refers here to one that almost all geologists would agree contains too much lateral variation than could be reasonably expected at the site. Conversely, a smooth model is one that most geologists would agree does not contain enough lateral variation than could be reasonably expected at the site. Clearly, not all geologists can be consulted to offer an opinion, so that the geophysicist must try to imagine the range of opinions that geologists would give, by consulting a few for example, and/or by using his own geological skill, observation, and reasoning power. It is fair to say however, in most cases, that the final assessment of whether a model is implausibly rough or reasonably smooth ultimately comes down to the judgment and experience of the geophysical interpreter.

The reason that a trade-off exists between model roughness and data misfit is readily understood in the context of seismic refraction tomography. Rough slowness models generate predicted first-arrival travel times that vary greatly from station to station along the survey line. This is because, in general, the complexity of a geophysical response

reflects the complexity of the underlying geological model that generates it. The measured first-arrival travel times also contain a certain amount of station-to-station variability from random noise in the measurements. A set of predicted travel-times that very nearly matches the measured travel-times is actually not desired by geophysicists because many of the energy signatures are simply random measurement noise. In this way, rough slowness models that generate rough travel time responses, while achieving a very low misfit to the data, are not likely to portray realistic physical models of the subsurface. Geophysicists instead prefer to construct smooth slowness models that hopefully portray a physically reasonable underlying geological structure without over-fitting the data. In the final analysis, there is only so much structure that a geophysicist can introduce into the model before starting to fit the noise.

A regularized inverse problem is one that negotiates the trade-off between a specified model attribute, such as roughness, and data misfit. The seismic refraction tomography of Zelt and Smith (1992) is a regularized inverse problem based on a damped least-squares approach. To negotiate the trade-off, Zelt and Smith (1992) declare an objective function that, in effect, involves a linear combination of model roughness and data misfit. The relative contribution of each term in the objective function is controlled by specifying a damping factor (D). The goal is to minimize the objective function for different values of D . As D is increased, smoother models are given preference at the expense of an increased data misfit. Conversely, as D is decreased, the algorithm returns

rougher models with lower values of the misfit. The geophysicist decides an optimal value of D , somewhat subjectively.

To determine the effect of D on model roughness, tomographic inversions were run for a number of different trial values of D . A graph of misfit versus the model roughness at each iteration was created for each trial. These misfit versus roughness graphs are essentially convergence graphs that portray, at each iteration, the attributes of each model in the iterative sequence (Figure 12). The processing of Line 3 was completed prior to Line 2; therefore the models will be displayed in reverse numerical order.

As shown in Figure 12, trial damping values of $D=0.005, 0.009, 0.020, 0.030, 0.050, 0.060, 0.120, 0.200$, and 0.250 were chosen. These values of D provide an adequate sampling of this parameter while maintaining stable convergence of the tomographic model reconstruction algorithm. Selecting values of D outside this range yielded unstable performance of the tomography software.

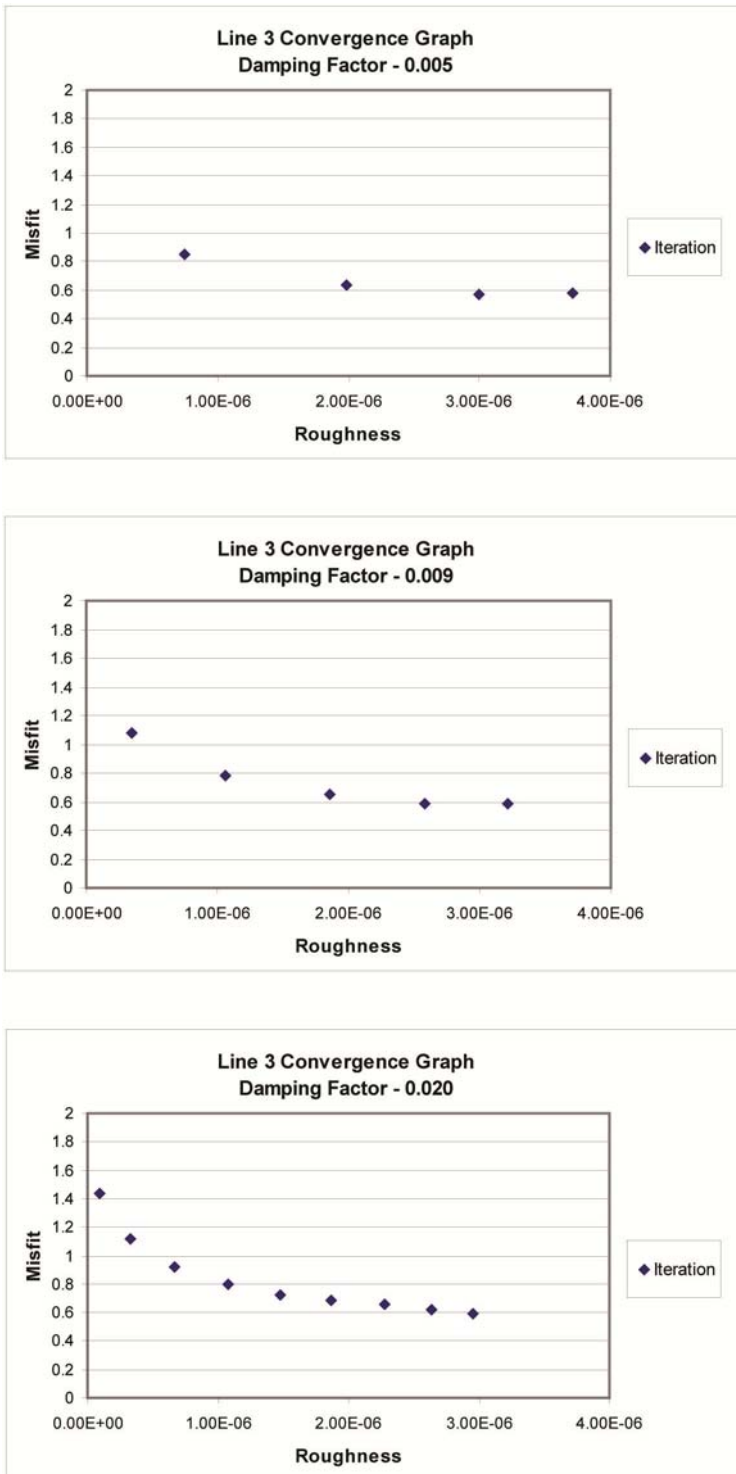


Figure 12. Line 3 convergence graphs for the damping factor trials.

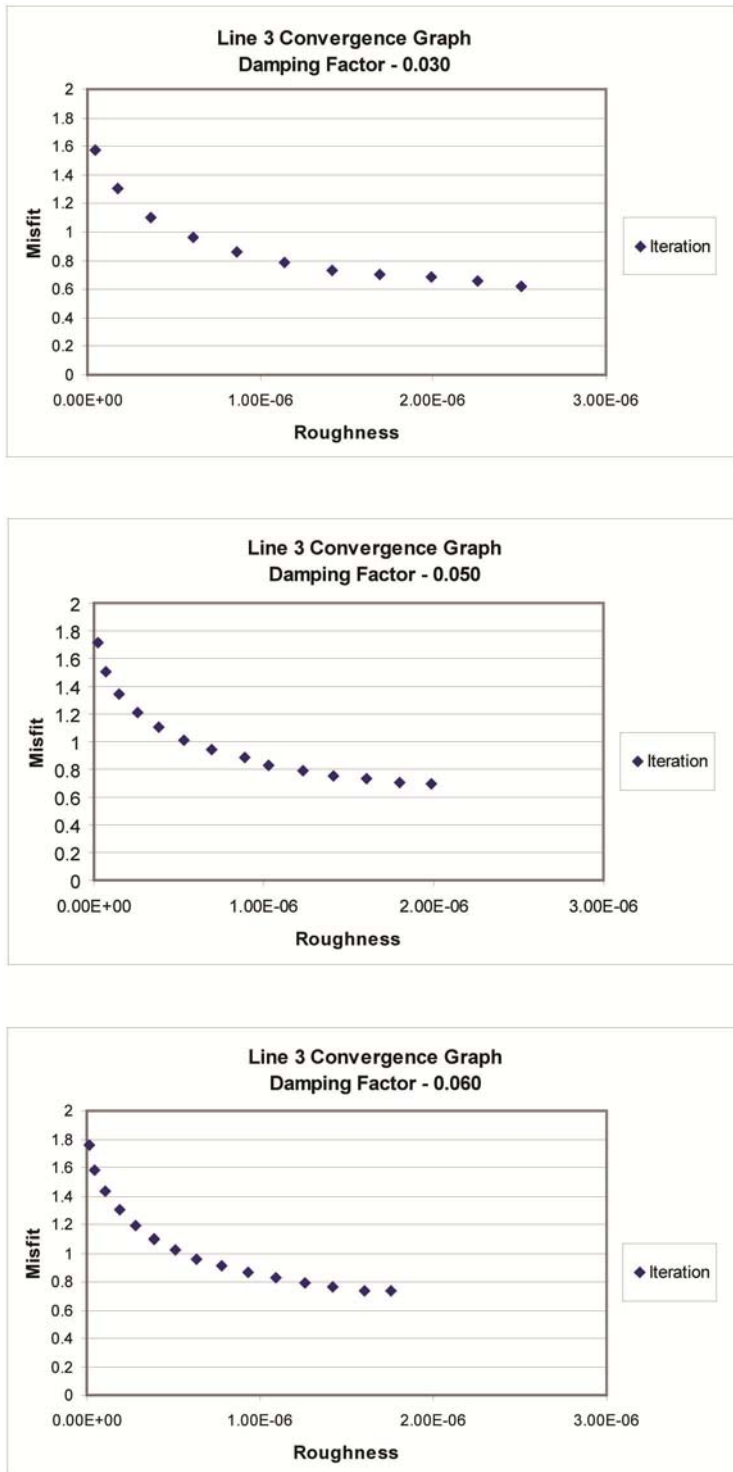


Figure 12 (continued).

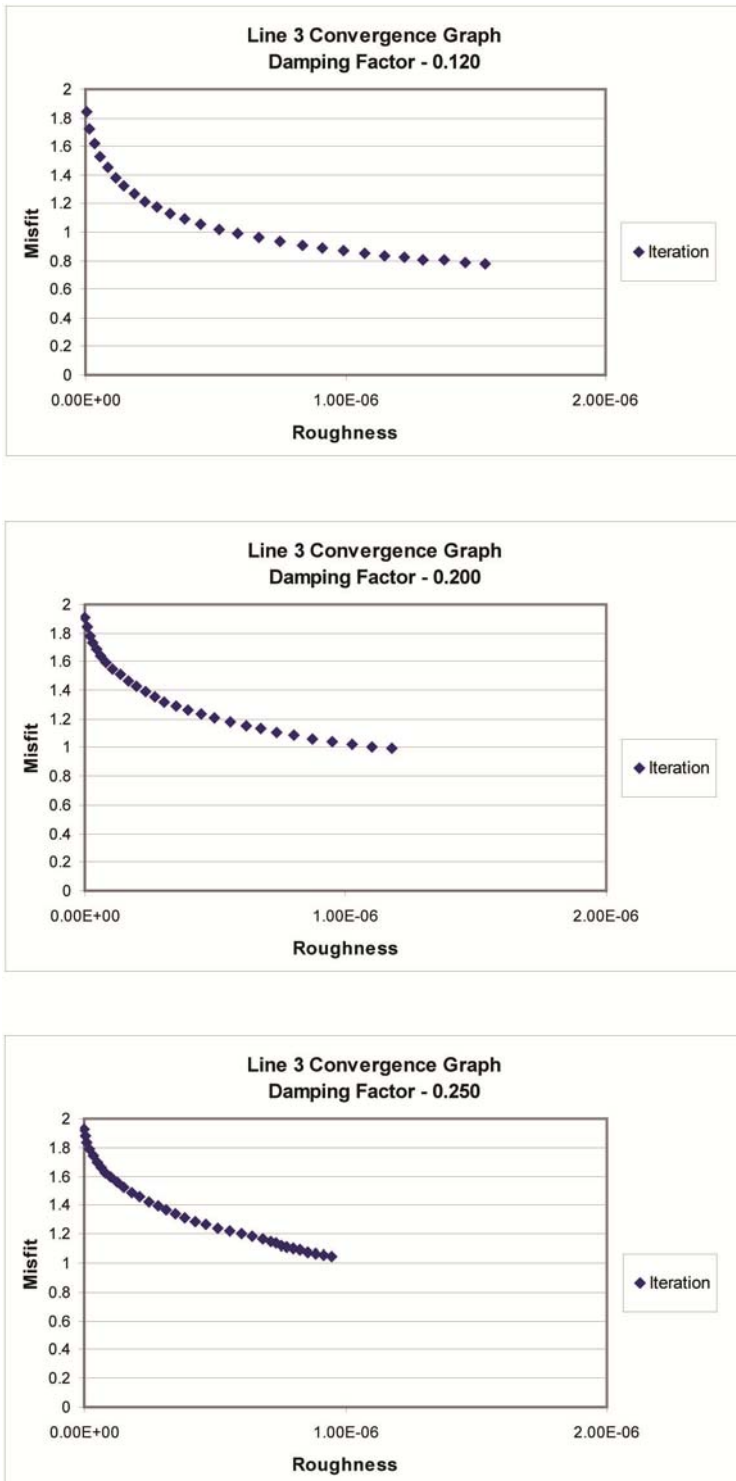


Figure 12 (continued).

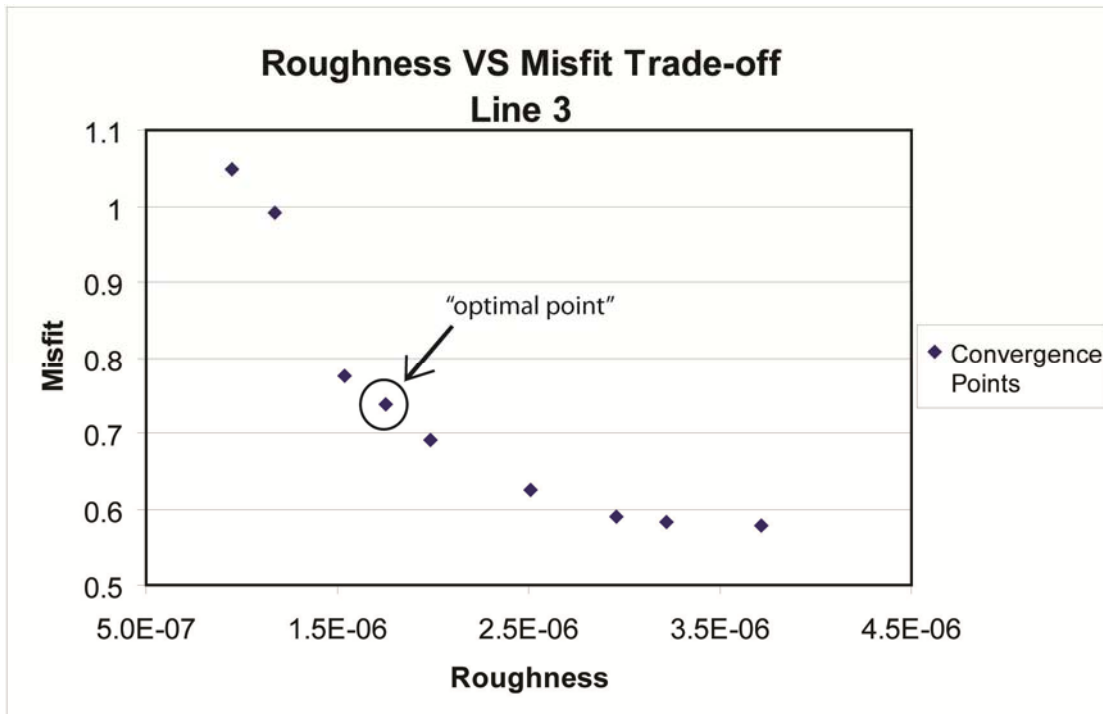


Figure 13. Roughness versus misfit trade-off graph of convergence points from Figure 12 for Line 3. The optimal point is shown.

The model to which the tomographic algorithm converged was chosen from each D trial.

The key attributes (misfit and roughness) of these converged models were plotted to create a trade-off, or “L” curve. The model that falls closest to the origin is at the “knee of the curve” or the optimal point. Shown in Figure 13, this is the point where the trade-off between misfit and roughness is balanced and represents the preferred final model of $h(x)$. This process was repeated for Line 2 and the results are displayed in Figures 14 and 15.

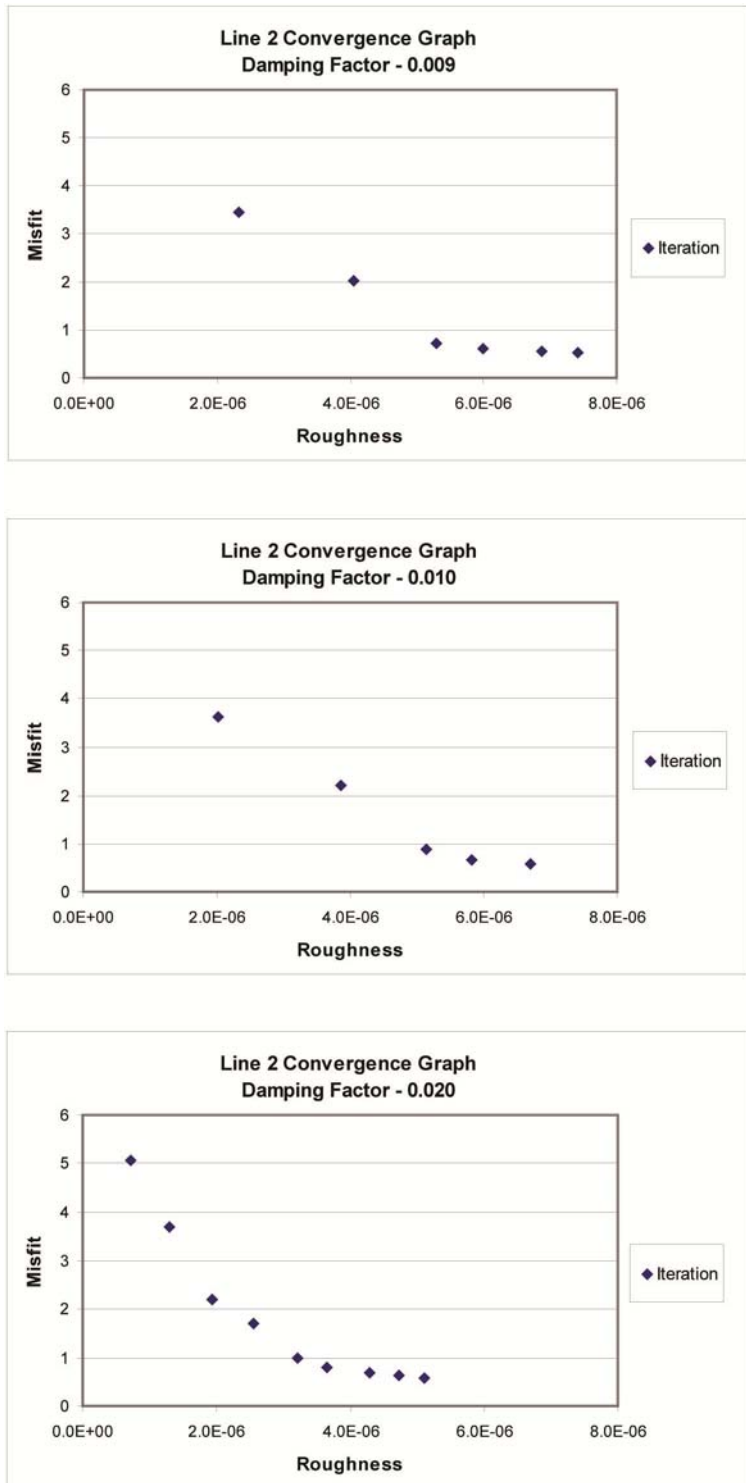


Figure 14. Line 2 convergence graphs for the damping factor trials.

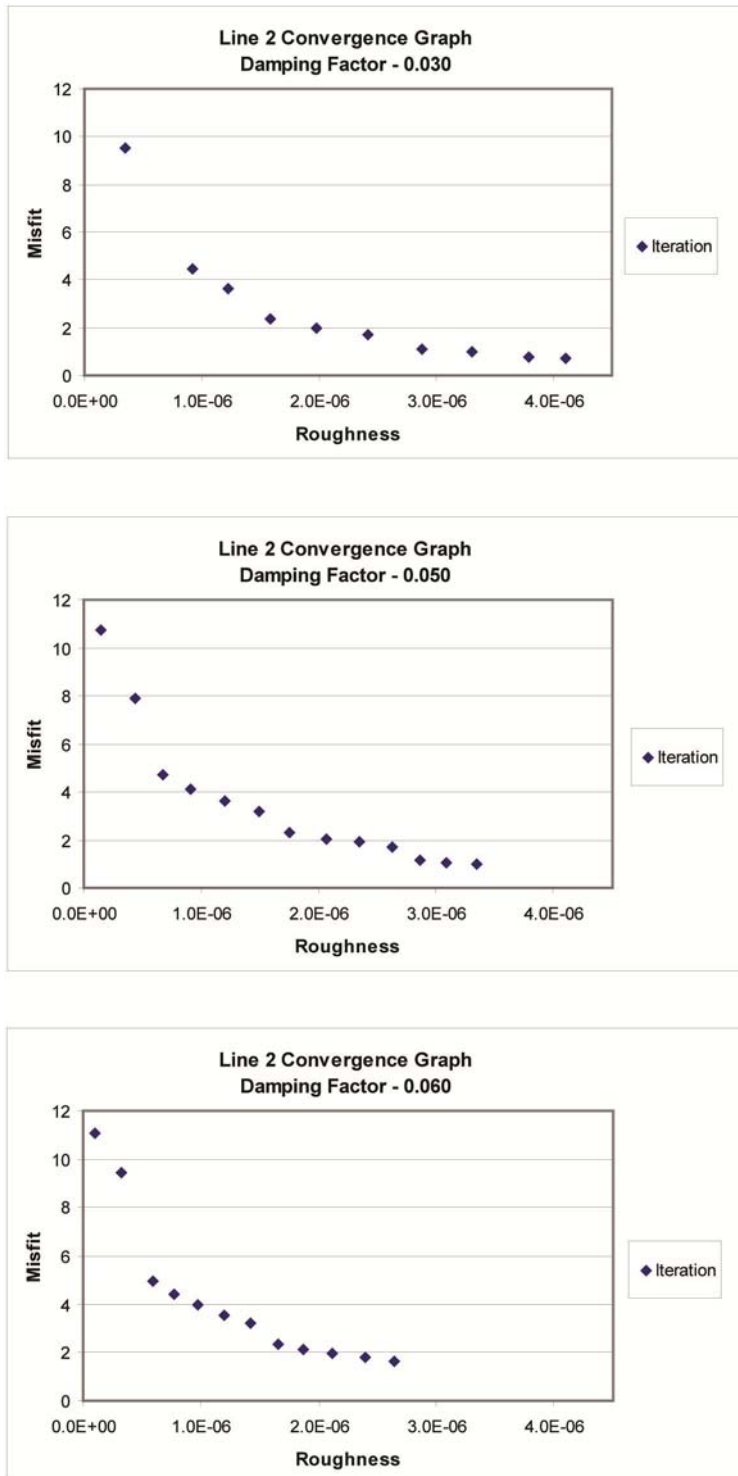


Figure 14 (continued).

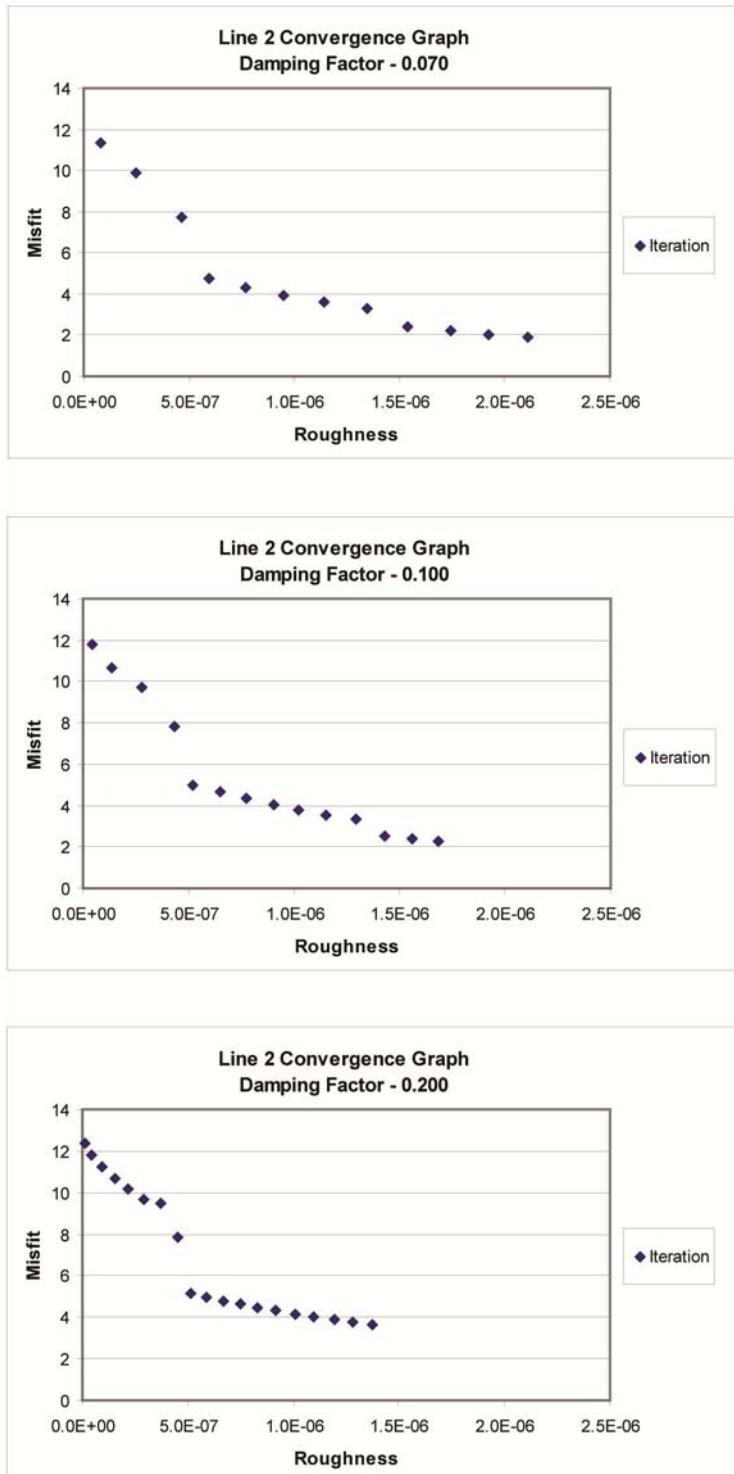


Figure 14 (continued).

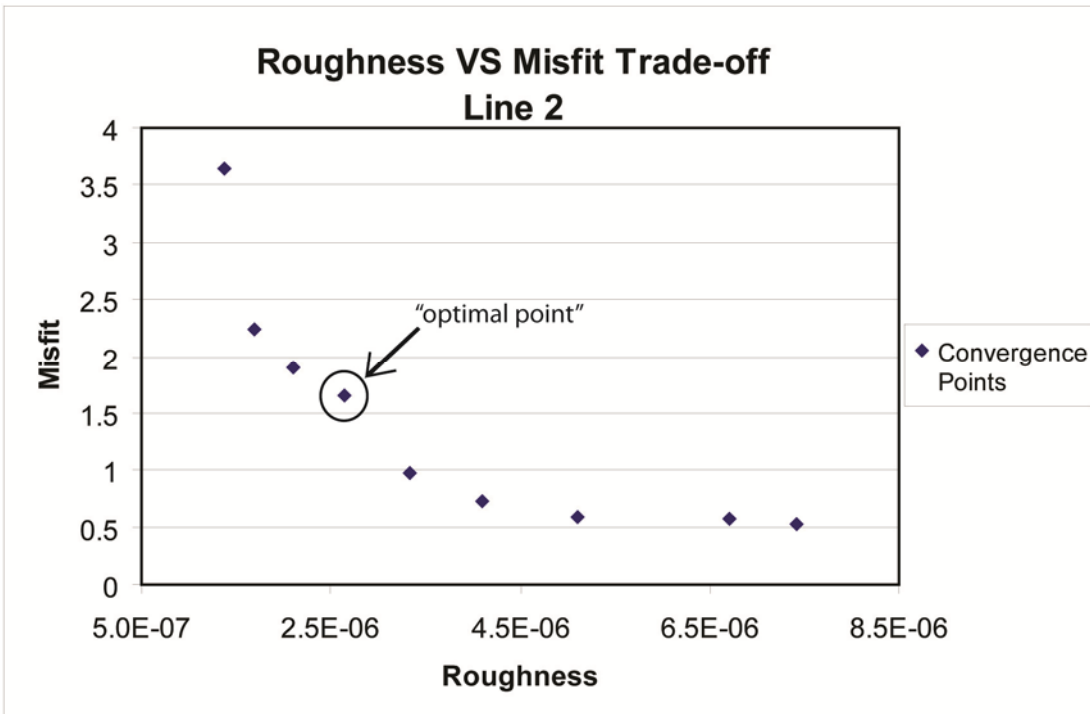


Figure 15. Roughness versus misfit trade-off graph of convergence points from Figure 14 for Line 2. The optimal point is shown.

RESULTS AND INTERPRETATION

Topography

The tabulated topographic data are provided in Appendix C. These data were used to construct topographic profiles along each of the three seismic lines (Figure 16). Line 1 is the only line that intersects an exposure of the HCS layer (Figure 17); this occurs between 90-96 m horizontally and approximately 6-7 m vertically below the survey datum. An important aspect of Line 1 is that the HCS exposure permits ground truthing of the seismic refraction tomograms. The HCS layer is not exposed across on the south side of the stream on Line 1 because it is buried below soil eroded from higher elevations on the stream bank.

Because Lines 2 and 3 elevations are above that of the HCS layer, these lines enable continuous seismic imaging of the underlying HCS layer. Line 1 has the greatest topographical variation at 7.31 m vertically, Line 3 has the smallest topographical variation at a total of 0.84 m, and Line 2 has an intermediate topographical variation of 3 m.

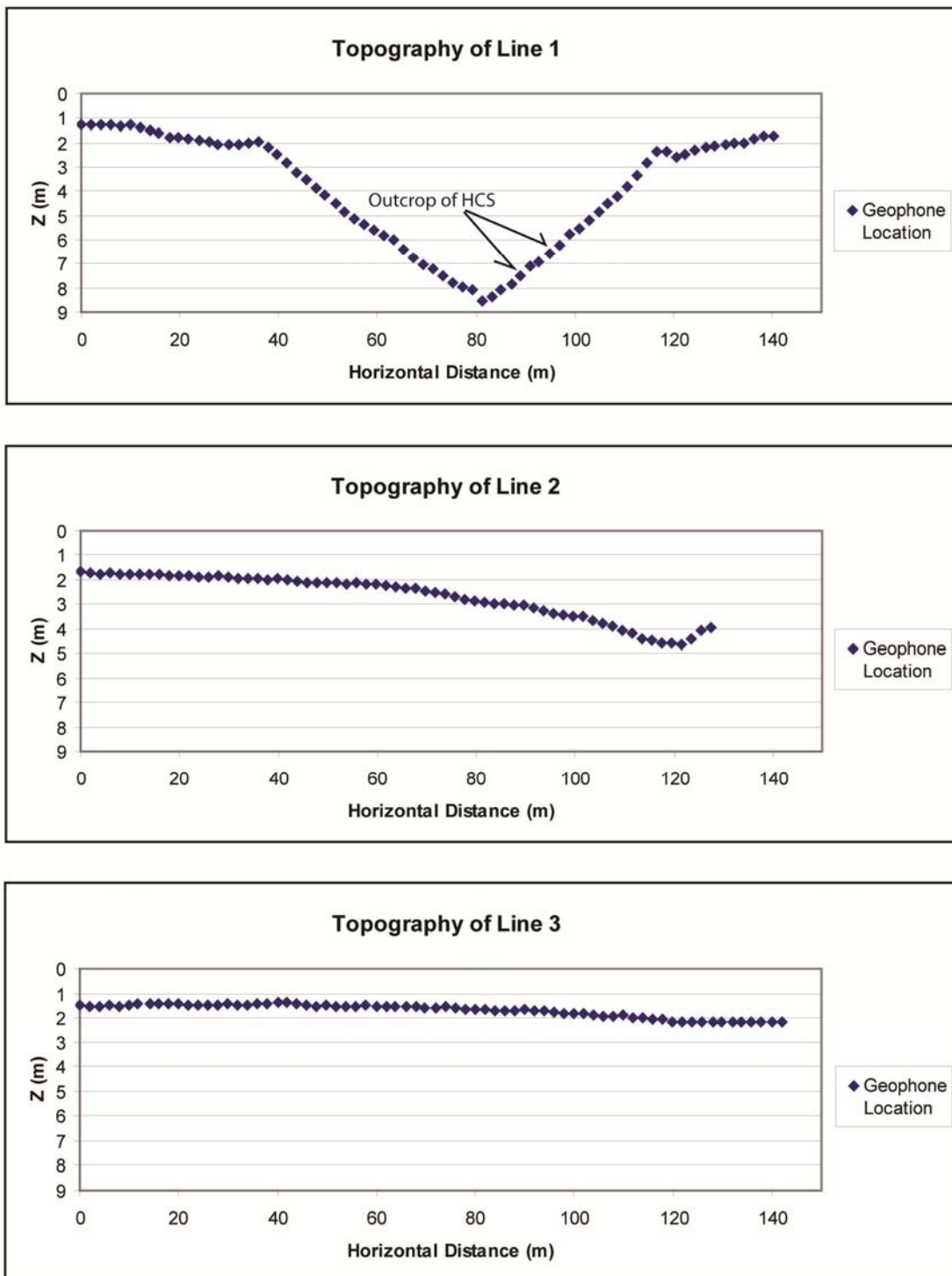


Figure 16. Graphs that represent the topography of Lines 1 through 3. Each diamond represents one geophone location, approximate exposure of HCS shown on Line 1.

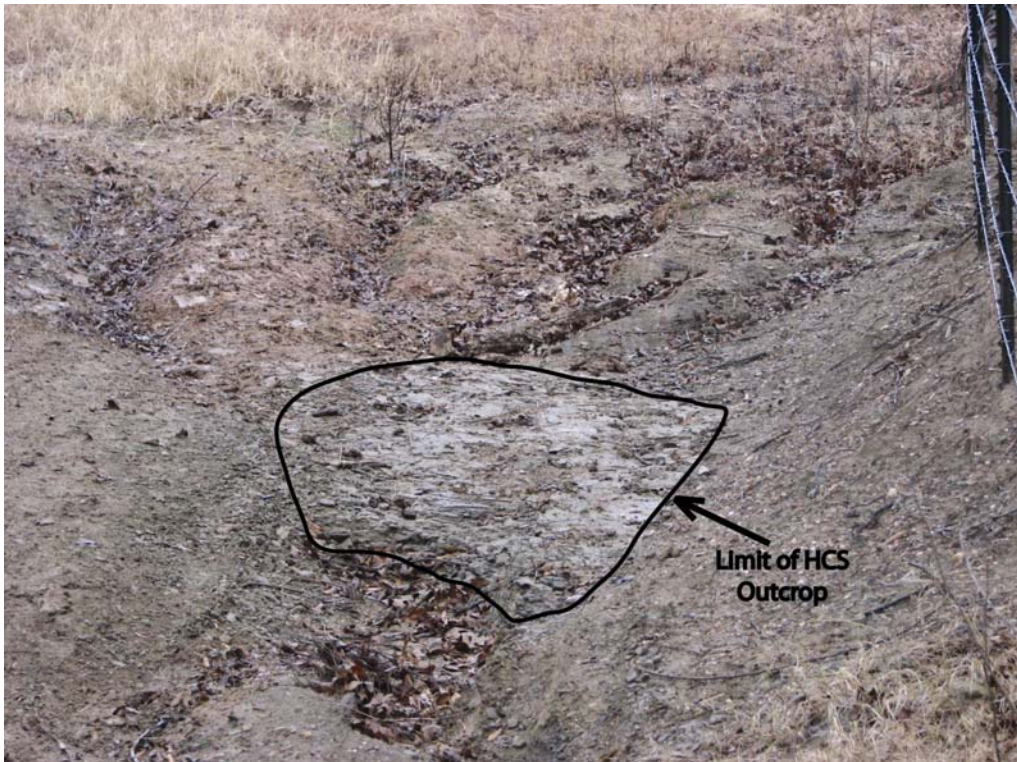


Figure 17. A view facing north of the HCS exposure in Line 1.

Seismic Survey

A seismogram is a graph of seismic energy with two-way travel-time from a shot to a subsurface reflector plotted along the y axis and horizontal distance from shotpoint to receiver on the x axis. A representative seismogram is shown in Figure 18. The first arrival time of the energy at each geophone location is the most important input information as explained previously; therefore, a table compiling all first arrivals for Lines 2 and 3 is in Appendix D.

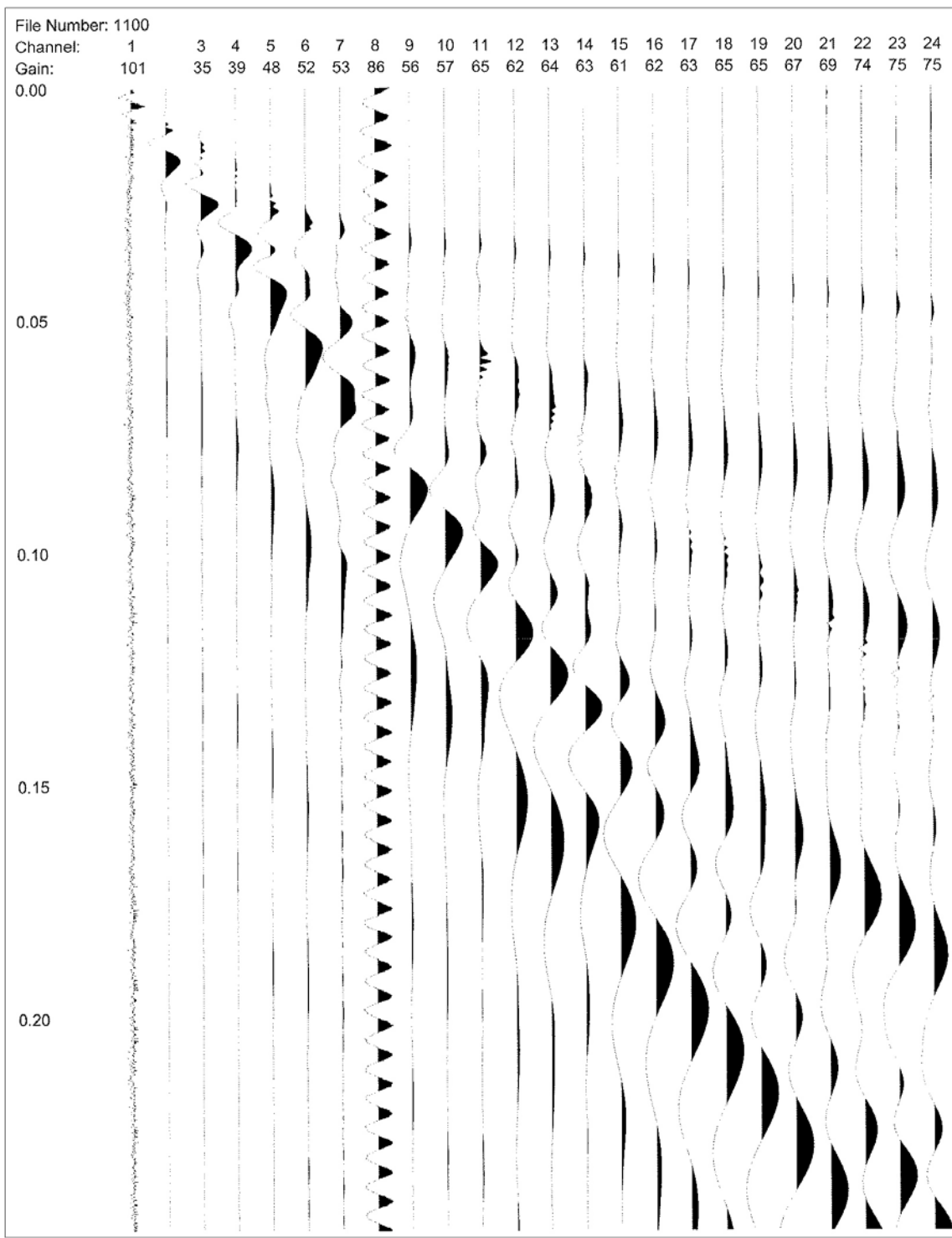


Figure 18. A representative seismogram taken during the Brazos K-T Boundary study.

Tomographic Model

As mentioned previously, the processing of Line 3 was completed prior to Line 2, therefore the reconstructed models will be described in that order. The optimal value of damping factor D for the Line 3 data set, as chosen from the optimal point in Figure 13, is 0.060. The preferred estimate of $h(x)$ was extracted from the corresponding model and is displayed in Figure 19. The model-derived $h(x)$ undulates in an irregular pattern and is characterized by a relief of roughly 1 m. The overall trend is largely uncorrelated with the topography.

The optimal value of the damping factor D for the Line 2 data set, chosen from the optimal point in Figure 15, is also 0.060. The preferred estimate for $h(x)$ was extracted from the model corresponding to the optimal point and is displayed in Figure 20. The model-derived $h(x)$ undulates with an irregular pattern and has relief 1.04 m over much of the line, until the final approximately 18 m of the model where it dips an additional 0.69 m and becomes highly oscillatory. The overall trend is largely uncorrelated with the topography.

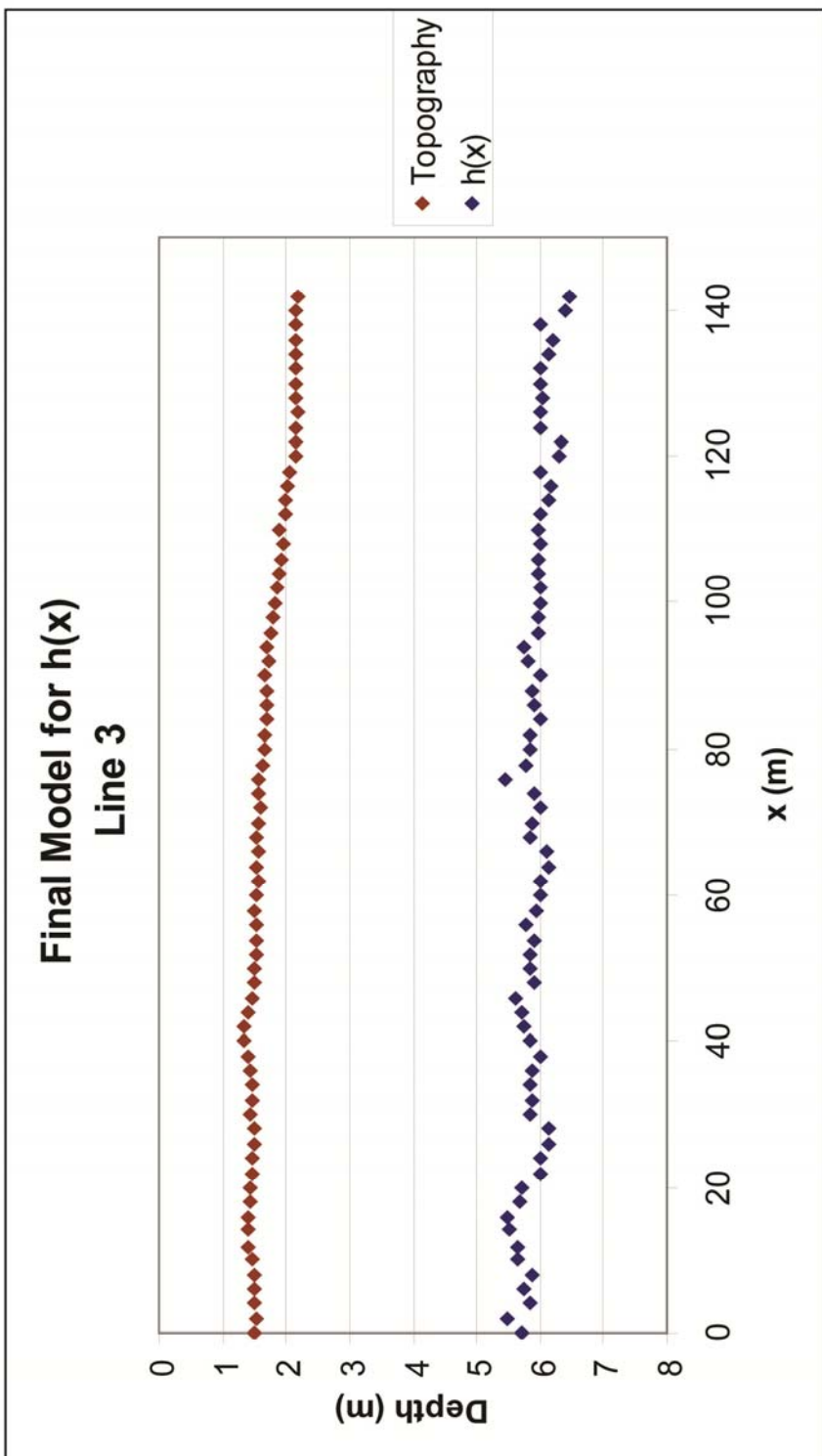


Figure 19. Final tomographic model of $h(x)$ from the Line 3 data set.

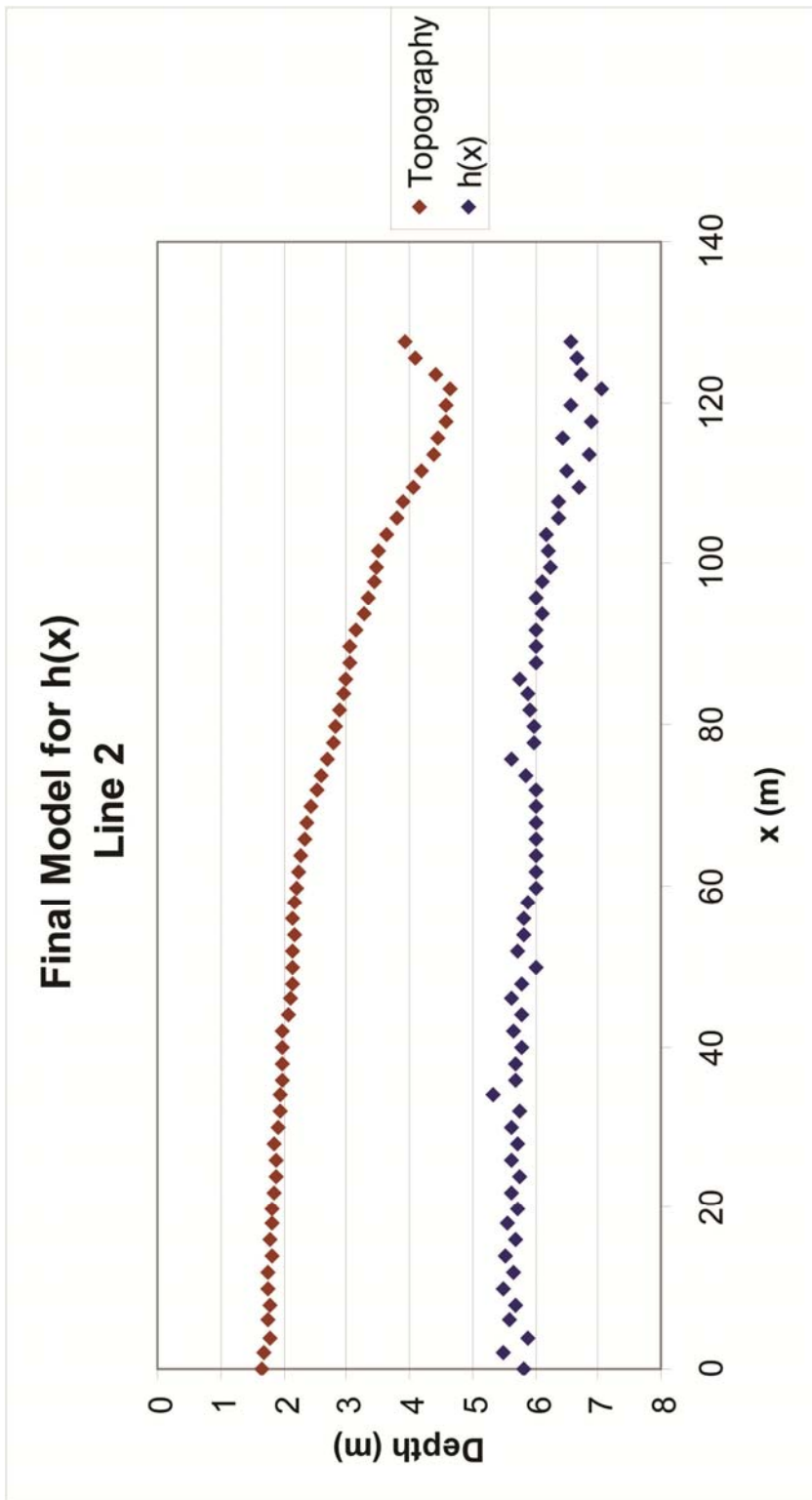


Figure 20. Final tomographic model of $h(x)$ from the Line 2 data set.

The oscillatory behavior of $h(x)$ near the end of Line 2 raises questions about the ability of the tomographic software to handle significant variations in topography while resolving shallow interfaces. Geologically speaking, a lateral discontinuity of the HCS layer is conceivable (Yancey, 1996). On the other hand, it is also possible that the reconstructed interface oscillations are unstable artifacts of the Zelt and Smith (1992) modeling algorithm. It is noteworthy that the oscillations correspond to locations beneath a significant elevation drop in the surface topography. This drop in topography brings the surface to within 1.4 m of the projected depth of the HCS layer. This close proximity is challenging to explain on geological grounds. A possible explanation for the apparent HCS layer oscillations is that the $h(x)$ reconstruction may be less well-constrained at the ends of the seismic lines because a less complete subsurface ray coverage compared to the line interiors.

It is interesting to note that the undulations do not vary in terms of x when D is changed. Figure 21 is a combined plot of $h(x)$ D of 0.005, 0.060, and 0.200 for Line 3, which clearly shows that the undulations only vary in amplitude with the change in D . This is significant because it demonstrates that the tomographic software is consistent in its ray-tracing pathways and ability to match travel-time data. This effect is demonstrated again in Figure 22.

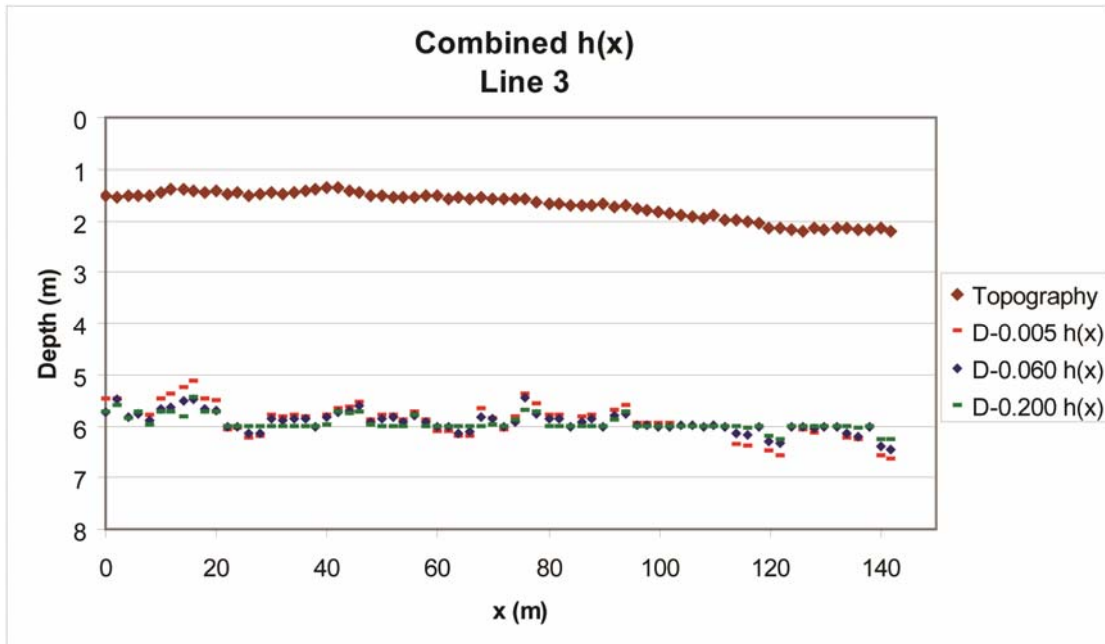


Figure 21. Combined $h(x)$ plot for the spectrum of D for Line 3. Note the inverse relationship of D and amplitude of $h(x)$.

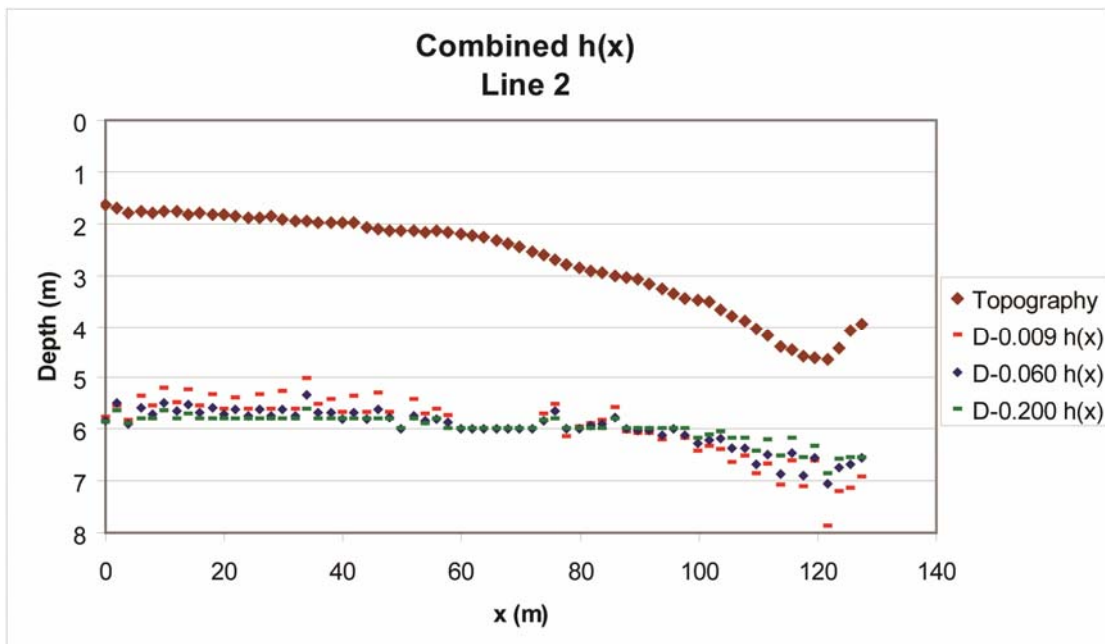


Figure 22. Combined $h(x)$ plot for the spectrum of D for Line 2. Note the inverse relationship of D and amplitude of $h(x)$.

The undulations that are present in the final $h(x)$ for both Line 2 and 3 can be compared, where exposures permit, to observed undulations of the HCS layer. As shown in Figure 23, the undulations of the HCS as exposed in Cottonmouth Creek can be on the order of several m horizontally with amplitude of less than a meter. The undulations presented in the tomographic model reconstructions are roughly 4-8 m horizontally with amplitude of approximately 0.5-1.0 m.



Figure 23. A view of the top of the HCS layer down stream of Line 1 (backpack for scale).

CONCLUSION AND RECOMMENDATIONS

This study has shown that near-surface seismic tomography is capable of interpreting large scale features of the HCS associated with the KTB. The large scale orientation of the HSC is clearly shown in the two survey lines that were studied. Representations of these layers are shown in graph form created by analyzing the seismic data using the tomographic model based on the work of Zelt and Smith (1992). The contrast in density between the overburden and the HCS layer provided a pathway for the refracted seismic waves that enabled the use of seismic tomography.

This tomographic program was proven to map small scale features such as undulations that appear in the HCS. It is important that these features can be mapped because the undulations are a significant feature of the HCS and shows that the tomographic program was successful in providing an accurate 2-D view of the layer. The sandstone complex is important to the discussion of the depositional history of the KTB because there are competing theories about its depositional origin. To better understand the events at the end of the Cretaceous it is important to increase knowledge of the geology of the KTB through means available to researchers. Remote sensing through seismic refraction such as used in this study is one of the methods that can provide this information.

Future research should focus on refinement of the tomographic method used in this study. Tests should be run to determine how the model reacts when it encounters a lateral discontinuity of the HCS so that the signature is easily determined. Once the program is refined, further seismic mapping can be performed between point data to create fence diagrams to create a 3-D image of the HCS to determine spacial variability and continuity of this component of the KTB.

REFERENCES

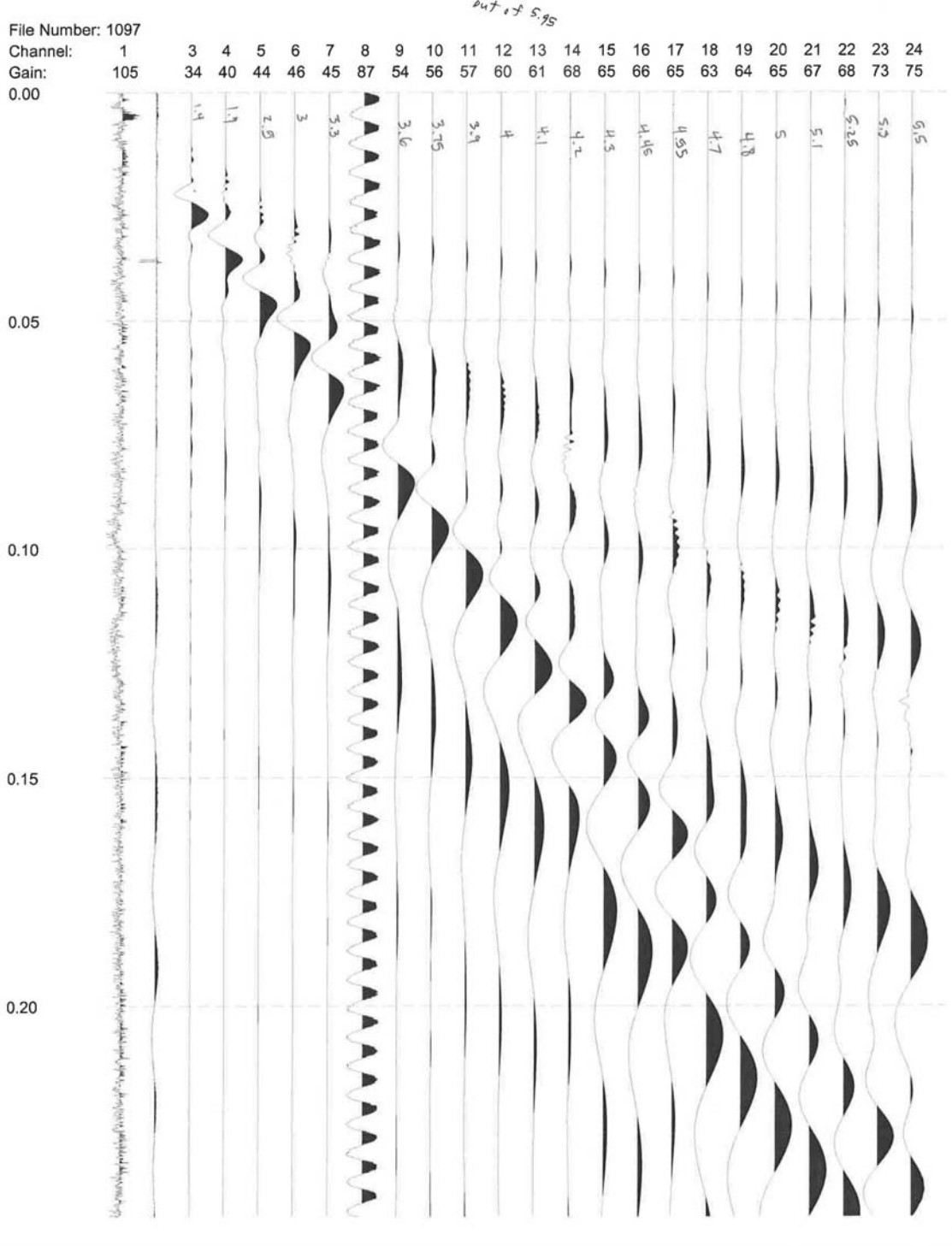
- Adatte, T., G. Keller, and G. R. Baum, 2011, Age and origin of the Chicxulub impact and sandstone complex, Brazos River, Texas: evidence from lithostratigraphy and sedimentology, *in* Keller, G., and T. Adatte, eds., The end-Cretaceous mass extinction and the Chicxulub impact in Texas: Society for Sedimentary Geology, SEPM Special Publication, **100**, 43-80.
- Alvarez, L. W., W. Alvarez, F. Asaro, and H.V. Michel, 1980, Extraterrestrial cause for the Cretaceous-Tertiary extinction: *Science*, **208**(4448), 1095-1108.
- Heymann, D., T. E. Yancey, W. S. Wolbach, M. H. Thiemens, E. A. Johnson, D. Roach, and S. Moecker, 1998, Geochemical markers of the Cretaceous-Tertiary boundary event at Brazos River, Texas, USA: *Geochimica et Cosmochimica Acta*, **62**, 173-181.
- Geostuff. <http://www.geostuff.com/RollboxDS.pdf>, 2008, Rollalong Switches. Retrieved 2/8/08.
- Jakosky, J. J., 1957, Exploration Geophysics: Newport Beach, Trija Publishing Co.
- Keller, G., T. Adatte, Z. Berner, M. Harting, G. Baum, M. Prauss, A. Tantawy, and D. Stueben, 2007, Chicxulub impact predates K-T boundary: New evidence from Brazos, Texas: *Earth and Planetary Science Letters*, **255**, 339-356.
- Keller, G., S. Abramovich, T. Adatte, and Z. Berner, 2011, Biostratigraphy, age of Chicxulub impact, and depositional environment of the Brazos River KTB sequences, *in* Keller, G., and T. Adatte, eds., The end-Cretaceous mass extinction

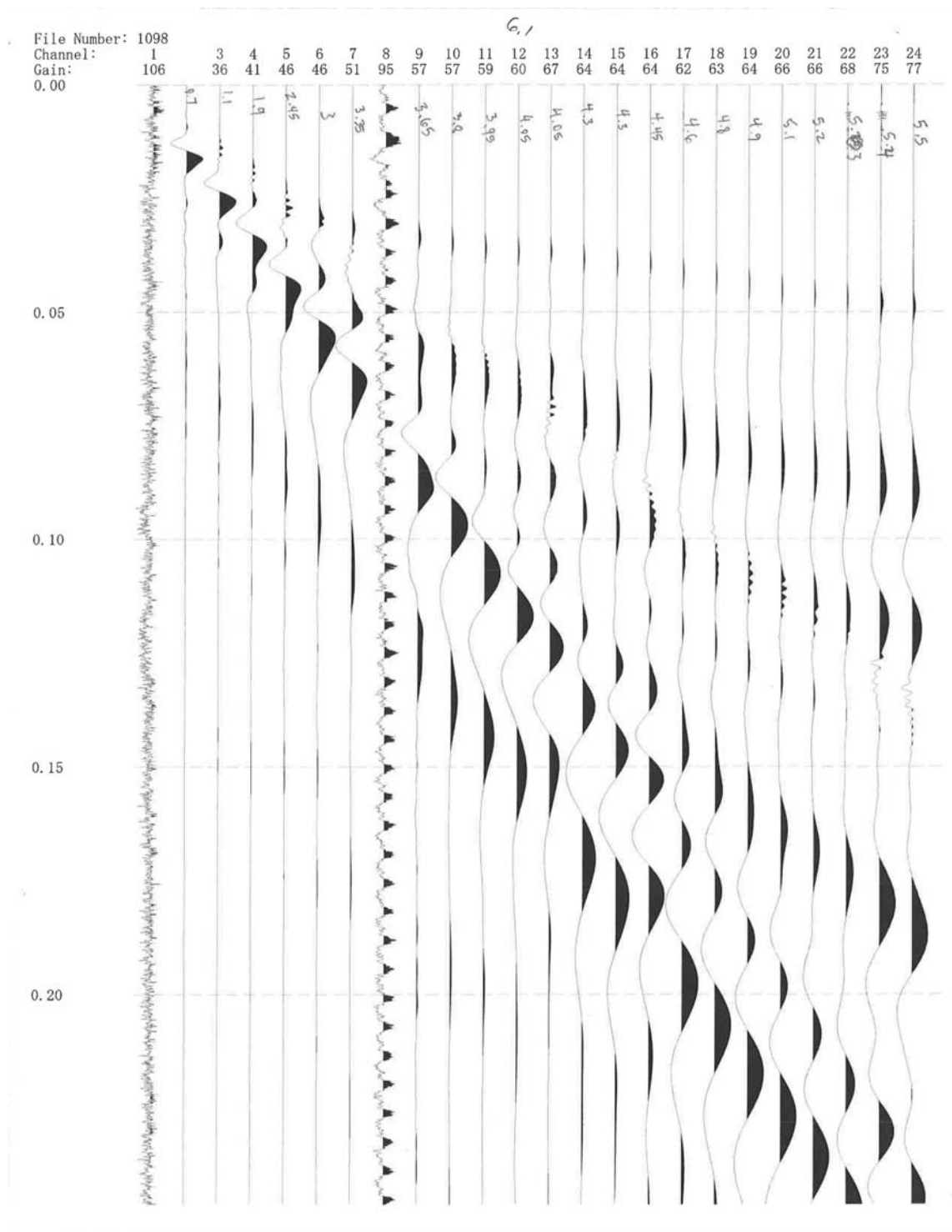
- and the Chicxulub impact in Texas: Society for Sedimentary Geology, SEPM Special Publication, **100**, 81-122.
- Knight, R. J., and A. L. Endres, 2005, An introduction to rock physics principles for near-surface geophysics, *in* Butler, D., ed., Near-Surface Geophysics: Tulsa, Society of Exploration Geophysicists, **13**, 60.
- Kring, D. A., 2007, The Chicxulub impact event and its environmental consequences at the Cretaceous-Tertiary boundary: Palaeogeography, Palaeoclimatology, Palaeoecology, **255**, 4-21.
- Molina, E., L. Alegret, I. Arenillas, J. A. Arz, N. Gallala, J. Hardenbol, K. von Salis, E. Steurbraut, N. Vandenbergh, and D. Zahgibib-Turki, 2006, The global boundary stratotype section and point for the base of the Danian stage (Paleocene, Paleogene, “Tertiary”, Cenozoic) at El Kef, Tunisia-original definition and revision: Episodes, **29**, 263-273.
- Pelton, J., 2005, Near-Surface Seismology: Surface-Based Methods, *in* Butler, D., ed., Near-Surface Geophysics: Tulsa, Society of Exploration Geophysicists, **13**, 219-255.
- Pilkington, M., and A. R. Hildebrand, 2000, Three-dimensional magnetic imaging of the Chicxulub Crater: Journal of Geophysical Research, **105**, 23,497-23,491.
- Redpath, B., 1973, Seismic refraction exploration for engineering site investigations. U. S. D. O. Commerce: Springfield, Explosive Excavation Research Laboratory.

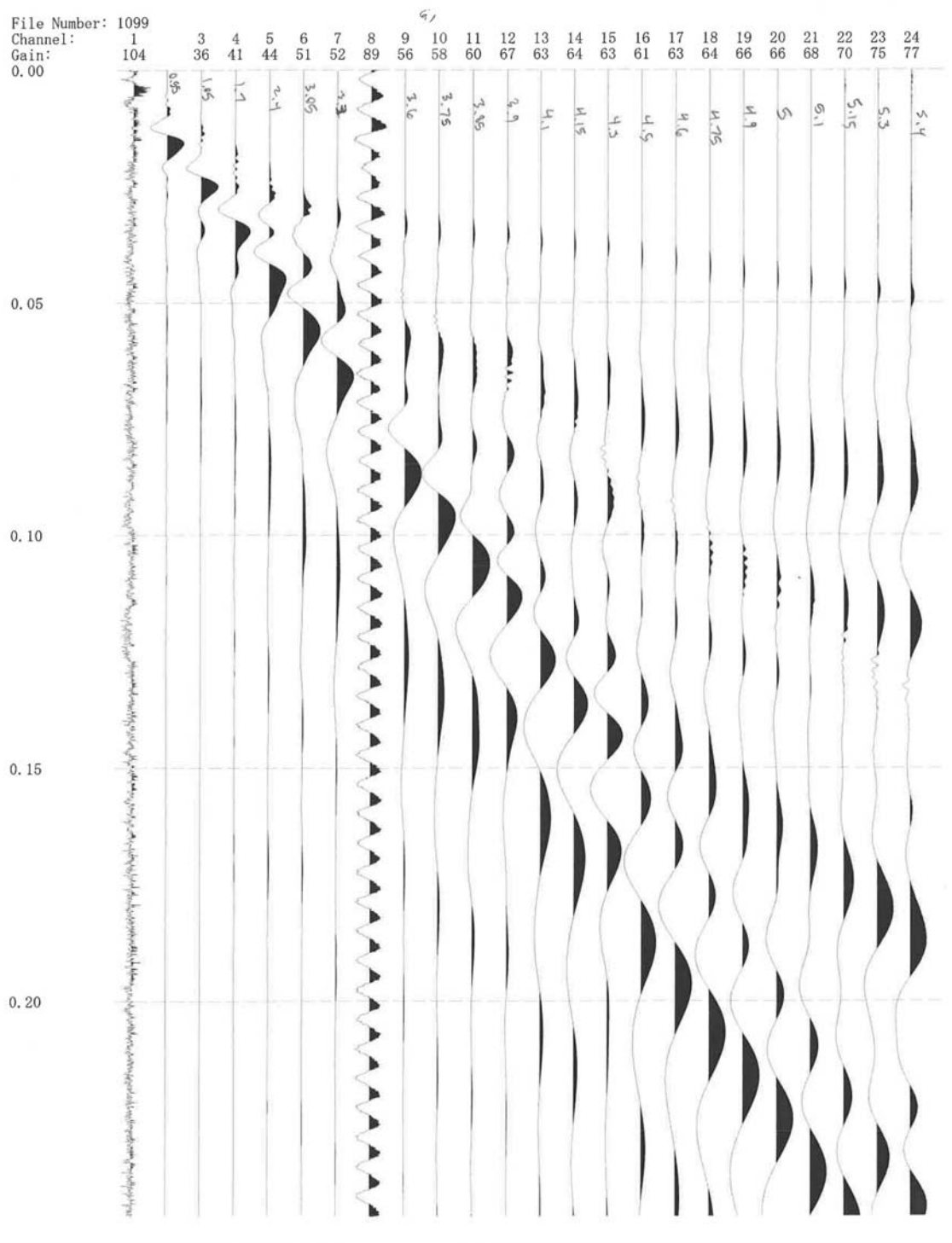
- Satti, S. A., 2000, Integrated geophysical study of near-surface faults in the Wilcox Group, Texas, with application to lignite mining: M.S. thesis, Texas A&M University.
- Schulte, P., R. Speijer, H. Mai, and A. Kontny, 2006, The Cretaceous-Paleogene (K-P) boundary at Brazos, Texas: Sequence stratigraphy, depositional events and the Chicxulub impact: *Sedimentary Geology*, **184**, 77-109.
- Sepkoski Jr., J. J., 1986, Phanerozoic overview of mass extinction, *in* Raup, D. M., and D. Jablonski, eds., *Patterns and Processes in the History of Life*: Springer Verlag, 277-295.
- Sharma, P. V., 1997, *Environmental and Engineering Geophysics*: Cambridge, Cambridge University Press.
- Sole, R. V., and M. Newman, 2002, The Earth system: biologically and ecological dimensions of global environmental change, *in* Encyclopedia of Global Environmental Change, 297-301.
- Yancey, T. E., 1996, Stratigraphy and depositional environments of the Cretaceous-Tertiary boundary complex and basal Paleocene section, Brazos River, Texas: Gulf Coast Association of Geological Societies Transactions, **46**, 433-442.
- Zelt, C. A., and R. B. Smith, 1992, Seismic travelttime inversion for 2-D crustal velocity structure: *Geophysics Journal International*, **108**, 16-34.

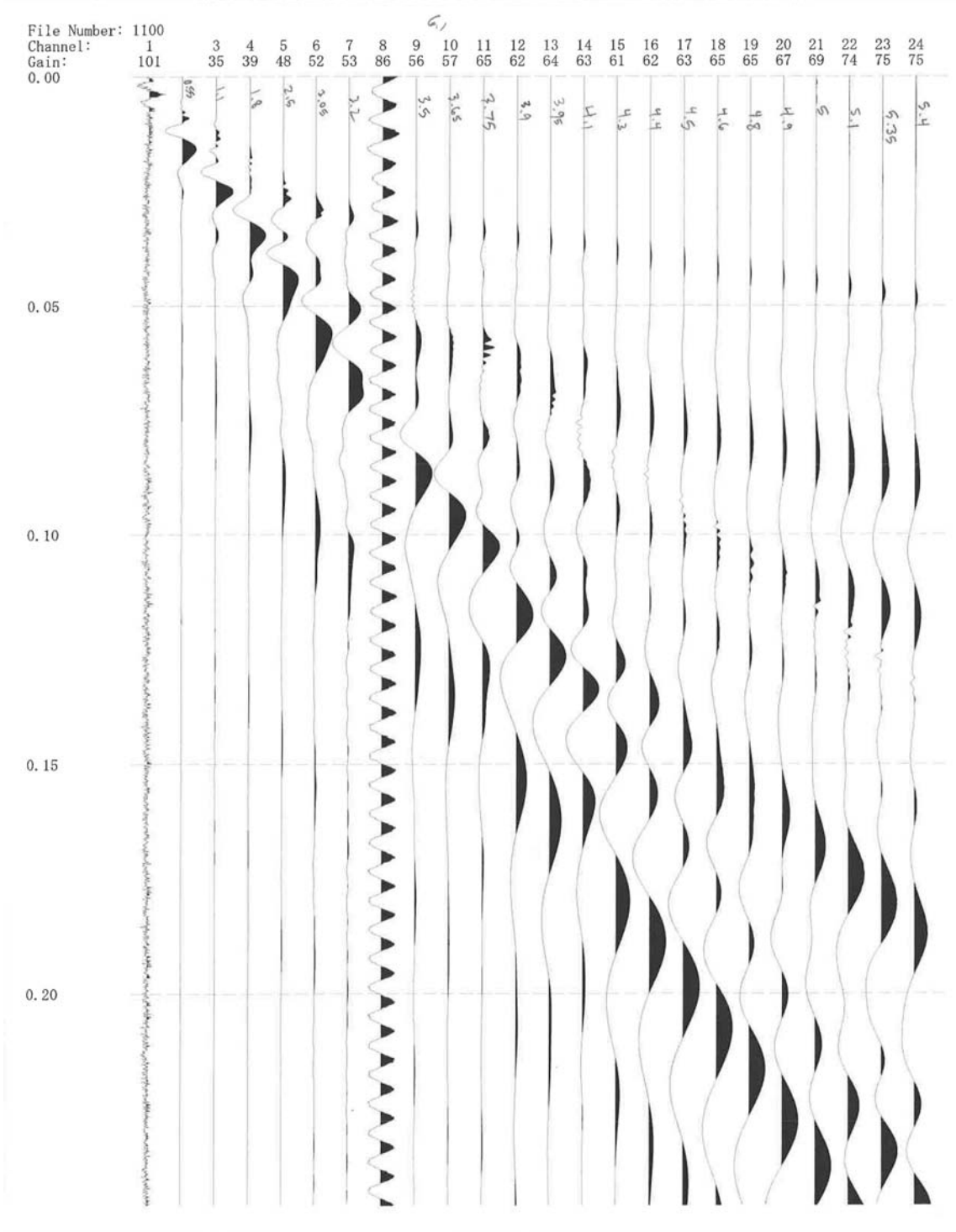
APPENDIX A

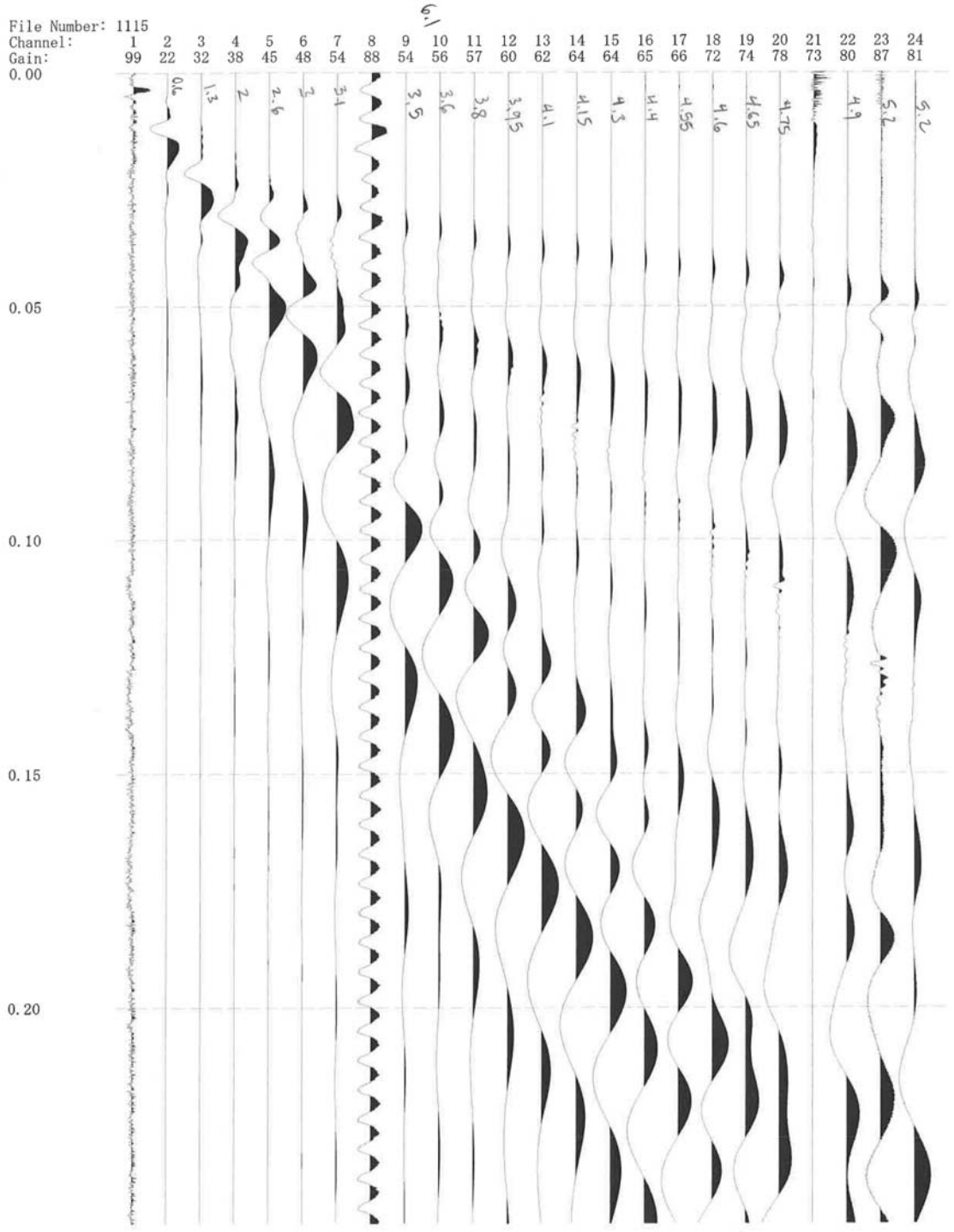
SELECT FIELD COLLECTED SEISMOGRAMS

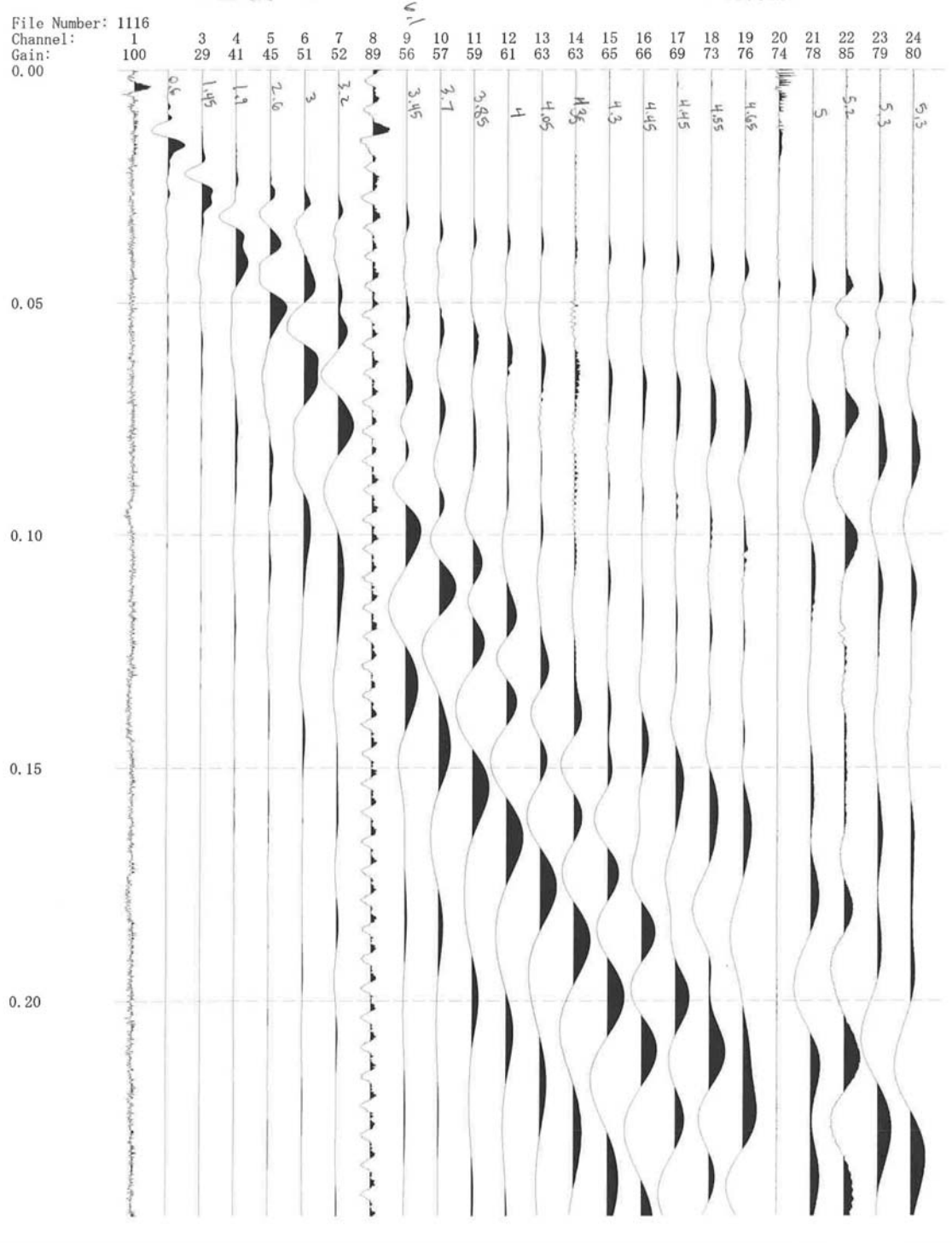












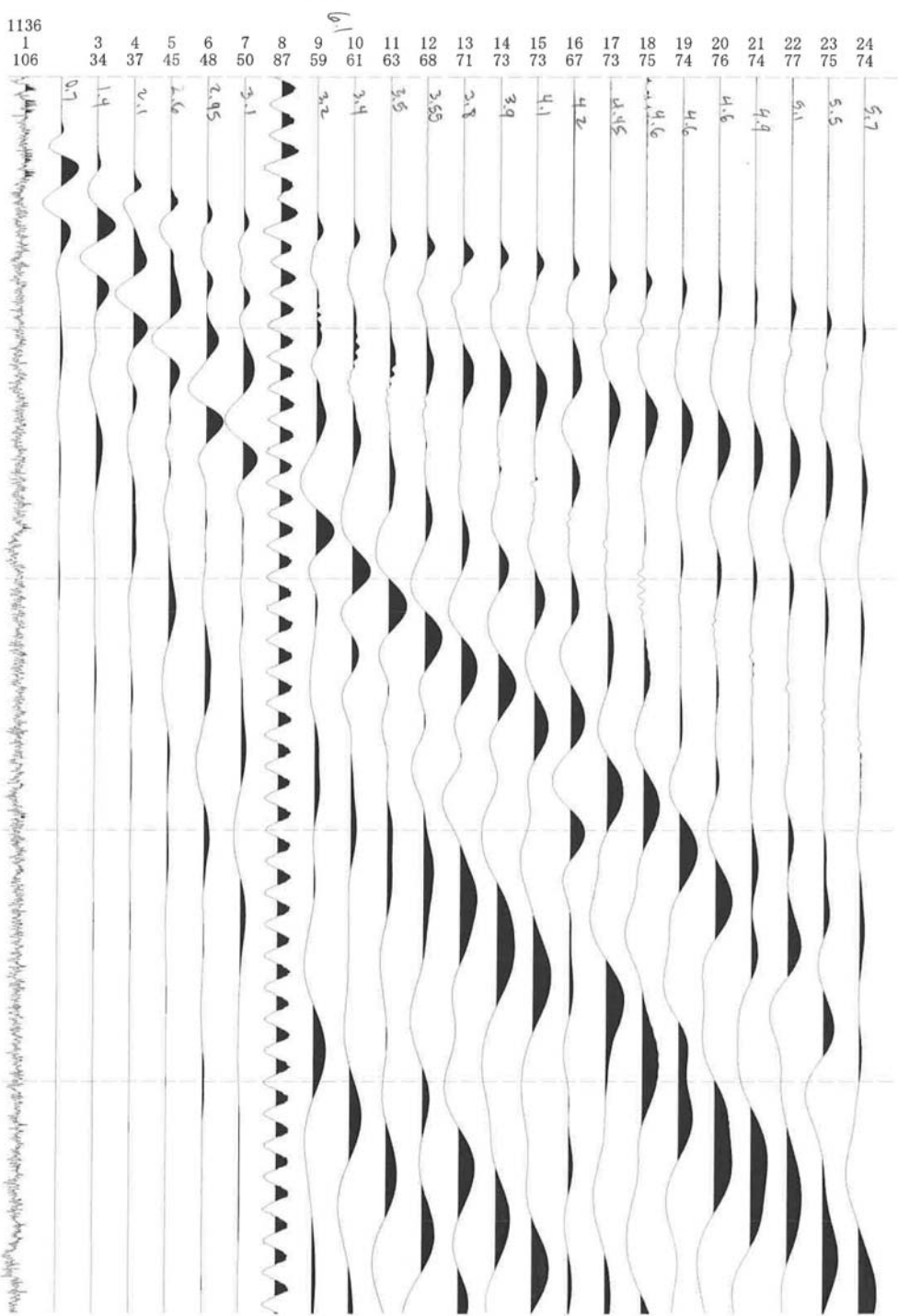
File Number: 1136
Channel: 1 3 4 5 6 7 8 9 10 11 12 13 14 15 16 17 18 19 20 21 22 23 24
106 34 37 45 48 50 87 59 61 63 68 71 73 73 67 73 75 74 76 74 77 75 74
Gain: 0.00

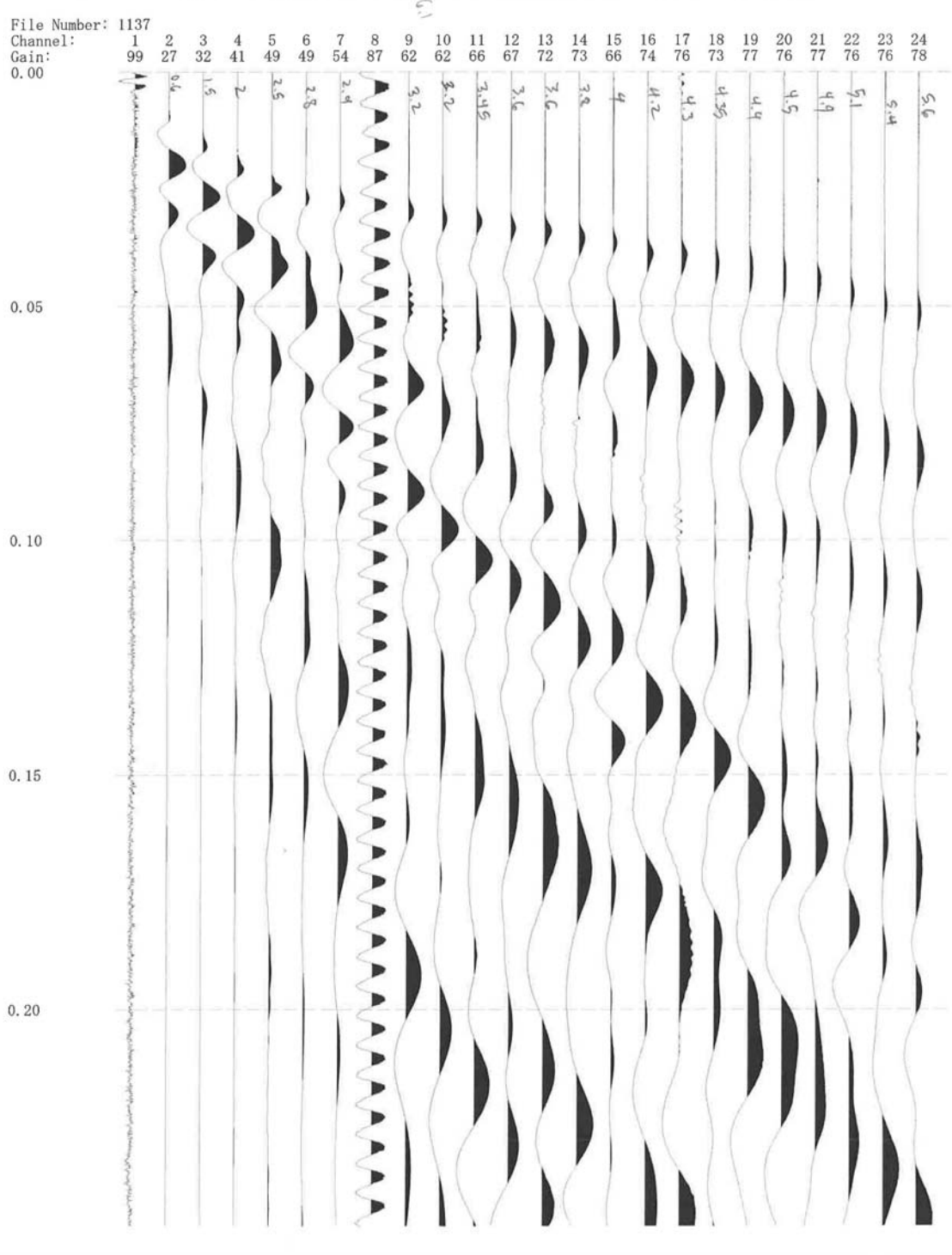
0.05

0.10

0.15

0.20



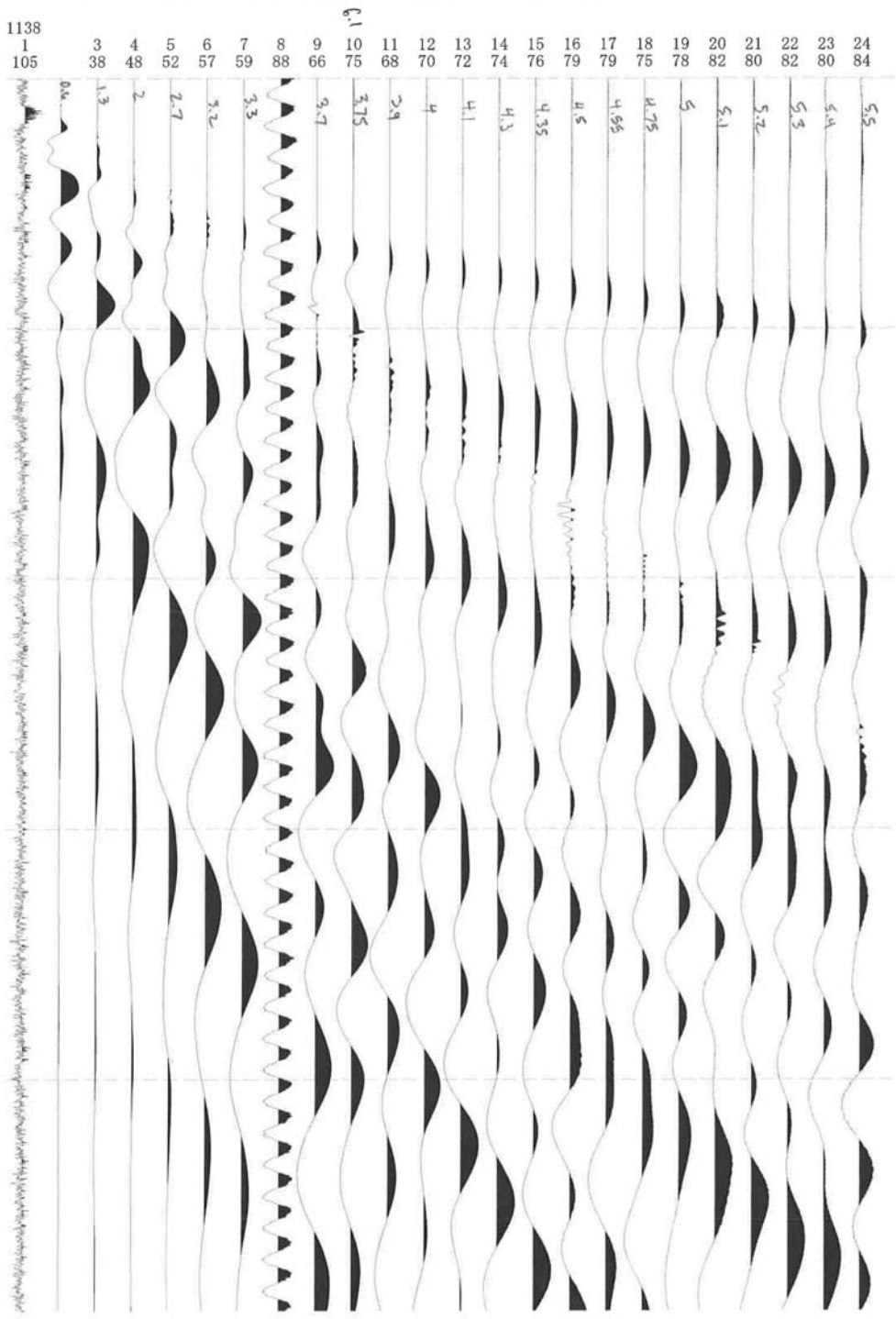


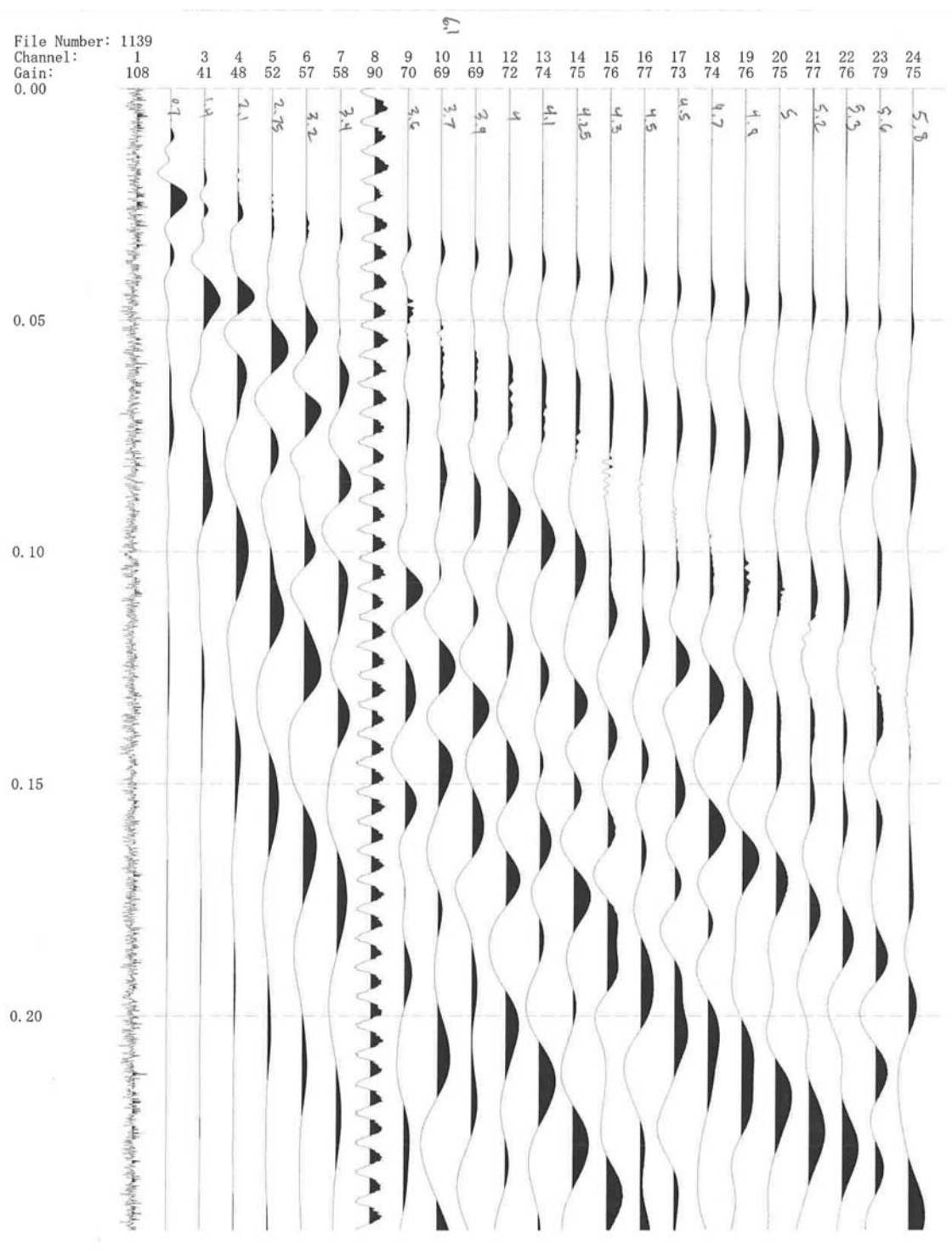
File Number: 1138

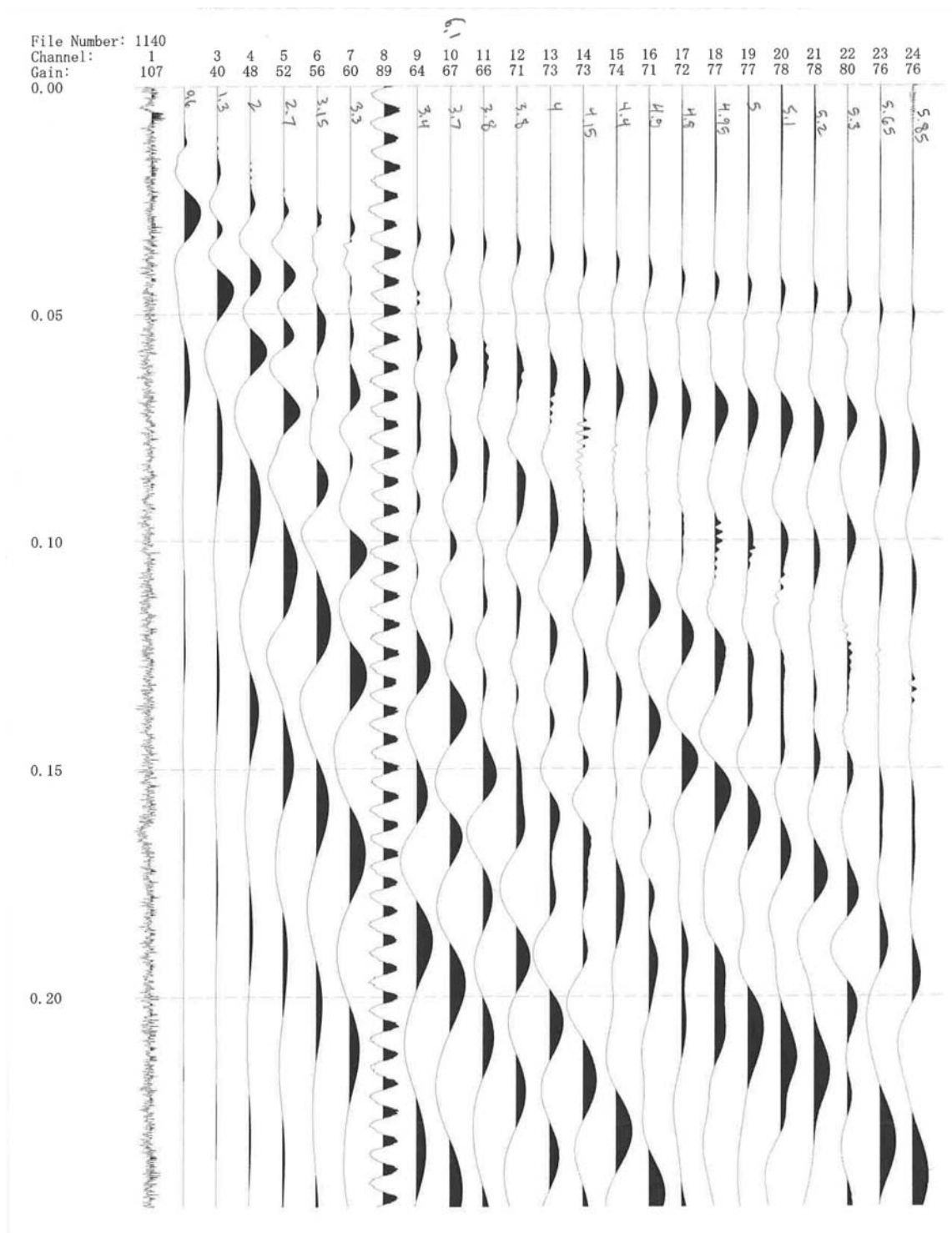
Channel: 1

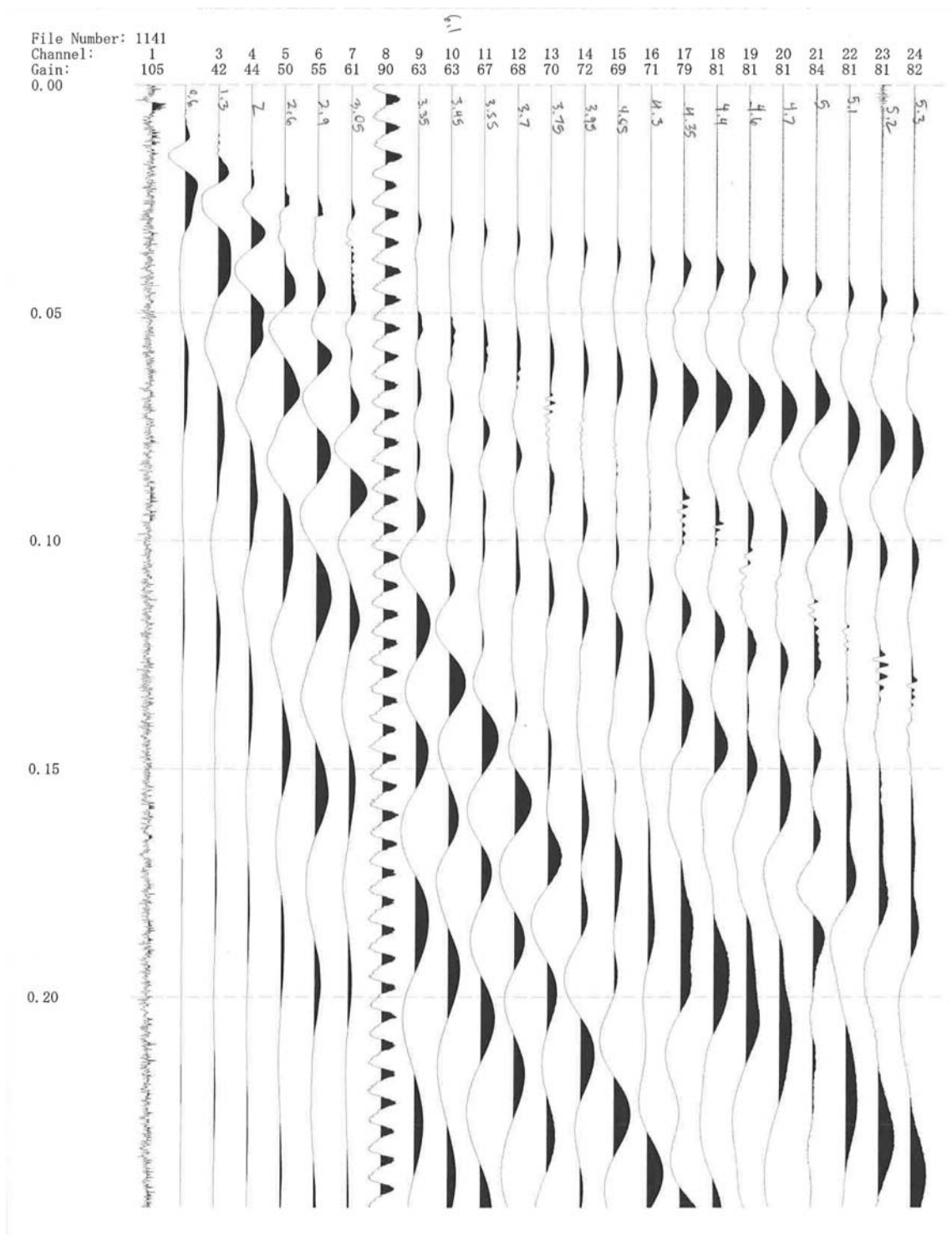
Gain: 105

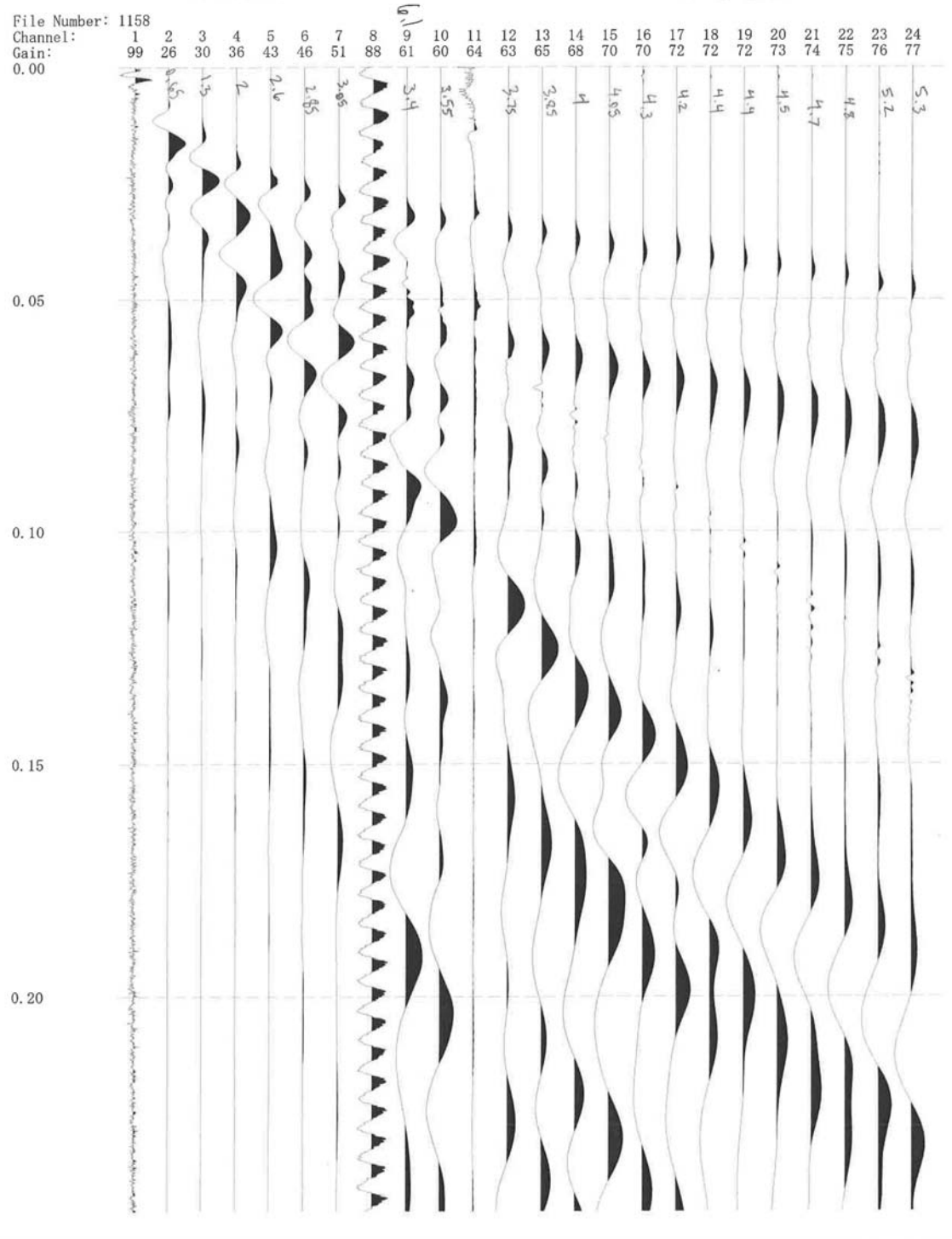
0.00

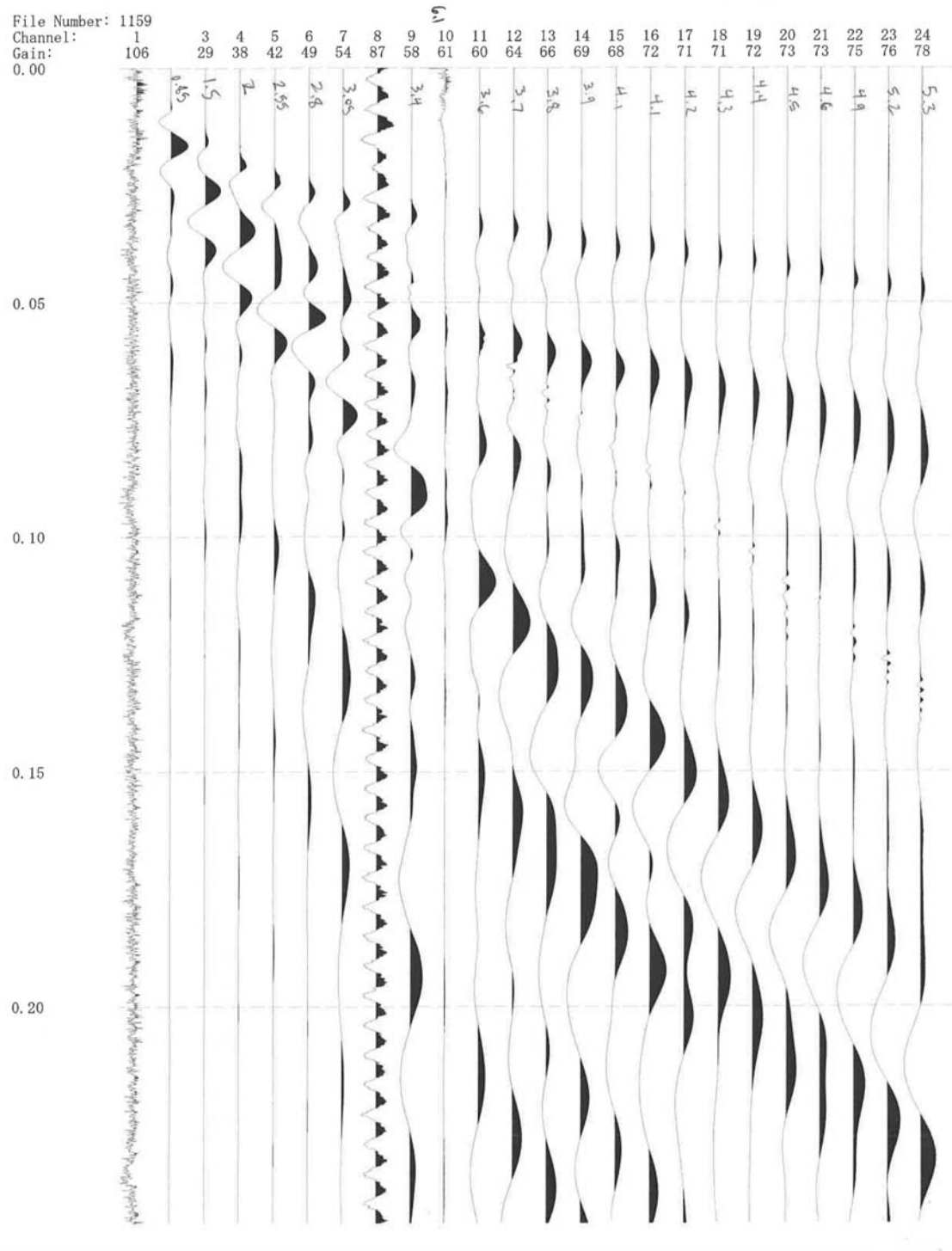


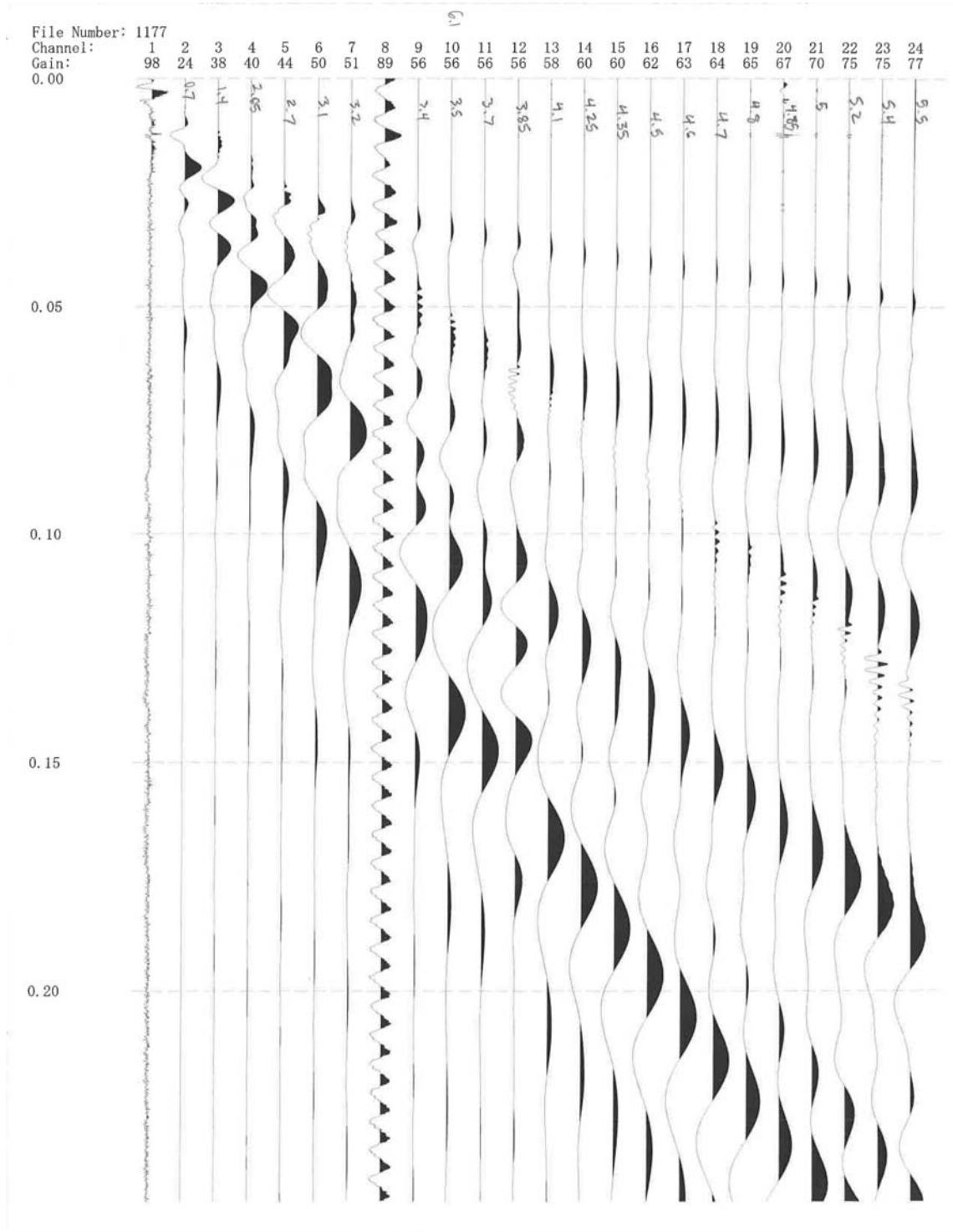


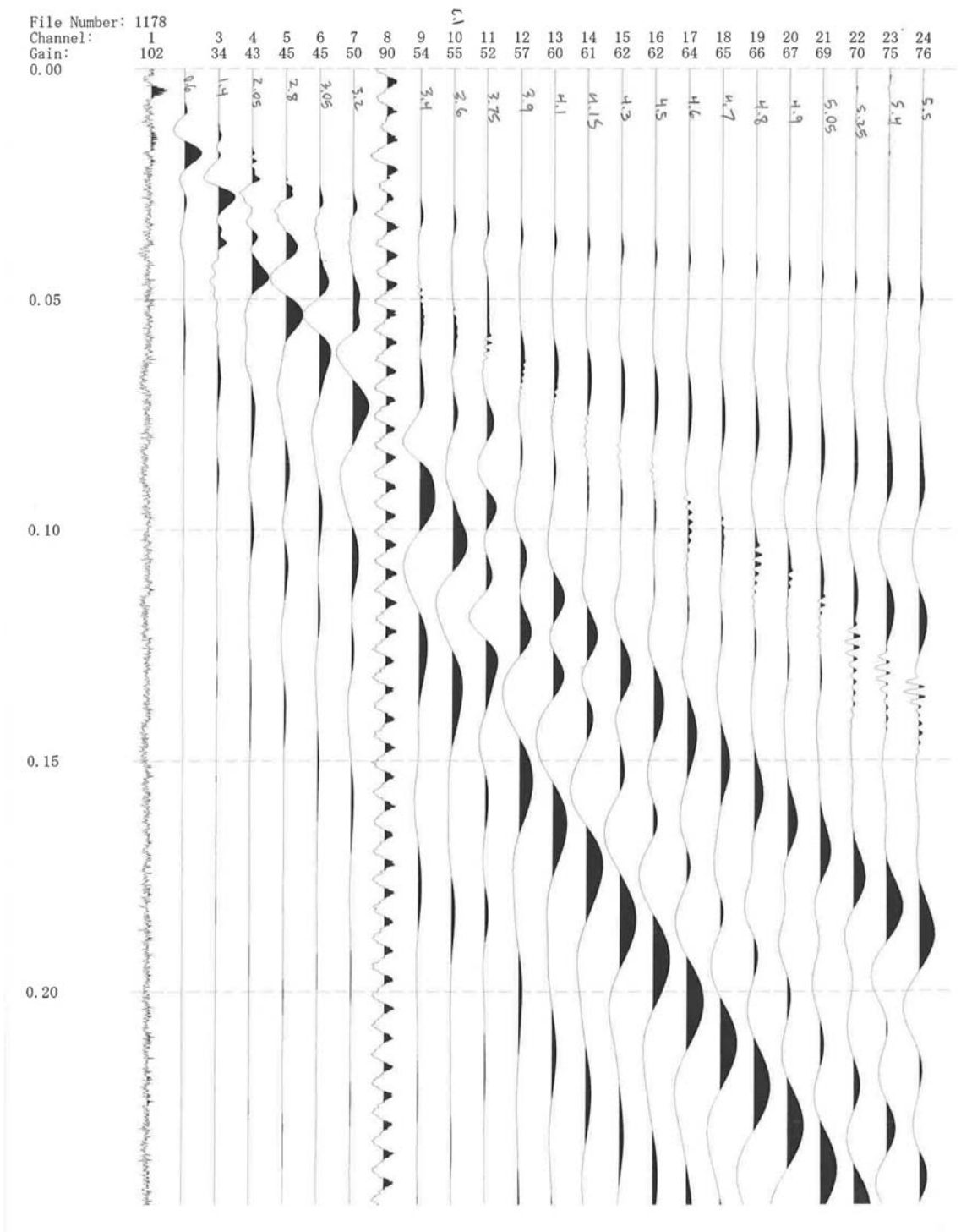


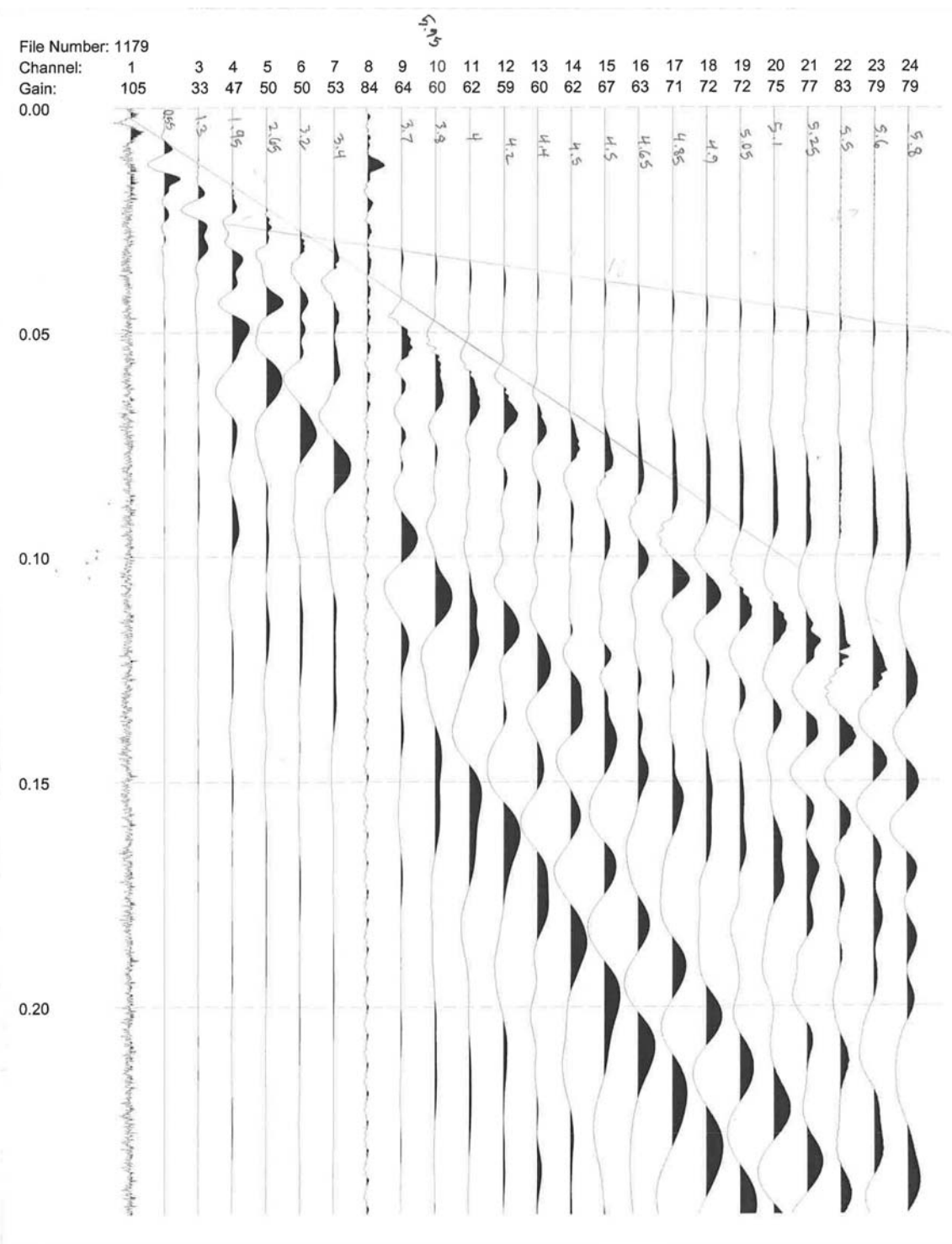


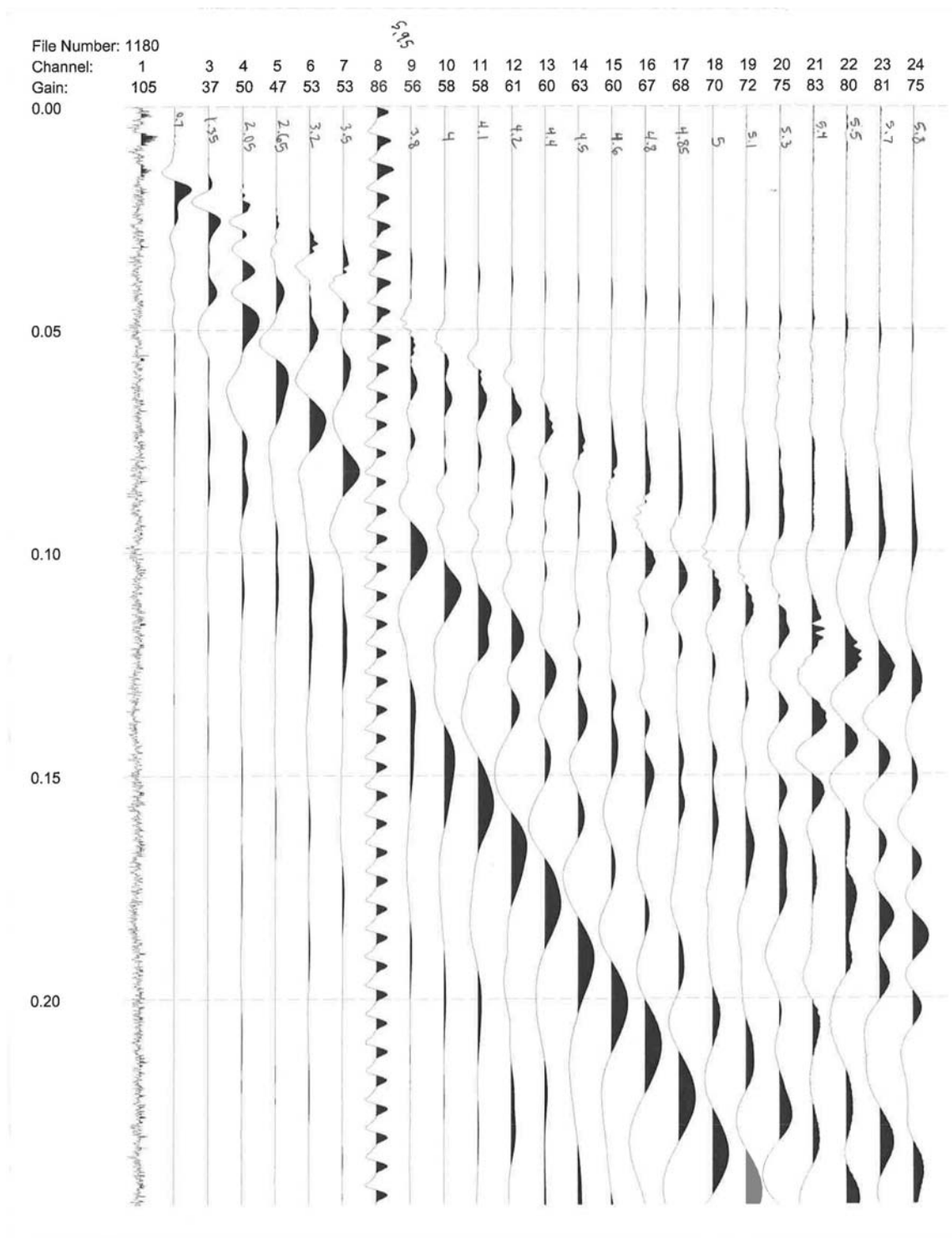


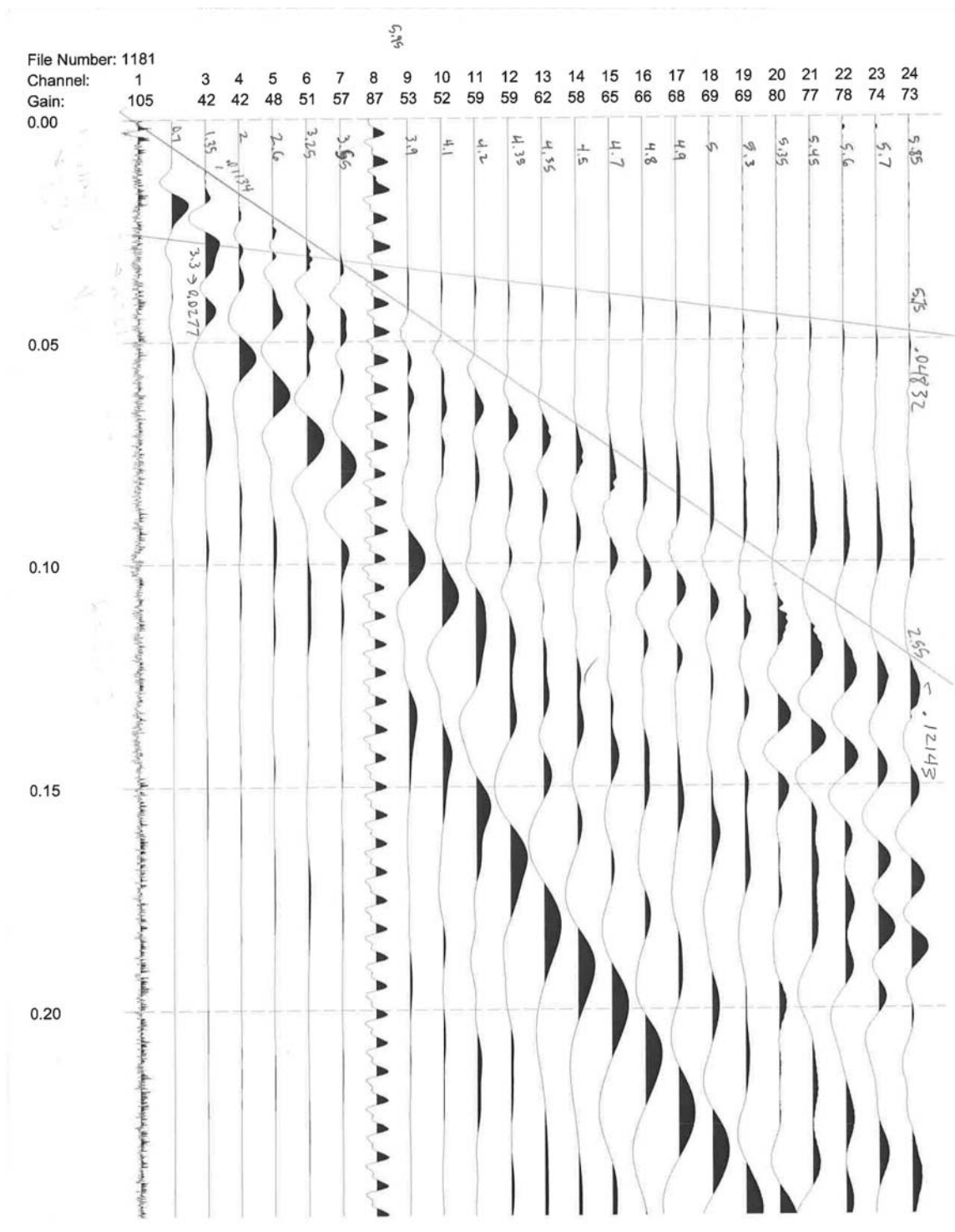


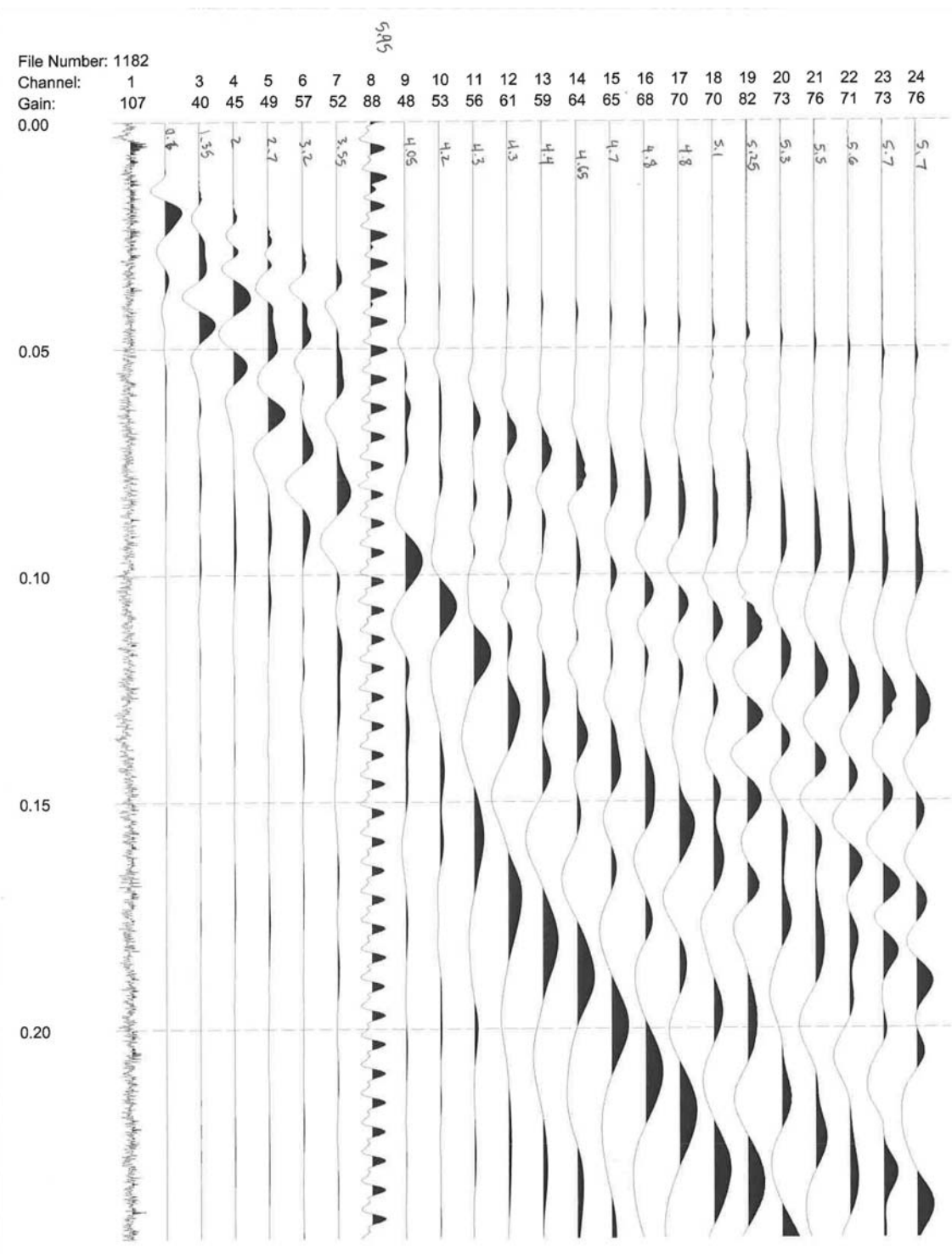


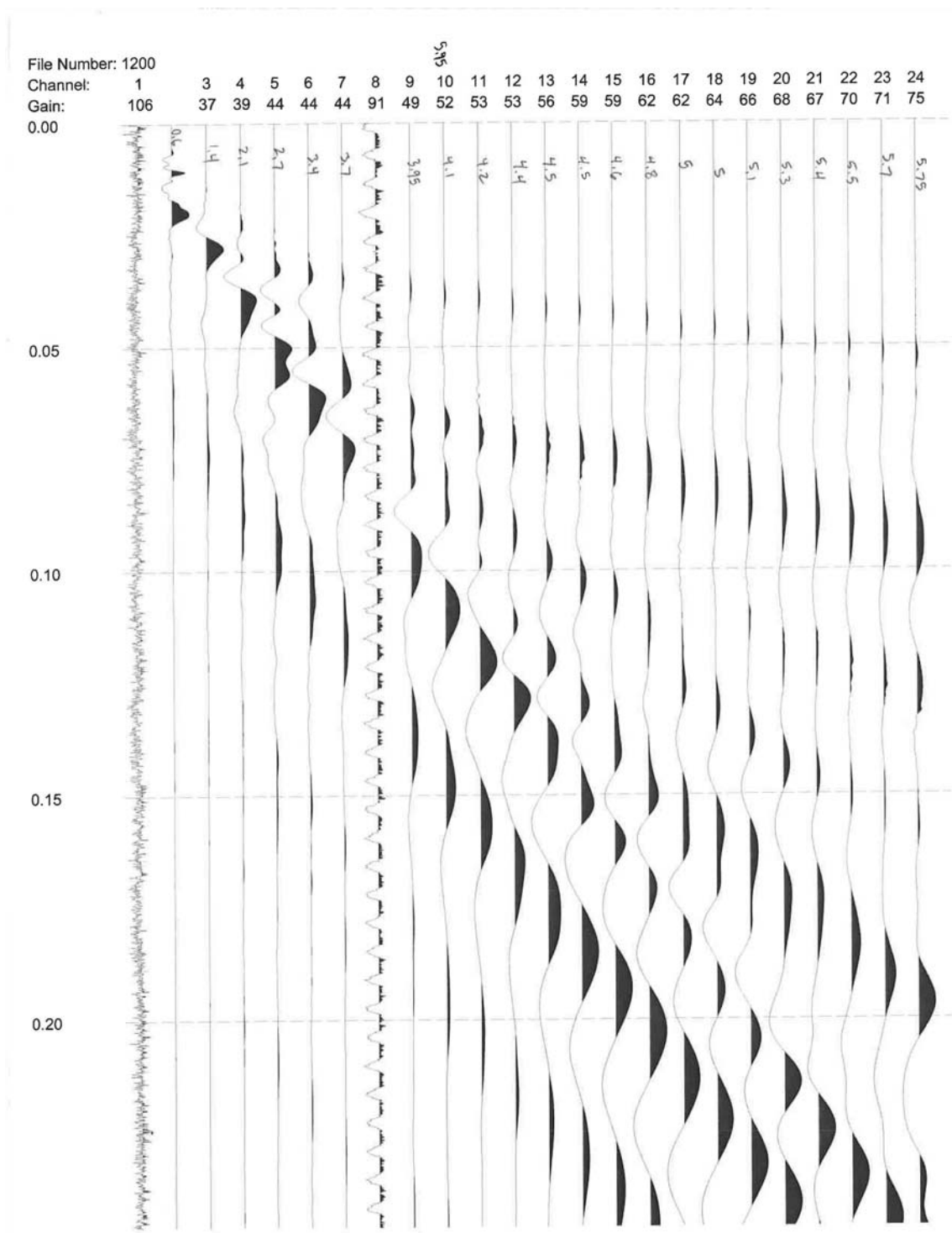


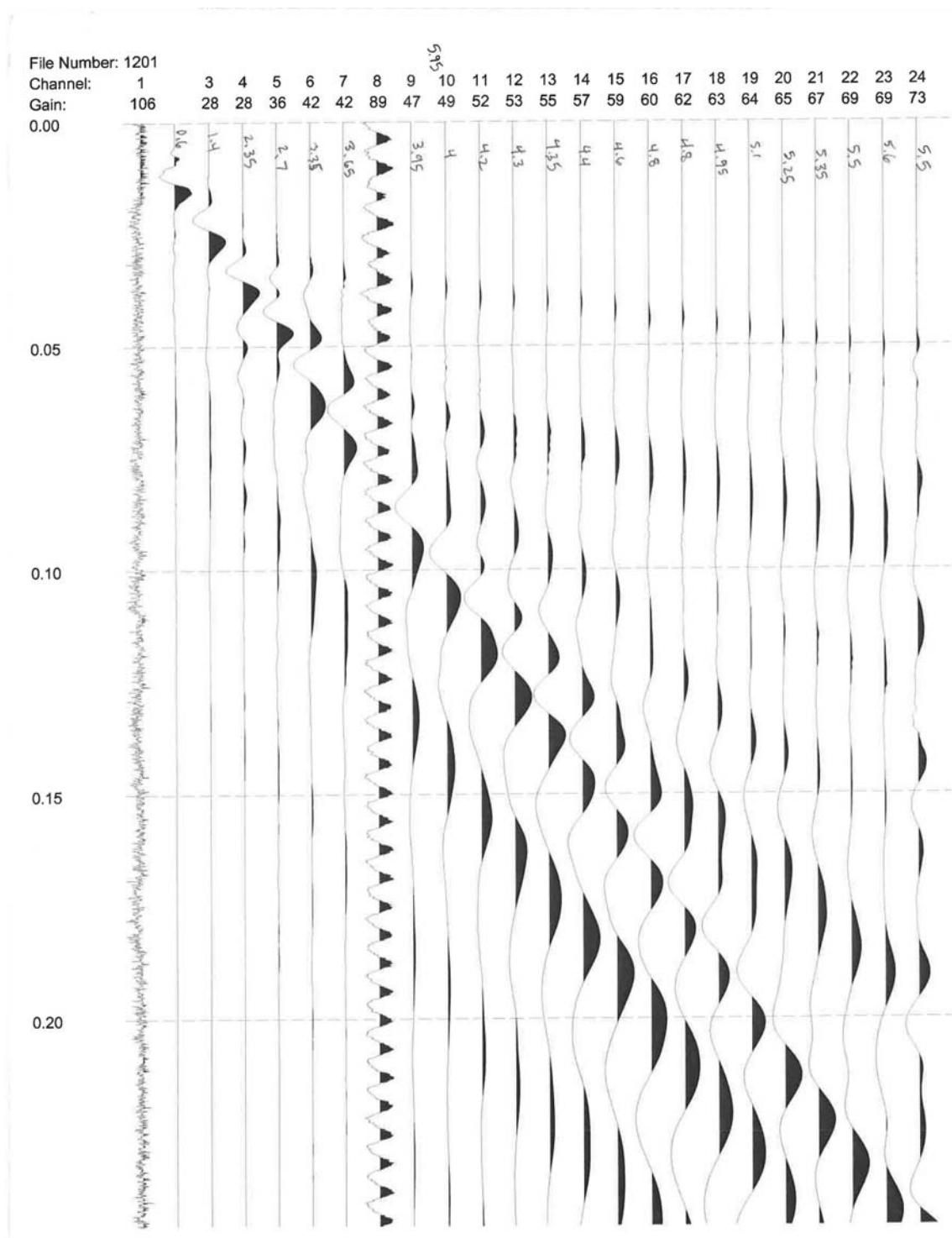


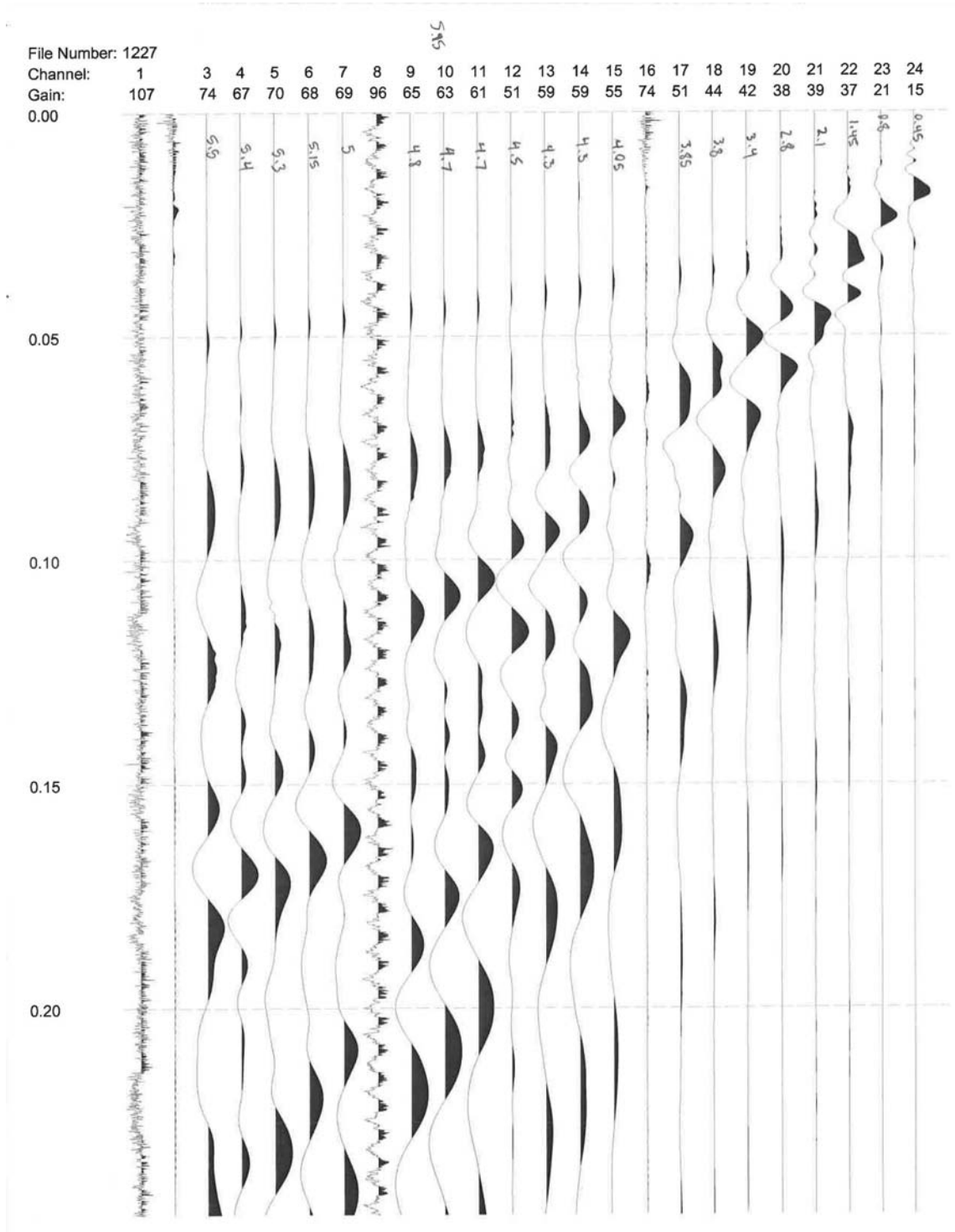


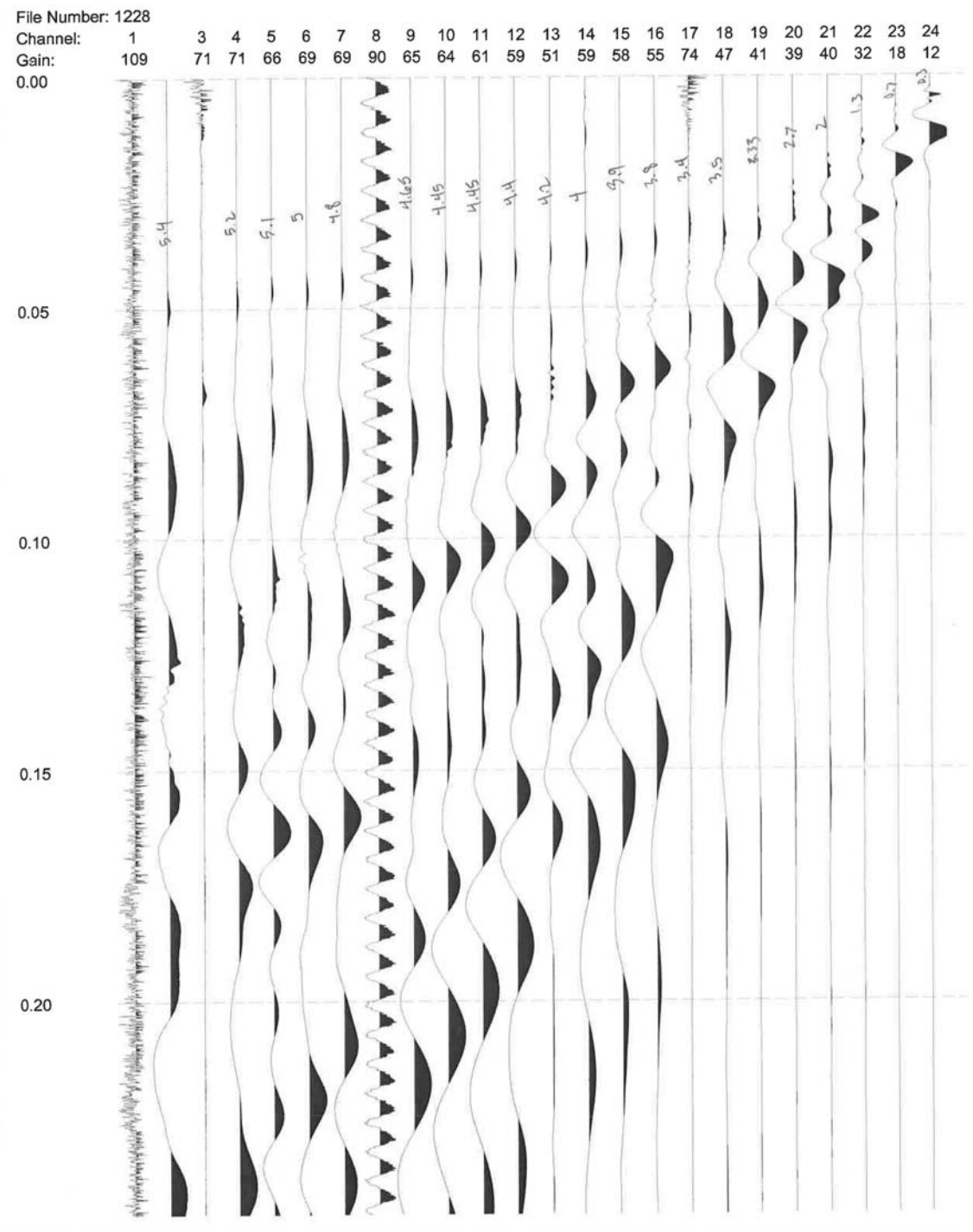


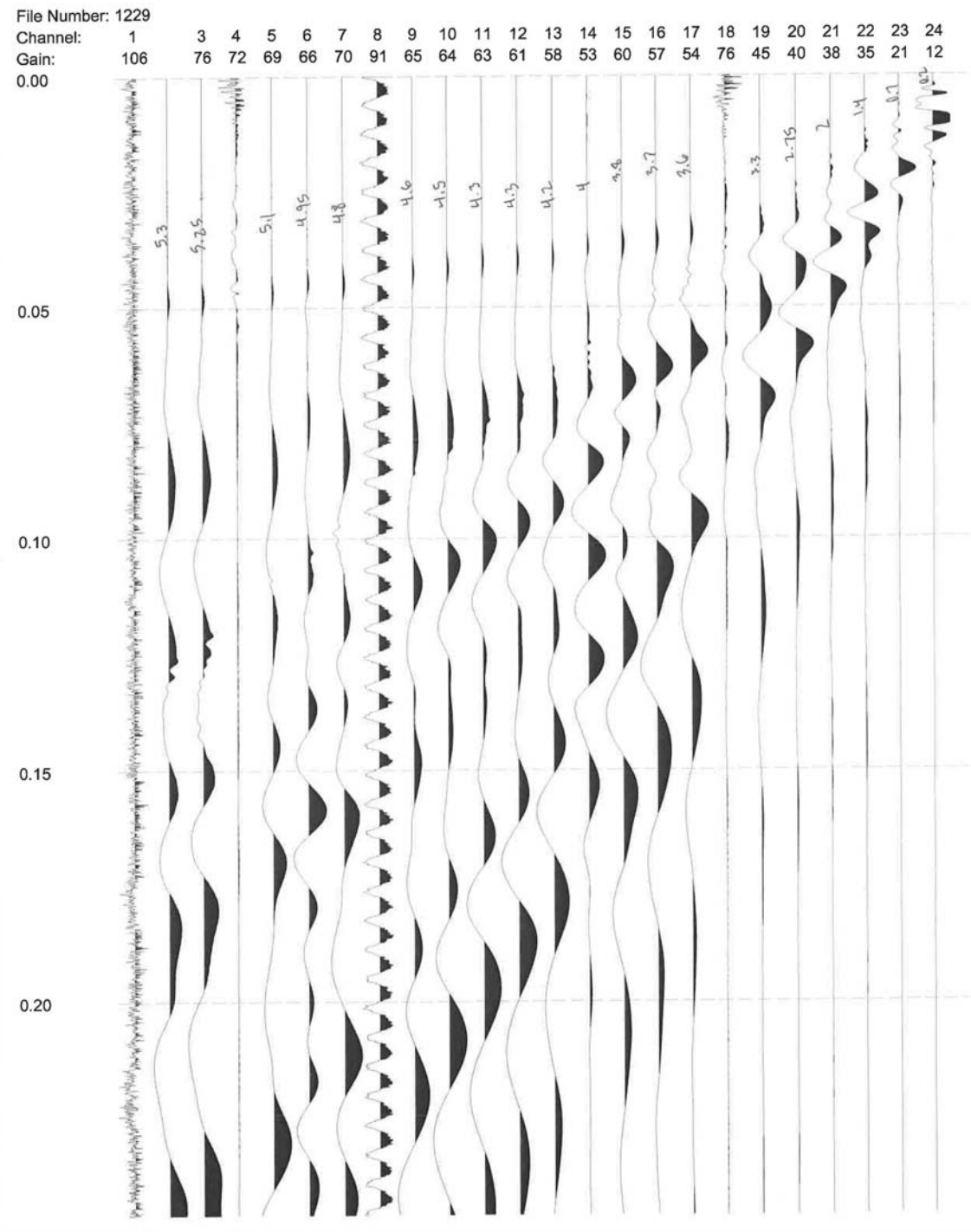












File Number: 1230

Channel:

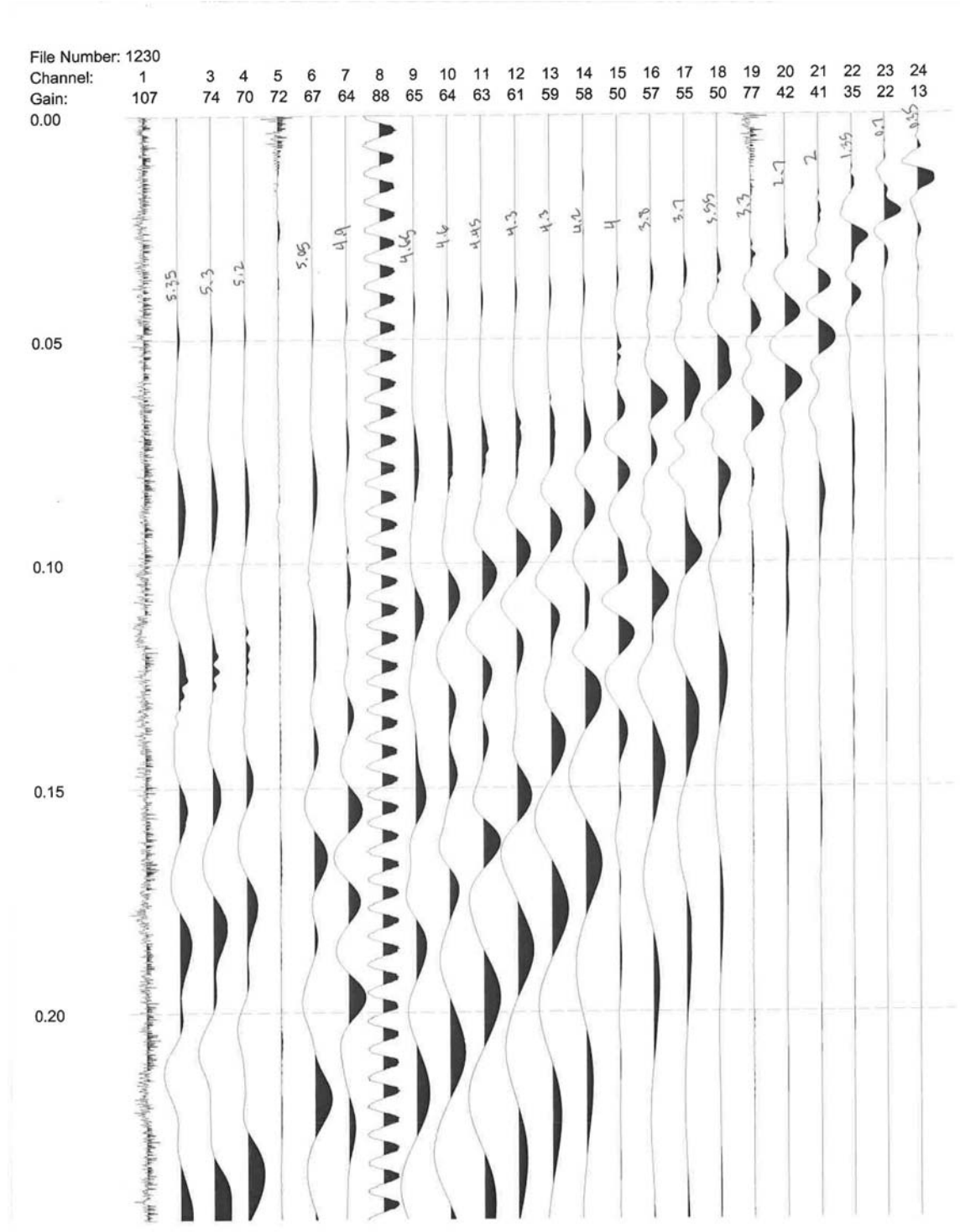
1 3 4 5 6 7 8 9 10 11 12 13 14 15 16 17 18 19 20 21 22 23 24
107 74 70 72 67 64 88 65 64 63 61 59 58 50 57 55 50 77 42 41 35 22 13
Gain:
0.00

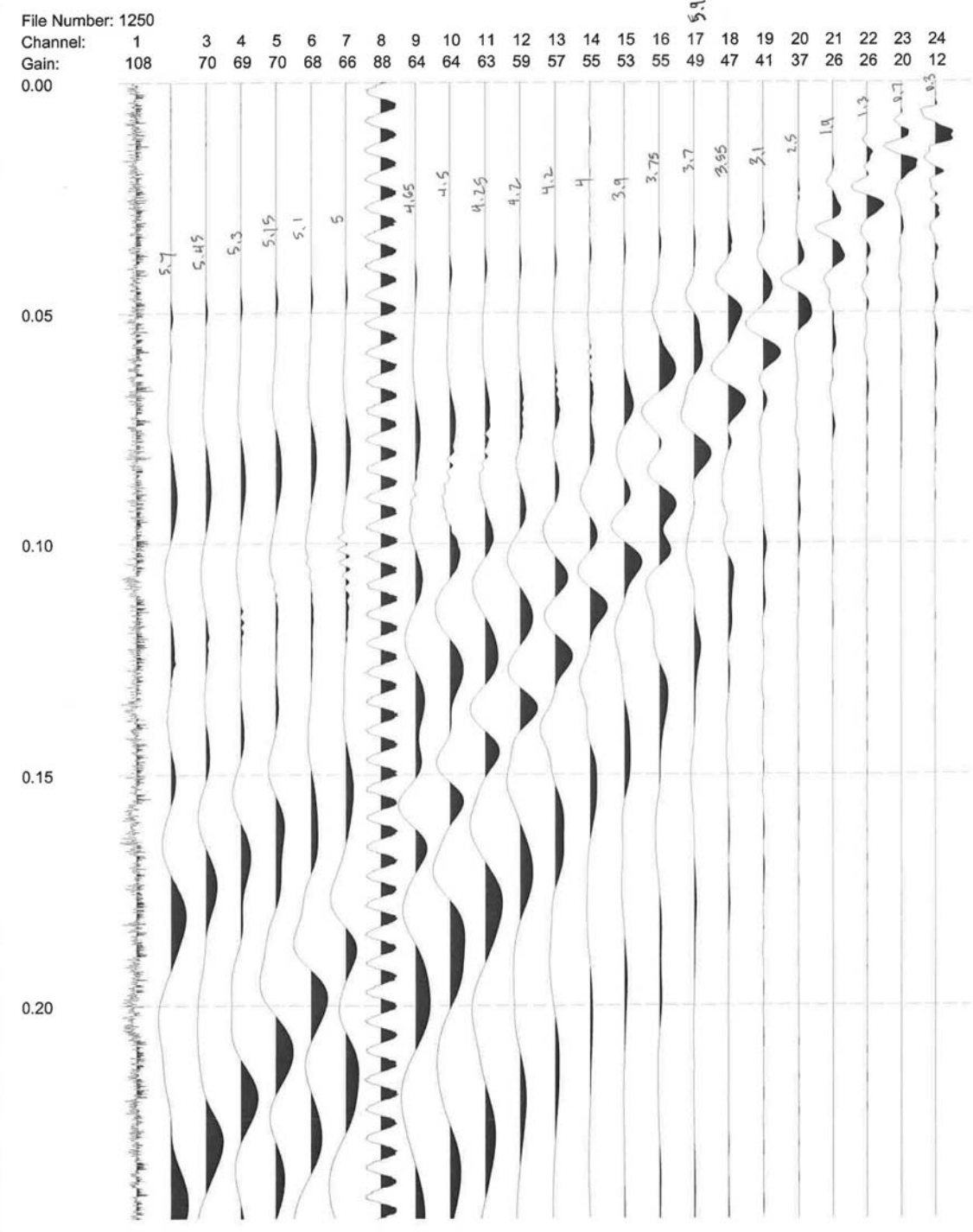
0.05

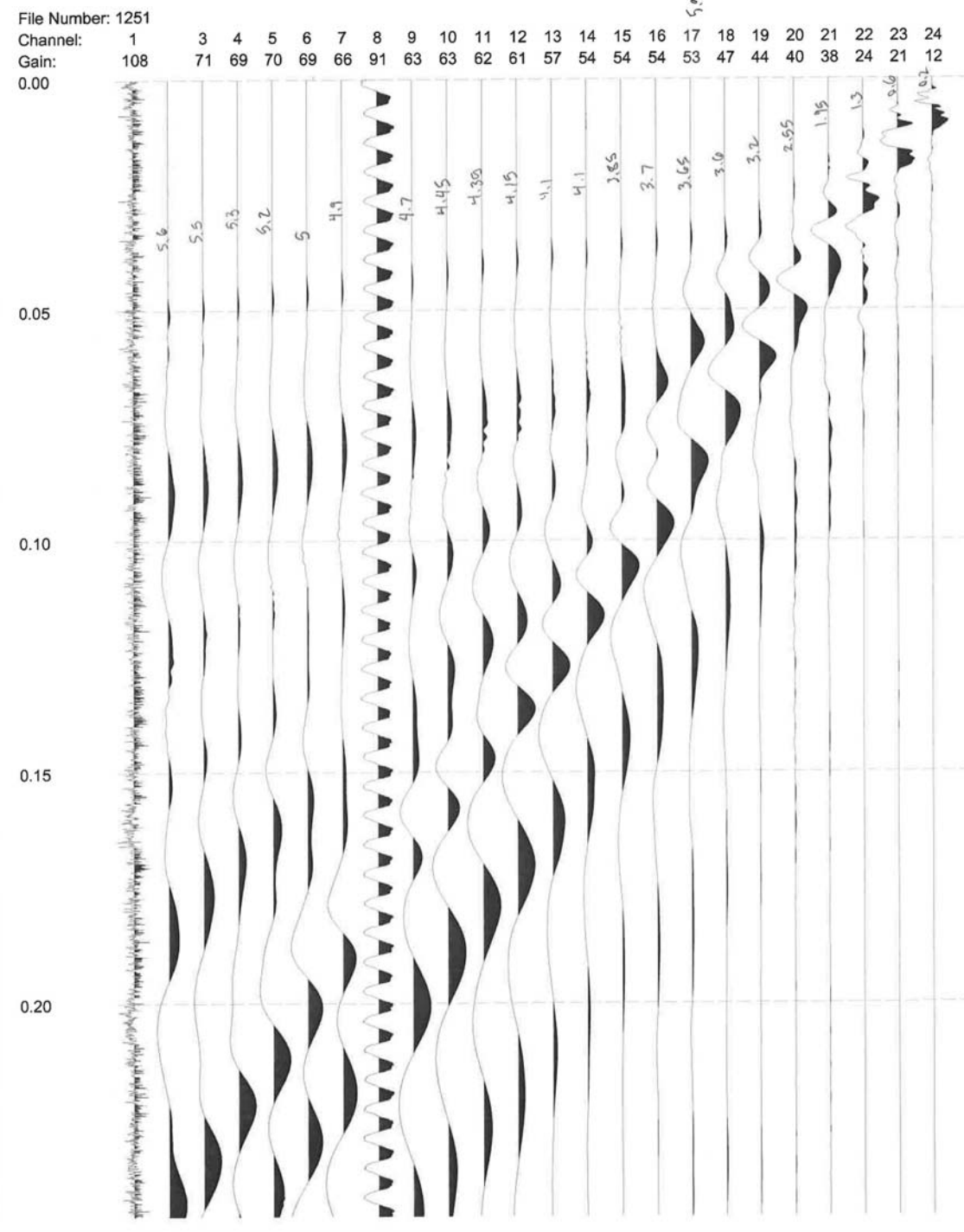
0.10

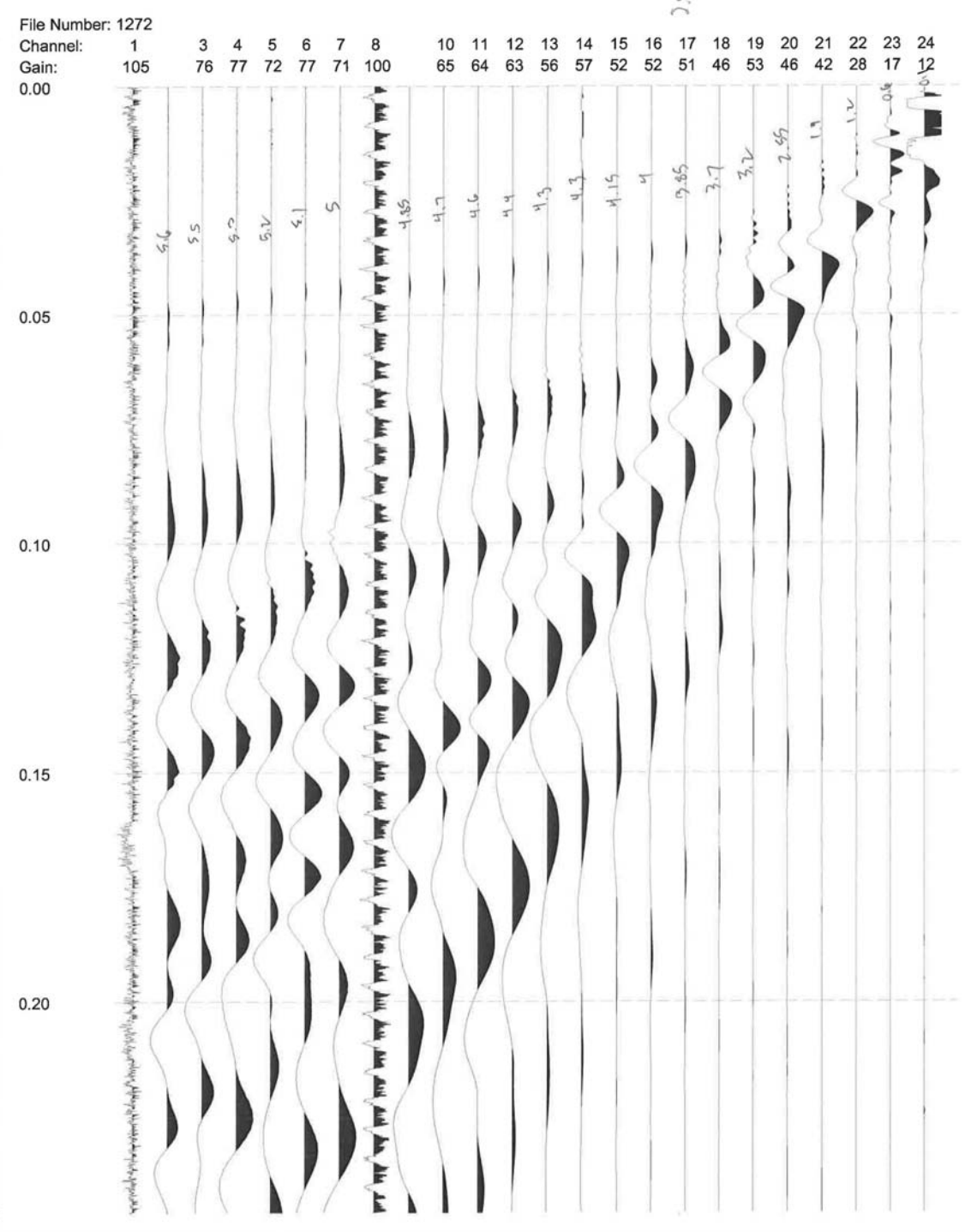
0.15

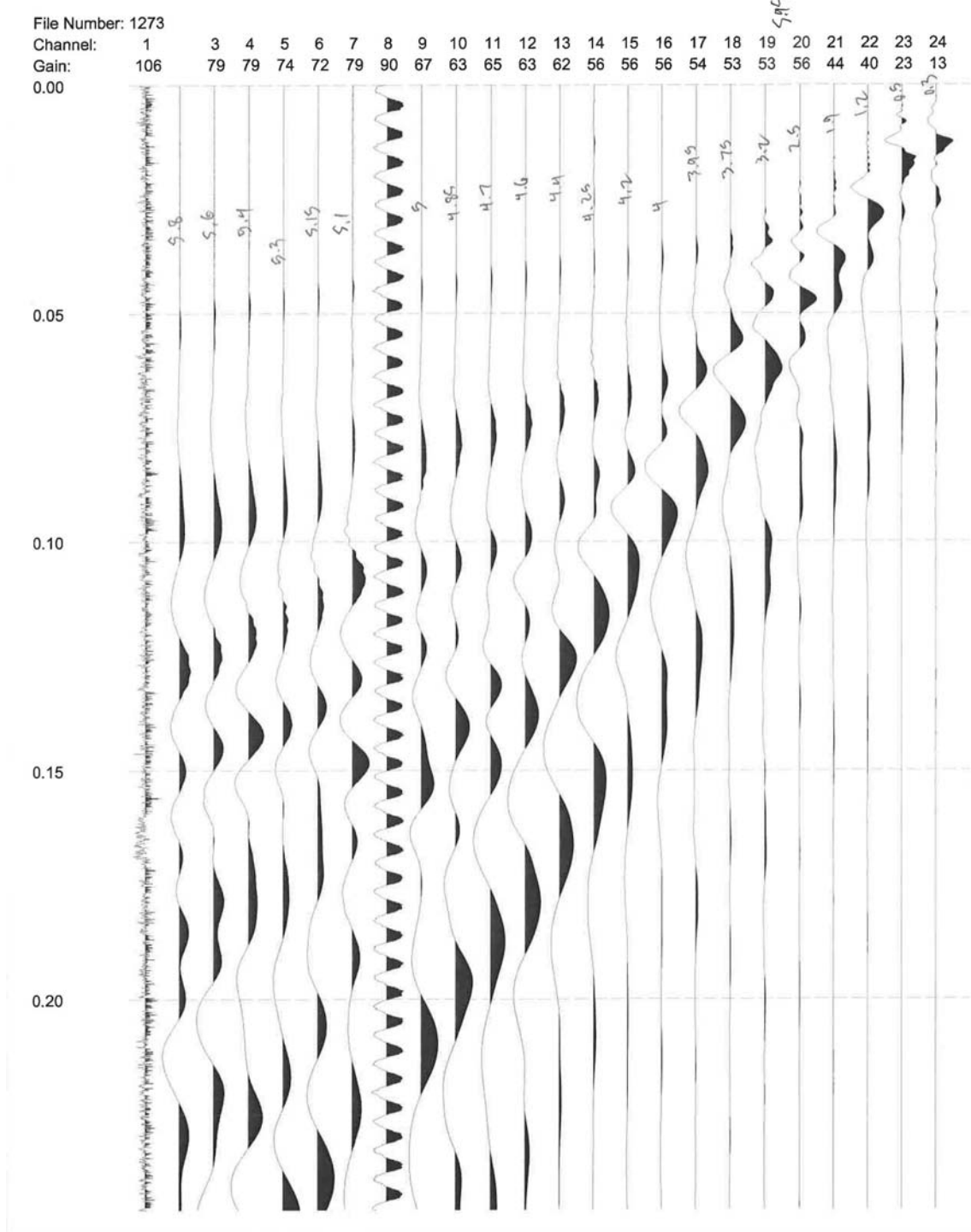
0.20

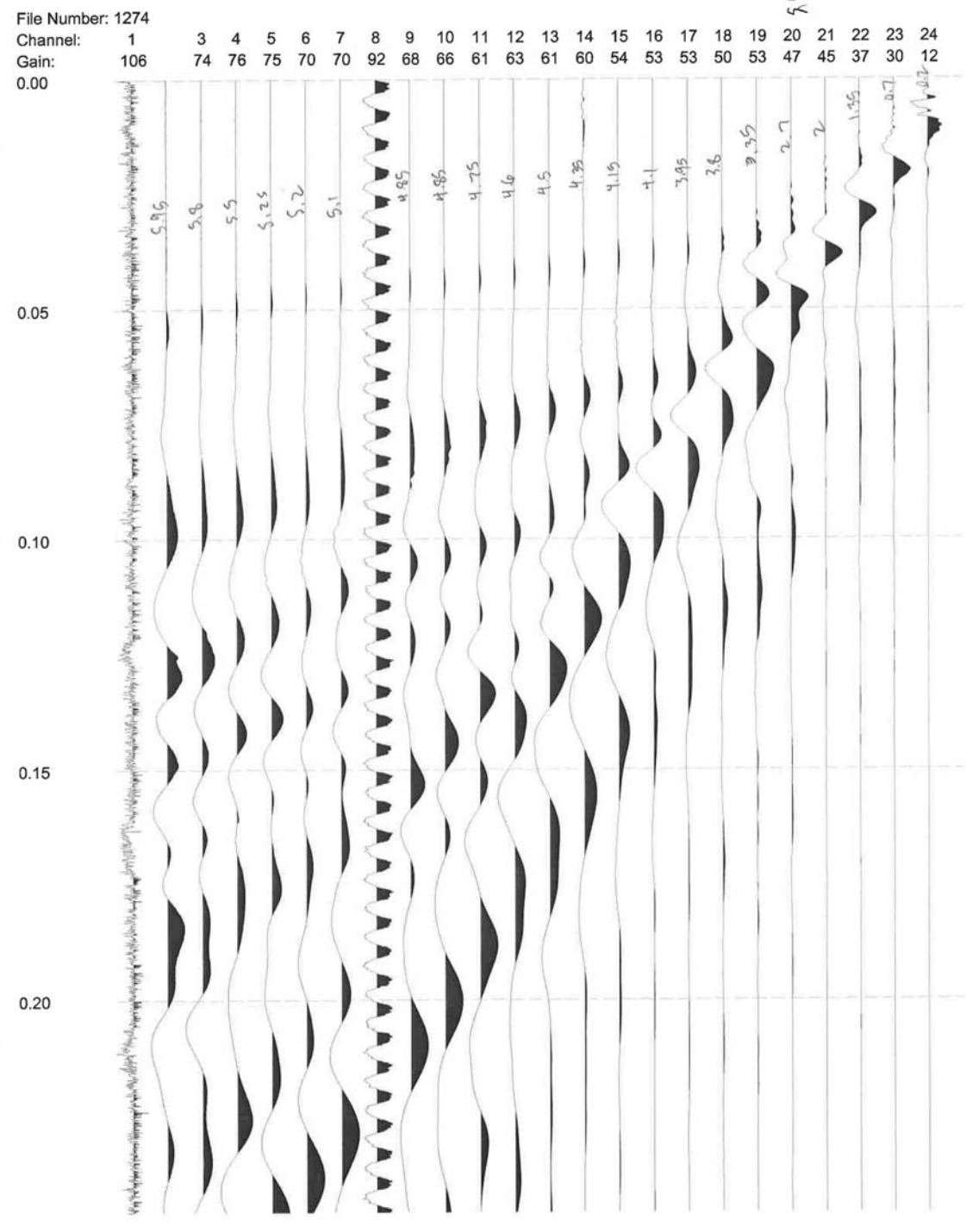


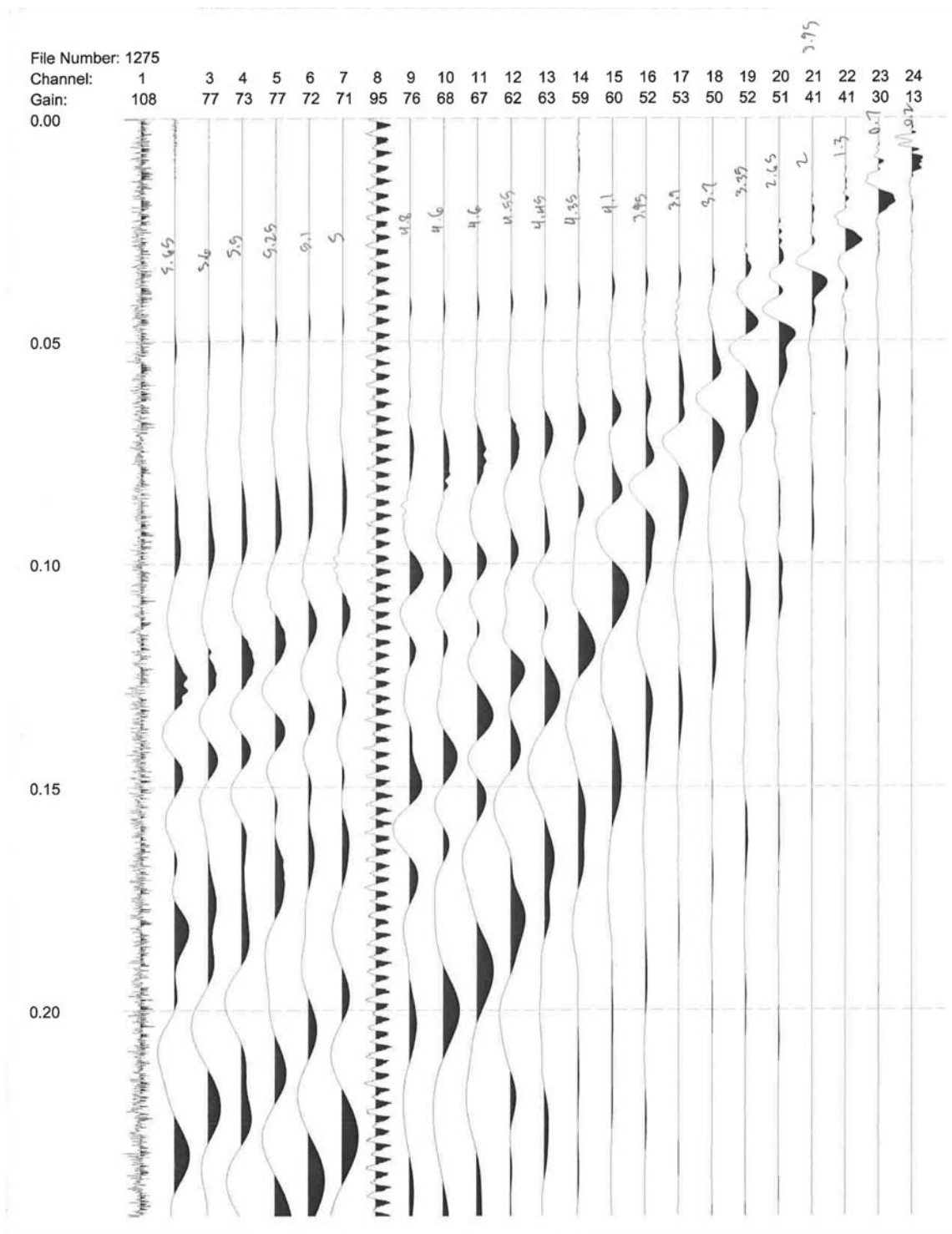












APPENDIX B
INITIAL MODEL INPUT FILES

LINE 2

r.IN File:

```

pltpar (plotting parameters)...
0    ! isep
3    ! itx
1    ! idata
1    ! imod
2    ! iray
0    ! ibnd
2    ! isum
292. ! xwndow
175. ! ywndow
1    ! ircol
1    ! itcol
1    ! idump
axepar (axes parameters)...
0.12752   ! xmax
0.12752   ! xmm
0.020     ! zmax
0.020     ! zmm
10.       ! tmax
10.       ! tmm
3.5       ! albht
15.       ! orig
10.       ! sep
ray-tracing parameters...
1        ! imodf
0        ! ibsmth
0        ! i2pt
83       ! number of entries in ishot
1        ! ishot(1)
1        ! ishot(2)
1        ! ishot(3)
1        ! ishot(4)
1        ! ishot(5)
1        ! ishot(6)
1        ! ishot(7)
1        ! ishot(8)
1        ! ishot(9)
1        ! ishot(10)
1        ! ishot(11)
1        ! ishot(12)
1        ! ishot(13)
1        ! ishot(14)
1        ! ishot(15)
1        ! ishot(16)
1        ! ishot(17)
1        ! ishot(18)
1        ! ishot(19)
1        ! ishot(20)

```

```
1      ! ishot(21)
1      ! ishot(22)
1      ! ishot(23)
1      ! ishot(24)
1      ! ishot(25)
1      ! ishot(26)
1      ! ishot(27)
1      ! ishot(28)
1      ! ishot(29)
1      ! ishot(30)
1      ! ishot(31)
1      ! ishot(32)
1      ! ishot(33)
1      ! ishot(34)
1      ! ishot(35)
1      ! ishot(36)
1      ! ishot(37)
1      ! ishot(38)
1      ! ishot(39)
1      ! ishot(40)
1      ! ishot(41)
1      ! ishot(42)
-1      ! ishot(43)
-1      ! ishot(44)
-1      ! ishot(45)
-1      ! ishot(46)
-1      ! ishot(47)
-1      ! ishot(48)
-1      ! ishot(49)
-1      ! ishot(50)
-1      ! ishot(51)
-1      ! ishot(52)
-1      ! ishot(53)
-1      ! ishot(54)
-1      ! ishot(55)
-1      ! ishot(56)
-1      ! ishot(57)
-1      ! ishot(58)
-1      ! ishot(59)
-1      ! ishot(60)
-1      ! ishot(61)
-1      ! ishot(62)
-1      ! ishot(63)
-1      ! ishot(64)
-1      ! ishot(65)
-1      ! ishot(66)
-1      ! ishot(67)
-1      ! ishot(68)
-1      ! ishot(69)
-1      ! ishot(70)
-1      ! ishot(71)
-1      ! ishot(72)
-1      ! ishot(73)
-1      ! ishot(74)
```

```
-1      ! ishot(75)
-1      ! ishot(76)
-1      ! ishot(77)
-1      ! ishot(78)
-1      ! ishot(79)
-1      ! ishot(80)
-1      ! ishot(81)
-1      ! ishot(82)
-1      ! ishot(83)
83      ! number of entries in xshot
0.00000  ! xshot(1)
0.00193  ! xshot(2)
0.00392  ! xshot(3)
0.00602  ! xshot(4)
0.00796  ! xshot(5)
0.00995  ! xshot(6)
0.01193  ! xshot(7)
0.01392  ! xshot(8)
0.01588  ! xshot(9)
0.01791  ! xshot(10)
0.01991  ! xshot(11)
0.02193  ! xshot(12)
0.02393  ! xshot(13)
0.02588  ! xshot(14)
0.02787  ! xshot(15)
0.02993  ! xshot(16)
0.03190  ! xshot(17)
0.03393  ! xshot(18)
0.03593  ! xshot(19)
0.03787  ! xshot(20)
0.03990  ! xshot(21)
0.04189  ! xshot(22)
0.04393  ! xshot(23)
0.04589  ! xshot(24)
0.04788  ! xshot(25)
0.04988  ! xshot(26)
0.05182  ! xshot(27)
0.05384  ! xshot(28)
0.05585  ! xshot(29)
0.05781  ! xshot(30)
0.05981  ! xshot(31)
0.06177  ! xshot(32)
0.06384  ! xshot(33)
0.06579  ! xshot(34)
0.06785  ! xshot(35)
0.06979  ! xshot(36)
0.07180  ! xshot(37)
0.07378  ! xshot(38)
0.07575  ! xshot(39)
0.07776  ! xshot(40)
0.07982  ! xshot(41)
0.08174  ! xshot(42)
0.12752  ! xshot(43)
0.12553  ! xshot(44)
```

```
0.12355      ! xshot(45)
0.12160      ! xshot(46)
0.11957      ! xshot(47)
0.11761      ! xshot(48)
0.11556      ! xshot(49)
0.11362      ! xshot(50)
0.11165      ! xshot(51)
0.10964      ! xshot(52)
0.10761      ! xshot(53)
0.10567      ! xshot(54)
0.10366      ! xshot(55)
0.10171      ! xshot(56)
0.09970      ! xshot(57)
0.09772      ! xshot(58)
0.09570      ! xshot(59)
0.09374      ! xshot(60)
0.09173      ! xshot(61)
0.08975      ! xshot(62)
0.08774      ! xshot(63)
0.08574      ! xshot(64)
0.08378      ! xshot(65)
0.08174      ! xshot(66)
0.07982      ! xshot(67)
0.07776      ! xshot(68)
0.07575      ! xshot(69)
0.07378      ! xshot(70)
0.07180      ! xshot(71)
0.06979      ! xshot(72)
0.06785      ! xshot(73)
0.06579      ! xshot(74)
0.06384      ! xshot(75)
0.06177      ! xshot(76)
0.05981      ! xshot(77)
0.05781      ! xshot(78)
0.05585      ! xshot(79)
0.05384      ! xshot(80)
0.05182      ! xshot(81)
0.04988      ! xshot(82)
0.04788      ! xshot(83)
83          ! number of entries in zshot
0.00164      ! zshot(1)
0.00170      ! zshot(2)
0.00178      ! zshot(3)
0.00175      ! zshot(4)
0.00179      ! zshot(5)
0.00175      ! zshot(6)
0.00177      ! zshot(7)
0.00181      ! zshot(8)
0.00180      ! zshot(9)
0.00181      ! zshot(10)
0.00183      ! zshot(11)
0.00186      ! zshot(12)
0.00188      ! zshot(13)
0.00188      ! zshot(14)
```

```
0.00186      ! zshot(15)
0.00192      ! zshot(16)
0.00195      ! zshot(17)
0.00194      ! zshot(18)
0.00197      ! zshot(19)
0.00198      ! zshot(20)
0.00198      ! zshot(21)
0.00199      ! zshot(22)
0.00208      ! zshot(23)
0.00211      ! zshot(24)
0.00214      ! zshot(25)
0.00214      ! zshot(26)
0.00214      ! zshot(27)
0.00217      ! zshot(28)
0.00215      ! zshot(29)
0.00217      ! zshot(30)
0.00220      ! zshot(31)
0.00223      ! zshot(32)
0.00227      ! zshot(33)
0.00233      ! zshot(34)
0.00238      ! zshot(35)
0.00245      ! zshot(36)
0.00253      ! zshot(37)
0.00260      ! zshot(38)
0.00270      ! zshot(39)
0.00278      ! zshot(40)
0.00284      ! zshot(41)
0.00291      ! zshot(42)
0.00395      ! zshot(43)
0.00409      ! zshot(44)
0.00441      ! zshot(45)
0.00464      ! zshot(46)
0.00460      ! zshot(47)
0.00458      ! zshot(48)
0.00447      ! zshot(49)
0.00440      ! zshot(50)
0.00419      ! zshot(51)
0.00406      ! zshot(52)
0.00390      ! zshot(53)
0.00381      ! zshot(54)
0.00366      ! zshot(55)
0.00352      ! zshot(56)
0.00348      ! zshot(57)
0.00344      ! zshot(58)
0.00336      ! zshot(59)
0.00328      ! zshot(60)
0.00316      ! zshot(61)
0.00306      ! zshot(62)
0.00305      ! zshot(63)
0.00300      ! zshot(64)
0.00296      ! zshot(65)
0.00291      ! zshot(66)
0.00284      ! zshot(67)
0.00278      ! zshot(68)
```

```
0.00270      ! zshot(69)
0.00260      ! zshot(70)
0.00253      ! zshot(71)
0.00245      ! zshot(72)
0.00238      ! zshot(73)
0.00233      ! zshot(74)
0.00227      ! zshot(75)
0.00223      ! zshot(76)
0.00220      ! zshot(77)
0.00217      ! zshot(78)
0.00215      ! zshot(79)
0.00217      ! zshot(80)
0.00214      ! zshot(81)
0.00214      ! zshot(82)
0.00214      ! zshot(83)
2          ! number of entries in ray
1.3        ! ray(1)
2.3        ! ray(2)
2          ! number of entries in nsmax
25         ! nsmax(1)
25         ! nsmax(2)
2          ! number of entries in nray
50         ! nray(1)
50         ! nray(2)
1          ! number of entries in space
1.          ! space(1)
0.25       ! aamin
75.        ! aamax
inversion parameters
1          ! invr
2          ! number of entries in ivray
13         ! ivray(1)
23         ! ivray(2)
```

tx.IN File:

0.00000	1.00000	0.00000	0
0.01588	0.03025	0.00100	13
0.01991	0.03277	0.00100	13
0.02193	0.03361	0.00100	13
0.02787	0.03655	0.00100	13
0.03190	0.03866	0.00100	13
0.04189	0.04412	0.00100	13
0.04393	0.04496	0.00100	13
0.04589	0.04622	0.00100	13
0.00193	1.00000	0.00000	0
0.01791	0.03025	0.00100	13
0.01991	0.03151	0.00100	13
0.02193	0.03277	0.00100	13
0.02393	0.03361	0.00100	13
0.02787	0.03529	0.00100	13
0.03190	0.03739	0.00100	13
0.03393	0.03824	0.00100	13
0.04393	0.04412	0.00100	13
0.00602	1.00000	0.00000	0
0.02193	0.02951	0.00100	13
0.02393	0.03074	0.00100	13
0.02588	0.03156	0.00100	13
0.02787	0.03197	0.00100	13
0.03190	0.03402	0.00100	13
0.03393	0.03525	0.00100	13
0.03787	0.03770	0.00100	13
0.04189	0.04016	0.00100	13
0.00995	1.00000	0.00000	0
0.02588	0.02869	0.00100	13
0.02787	0.02951	0.00100	13
0.03190	0.03197	0.00100	13
0.03593	0.03402	0.00100	13
0.03990	0.03607	0.00100	13
0.04189	0.03730	0.00100	13
0.04393	0.03852	0.00100	13
0.04788	0.04057	0.00100	13
0.01392	1.00000	0.00000	0
0.02993	0.02869	0.00100	13
0.03190	0.02951	0.00100	13
0.03593	0.03197	0.00100	13
0.03990	0.03402	0.00100	13
0.04393	0.03648	0.00100	13
0.04589	0.03689	0.00100	13
0.04988	0.03934	0.00100	13
0.05384	0.04180	0.00100	13
0.01791	1.00000	0.00000	0
0.03393	0.02869	0.00100	13
0.03593	0.02992	0.00100	13
0.03990	0.03197	0.00100	13
0.04393	0.03443	0.00100	13
0.04788	0.03648	0.00100	13
0.04988	0.03689	0.00100	13

0.05384	0.04016	0.00100	13
0.05781	0.04221	0.00100	13
0.02193	1.00000	0.00000	0
0.03787	0.02869	0.00100	13
0.03990	0.02951	0.00100	13
0.04393	0.03197	0.00100	13
0.04788	0.03443	0.00100	13
0.04988	0.03525	0.00100	13
0.05384	0.03770	0.00100	13
0.05781	0.04016	0.00100	13
0.06177	0.04180	0.00100	13
0.02588	1.00000	0.00000	0
0.04189	0.02828	0.00100	13
0.04393	0.02951	0.00100	13
0.04788	0.03197	0.00100	13
0.05182	0.03402	0.00100	13
0.05384	0.03566	0.00100	13
0.05781	0.03689	0.00100	13
0.06177	0.04016	0.00100	13
0.06579	0.04139	0.00100	13
0.02993	1.00000	0.00000	0
0.04589	0.02787	0.00100	13
0.04788	0.02910	0.00100	13
0.05182	0.03197	0.00100	13
0.05384	0.03320	0.00100	13
0.05781	0.03525	0.00100	13
0.06177	0.03770	0.00100	13
0.06579	0.03934	0.00100	13
0.06785	0.04016	0.00100	13
0.03393	1.00000	0.00000	0
0.04988	0.02705	0.00100	13
0.05182	0.02869	0.00100	13
0.05585	0.03033	0.00100	13
0.05981	0.03320	0.00100	13
0.06384	0.03525	0.00100	13
0.06579	0.03607	0.00100	13
0.06979	0.03811	0.00100	13
0.07378	0.03852	0.00100	13
0.03787	1.00000	0.00000	0
0.05384	0.02869	0.00100	13
0.05585	0.02951	0.00100	13
0.05981	0.03238	0.00100	13
0.06384	0.03402	0.00100	13
0.06579	0.03525	0.00100	13
0.06979	0.03730	0.00100	13
0.07180	0.03770	0.00100	13
0.07378	0.03811	0.00100	13
0.04189	1.00000	0.00000	0
0.05781	0.02869	0.00100	13
0.05981	0.02992	0.00100	13
0.06384	0.03197	0.00100	13
0.06785	0.03361	0.00100	13
0.06979	0.03484	0.00100	13
0.07378	0.03525	0.00100	13

0.07575	0.03689	0.00100	13
0.07982	0.04016	0.00100	13
0.04589	1.00000	0.00000	0
0.06177	0.02828	0.00100	13
0.06384	0.02910	0.00100	13
0.06785	0.03156	0.00100	13
0.07180	0.03320	0.00100	13
0.07378	0.03320	0.00100	13
0.07575	0.03443	0.00100	13
0.07982	0.03607	0.00100	13
0.08174	0.03689	0.00100	13
0.05182	1.00000	0.00000	0
0.06785	0.02828	0.00100	13
0.06979	0.02951	0.00100	13
0.07180	0.02951	0.00100	13
0.07378	0.03033	0.00100	13
0.07575	0.03115	0.00100	13
0.07982	0.03320	0.00100	13
0.08174	0.03443	0.00100	13
0.05585	1.00000	0.00000	0
0.06785	0.02623	0.00100	13
0.07180	0.02787	0.00100	13
0.07378	0.02828	0.00100	13
0.07575	0.02910	0.00100	13
0.07982	0.03197	0.00100	13
0.08174	0.03238	0.00100	13
0.12752	-1.00000	0.00000	0
0.11165	0.03033	0.00100	13
0.10761	0.03197	0.00100	13
0.10567	0.03279	0.00100	13
0.09970	0.03566	0.00100	13
0.09570	0.03730	0.00100	13
0.09173	0.04098	0.00100	13
0.08574	0.04344	0.00100	13
0.08378	0.04426	0.00100	13
0.12553	-1.00000	0.00000	0
0.10964	0.02951	0.00100	13
0.10761	0.03033	0.00100	13
0.10366	0.03279	0.00100	13
0.10171	0.03361	0.00100	13
0.09772	0.03525	0.00100	13
0.09374	0.03689	0.00100	13
0.08975	0.03934	0.00100	13
0.08774	0.04098	0.00100	13
0.12355	-1.00000	0.00000	0
0.10761	0.02787	0.00100	13
0.10366	0.03115	0.00100	13
0.10171	0.03115	0.00100	13
0.09772	0.03402	0.00100	13
0.09570	0.03607	0.00100	13
0.09173	0.03934	0.00100	13
0.08174	0.04344	0.00100	13
0.07982	0.04631	0.00100	13
0.12160	-1.00000	0.00000	0

0.10567	0.02746	0.00100	13
0.10366	0.02828	0.00100	13
0.09970	0.03033	0.00100	13
0.09570	0.03238	0.00100	13
0.09374	0.03320	0.00100	13
0.08975	0.03566	0.00100	13
0.08574	0.03770	0.00100	13
0.08174	0.04098	0.00100	13
0.11761	-1.00000	0.00000	0
0.10171	0.02623	0.00100	13
0.09970	0.02623	0.00100	13
0.09772	0.02705	0.00100	13
0.09570	0.02787	0.00100	13
0.08975	0.03197	0.00100	13
0.08574	0.03361	0.00100	13
0.07776	0.03934	0.00100	13
0.07575	0.04016	0.00100	13
0.11362	-1.00000	0.00000	0
0.09772	0.02623	0.00100	13
0.09570	0.02664	0.00100	13
0.09173	0.03033	0.00100	13
0.08774	0.03115	0.00100	13
0.08174	0.03525	0.00100	13
0.07982	0.03689	0.00100	13
0.07378	0.03934	0.00100	13
0.07180	0.04016	0.00100	13
0.10964	-1.00000	0.00000	0
0.09374	0.02582	0.00100	13
0.09173	0.02787	0.00100	13
0.08774	0.02910	0.00100	13
0.08378	0.03156	0.00100	13
0.08174	0.03279	0.00100	13
0.07776	0.03607	0.00100	13
0.07378	0.03770	0.00100	13
0.06979	0.03975	0.00100	13
0.10567	-1.00000	0.00000	0
0.08975	0.02541	0.00100	13
0.08574	0.02787	0.00100	13
0.08378	0.02869	0.00100	13
0.07982	0.03197	0.00100	13
0.07378	0.03525	0.00100	13
0.06979	0.03689	0.00100	13
0.06579	0.03934	0.00100	13
0.06384	0.04016	0.00100	13
0.10171	-1.00000	0.00000	0
0.08574	0.02541	0.00100	13
0.08378	0.02623	0.00100	13
0.07982	0.02951	0.00100	13
0.07575	0.03115	0.00100	13
0.07378	0.03279	0.00100	13
0.06979	0.03566	0.00100	13
0.06579	0.03689	0.00100	13
0.06177	0.03975	0.00100	13
0.09970	-1.00000	0.00000	0

0.08378	0.02582	0.00100	13
0.07982	0.02869	0.00100	13
0.07776	0.03074	0.00100	13
0.07378	0.03238	0.00100	13
0.07180	0.03279	0.00100	13
0.06579	0.03648	0.00100	13
0.05781	0.04057	0.00100	13
0.05585	0.04098	0.00100	13
0.09374	-1.00000	0.00000	0
0.07776	0.02787	0.00100	13
0.07378	0.02992	0.00100	13
0.07180	0.03074	0.00100	13
0.06579	0.03361	0.00100	13
0.06177	0.03566	0.00100	13
0.05781	0.03770	0.00100	13
0.05182	0.04098	0.00100	13
0.04988	0.04098	0.00100	13
0.08975	-1.00000	0.00000	0
0.07378	0.02787	0.00100	13
0.07180	0.02910	0.00100	13
0.06579	0.03197	0.00100	13
0.06384	0.03320	0.00100	13
0.06177	0.03443	0.00100	13
0.05781	0.03648	0.00100	13
0.05585	0.03607	0.00100	13
0.05182	0.03811	0.00100	13
0.08574	-1.00000	0.00000	0
0.06979	0.02787	0.00100	13
0.06579	0.02951	0.00100	13
0.06384	0.03033	0.00100	13
0.05981	0.03197	0.00100	13
0.05781	0.03361	0.00100	13
0.05384	0.03443	0.00100	13
0.05182	0.03525	0.00100	13
0.04988	0.03607	0.00100	13
0.08174	-1.00000	0.00000	0
0.06579	0.02869	0.00100	13
0.06384	0.02951	0.00100	13
0.05981	0.03197	0.00100	13
0.05585	0.03238	0.00100	13
0.05384	0.03361	0.00100	13
0.05182	0.03443	0.00100	13
0.04988	0.03525	0.00100	13
0.04788	0.03689	0.00100	13
0.07776	-1.00000	0.00000	0
0.06177	0.02910	0.00100	13
0.05981	0.03033	0.00100	13
0.05781	0.03156	0.00100	13
0.05585	0.03115	0.00100	13
0.05384	0.03197	0.00100	13
0.05182	0.03279	0.00100	13
0.04988	0.03361	0.00100	13
0.04788	0.03443	0.00100	13
0.07575	-1.00000	0.00000	0

0.05981	0.02787	0.00100	13
0.05781	0.02869	0.00100	13
0.05585	0.02869	0.00100	13
0.05384	0.02951	0.00100	13
0.05182	0.03033	0.00100	13
0.04988	0.03115	0.00100	13
0.04788	0.03279	0.00100	13
0.00000	0.00000	0.00000	-1

v.IN File:

1 .03990 .04189 .04393 .04589 .04788 .04988 .05182 .05384 .05585
 .05781
 1 0.3640 0.3640 0.3640 0.3640 0.3640 0.3640 0.3640 0.3640 0.3640
 0.3640
 0 0 0 0 0 0 0 0 0 0
 0
 1 .05981 .06177 .06384 .06579 .06785 .06979 .07180 .07378 .07575
 .07776
 1 0.3640 0.3640 0.3640 0.3640 0.3640 0.3640 0.3640 0.3640 0.3640
 0.3640
 0 0 0 0 0 0 0 0 0 0
 0
 1 .07982 .08174 .08378 .08574 .08774 .08975 .09173 .09374 .09570
 .09772
 1 0.3640 0.3640 0.3640 0.3640 0.3640 0.3640 0.3640 0.3640 0.3640
 0.3640
 0 0 0 0 0 0 0 0 0 0
 0
 1 .09970 .10171 .10366 .10567 .10761 .10964 .11165 .11362 .11556
 .11761
 1 0.3640 0.3640 0.3640 0.3640 0.3640 0.3640 0.3640 0.3640 0.3640
 0.3640
 0 0 0 0 0 0 0 0 0 0
 0
 1 .11957 .12160 .12355 .12553 .12752
 0 0.3640 0.3640 0.3640 0.3640 0.3640
 0 0 0 0 0
 1 .00000 .00193 .00392 .00602 .00796 .00995 .01193 .01392 .01588
 .01791
 1 0.3640 0.3640 0.3640 0.3640 0.3640 0.3640 0.3640 0.3640 0.3640
 0.3640
 0 0 0 0 0 0 0 0 0 0
 0
 1 .01991 .02193 .02393 .02588 .02787 .02993 .03190 .03393 .03593
 .03787
 1 0.3640 0.3640 0.3640 0.3640 0.3640 0.3640 0.3640 0.3640 0.3640
 0.3640
 0 0 0 0 0 0 0 0 0 0
 0
 1 .03990 .04189 .04393 .04589 .04788 .04988 .05182 .05384 .05585
 .05781
 1 0.3640 0.3640 0.3640 0.3640 0.3640 0.3640 0.3640 0.3640 0.3640
 0.3640
 0 0 0 0 0 0 0 0 0 0
 0
 1 .05981 .06177 .06384 .06579 .06785 .06979 .07180 .07378 .07575
 .07776
 1 0.3640 0.3640 0.3640 0.3640 0.3640 0.3640 0.3640 0.3640 0.3640
 0.3640
 0 0 0 0 0 0 0 0 0 0
 0
 1 .07982 .08174 .08378 .08574 .08774 .08975 .09173 .09374 .09570
 .09772

1 0.3640 0.3640 0.3640 0.3640 0.3640 0.3640 0.3640 0.3640 0.3640 0.3640
 0.3640
 0 0 0 0 0 0 0 0 0 0
 0
 1 .09970 .10171 .10366 .10567 .10761 .10964 .11165 .11362 .11556
 .11761
 1 0.3640 0.3640 0.3640 0.3640 0.3640 0.3640 0.3640 0.3640 0.3640 0.3640
 0.3640
 0 0 0 0 0 0 0 0 0 0
 0
 1 .11957 .12160 .12355 .12553 .12752
 0 0.3640 0.3640 0.3640 0.3640 0.3640
 0 0 0 0 0
 2 .00000 .00193 .00392 .00602 .00796 .00995 .01193 .01392 .01588
 .01791
 1 .00600 .00600 .00600 .00600 .00600 .00600 .00600 .00600 .00600
 .00600
 1 1 1 1 1 1 1 1 1 1
 1
 2 .01991 .02193 .02393 .02588 .02787 .02993 .03190 .03393 .03593
 .03787
 1 .00600 .00600 .00600 .00600 .00600 .00600 .00600 .00600 .00600
 .00600
 1 1 1 1 1 1 1 1 1 1
 1
 2 .03990 .04189 .04393 .04589 .04788 .04988 .05182 .05384 .05585
 .05781
 1 .00600 .00600 .00600 .00600 .00600 .00600 .00600 .00600 .00600
 .00600
 1 1 1 1 1 1 1 1 1 1
 1
 2 .05981 .06177 .06384 .06579 .06785 .06979 .07180 .07378 .07575
 .07776
 1 .00600 .00600 .00600 .00600 .00600 .00600 .00600 .00600 .00600
 .00600
 1 1 1 1 1 1 1 1 1 1
 1
 2 .07982 .08174 .08378 .08574 .08774 .08975 .09173 .09374 .09570
 .09772
 1 .00600 .00600 .00600 .00600 .00600 .00600 .00600 .00600 .00600
 .00600
 1 1 1 1 1 1 1 1 1 1
 1
 2 .09970 .10171 .10366 .10567 .10761 .10964 .11165 .11362 .11556
 .11761
 1 .00600 .00600 .00600 .00600 .00600 .00600 .00600 .00600 .00600
 .00600
 1 1 1 1 1 1 1 1 1 1
 1
 2 .11957 .12160 .12355 .12553 .12752
 0 .00600 .00600 .00600 .00600 .00600
 1 1 1 1 1
 2 .00000 .00193 .00392 .00602 .00796 .00995 .01193 .01392 .01588
 .01791

3 .09970 .10171 .10366 .10567 .10761 .10964 .11165 .11362 .11556
 .11761
 1 .00700 .00700 .00700 .00700 .00700 .00700 .00700 .00700 .00700
 .00700
 0 0 0 0 0 0 0 0 0 0
 3 .11957 .12160 .12355 .12553 .12752
 0 .00700 .00700 .00700 .00700 .00700
 0 0 0 0 0
 3 .00000 .00193 .00392 .00602 .00796 .00995 .01193 .01392 .01588
 .01791
 1 2.2000 2.2000 2.2000 2.2000 2.2000 2.2000 2.2000 2.2000 2.2000
 2.2000
 0 0 0 0 0 0 0 0 0 0
 0 3 .01991 .02193 .02393 .02588 .02787 .02993 .03190 .03393 .03593
 .03787
 1 2.2000 2.2000 2.2000 2.2000 2.2000 2.2000 2.2000 2.2000 2.2000
 2.2000
 0 0 0 0 0 0 0 0 0 0
 0 3 .03990 .04189 .04393 .04589 .04788 .04988 .05182 .05384 .05585
 .05781
 1 2.2000 2.2000 2.2000 2.2000 2.2000 2.2000 2.2000 2.2000 2.2000
 2.2000
 0 0 0 0 0 0 0 0 0 0
 0 3 .05981 .06177 .06384 .06579 .06785 .06979 .07180 .07378 .07575
 .07776
 1 2.2000 2.2000 2.2000 2.2000 2.2000 2.2000 2.2000 2.2000 2.2000
 2.2000
 0 0 0 0 0 0 0 0 0 0
 0 3 .07982 .08174 .08378 .08574 .08774 .08975 .09173 .09374 .09570
 .09772
 1 2.2000 2.2000 2.2000 2.2000 2.2000 2.2000 2.2000 2.2000 2.2000
 2.2000
 0 0 0 0 0 0 0 0 0 0
 0 3 .09970 .10171 .10366 .10567 .10761 .10964 .11165 .11362 .11556
 .11761
 1 2.2000 2.2000 2.2000 2.2000 2.2000 2.2000 2.2000 2.2000 2.2000
 2.2000
 0 0 0 0 0 0 0 0 0 0
 0 3 .11957 .12160 .12355 .12553 .12752
 0 2.2000 2.2000 2.2000 2.2000 2.2000
 0 0 0 0 0
 3 .00000 .00193 .00392 .00602 .00796 .00995 .01193 .01392 .01588
 .01791
 1 2.2000 2.2000 2.2000 2.2000 2.2000 2.2000 2.2000 2.2000 2.2000
 2.2000
 0 0 0 0 0 0 0 0 0 0
 0

```

3 .01991 .02193 .02393 .02588 .02787 .02993 .03190 .03393 .03593
.03787
1 2.2000 2.2000 2.2000 2.2000 2.2000 2.2000 2.2000 2.2000 2.2000
2.2000
0 0 0 0 0 0 0 0 0 0
0
3 .03990 .04189 .04393 .04589 .04788 .04988 .05182 .05384 .05585
.05781
1 2.2000 2.2000 2.2000 2.2000 2.2000 2.2000 2.2000 2.2000 2.2000
2.2000
0 0 0 0 0 0 0 0 0 0
0
3 .05981 .06177 .06384 .06579 .06785 .06979 .07180 .07378 .07575
.07776
1 2.2000 2.2000 2.2000 2.2000 2.2000 2.2000 2.2000 2.2000 2.2000
2.2000
0 0 0 0 0 0 0 0 0 0
0
3 .07982 .08174 .08378 .08574 .08774 .08975 .09173 .09374 .09570
.09772
1 2.2000 2.2000 2.2000 2.2000 2.2000 2.2000 2.2000 2.2000 2.2000
2.2000
0 0 0 0 0 0 0 0 0 0
0
3 .09970 .10171 .10366 .10567 .10761 .10964 .11165 .11362 .11556
.11761
1 2.2000 2.2000 2.2000 2.2000 2.2000 2.2000 2.2000 2.2000 2.2000
2.2000
0 0 0 0 0 0 0 0 0 0
0
3 .11957 .12160 .12355 .12553 .12752
0 2.2000 2.2000 2.2000 2.2000 2.2000
0 0 0 0 0
4 .00000 .12752
0 .01200 .01200

```

d.IN File:

```

0.12752 ! xmax
0.050 ! damping factor
0.001 ! velocity uncertainty [km/s]
0.00001 ! depth-to-boundary uncertainty [km]

```

LINE 3

r.IN File:

```

pltpar (plotting parameters)...
0    ! isep
3    ! itx
1    ! idata
1    ! imod
2    ! iray
0    ! ibnd
2    ! isum
292. ! xwndow
175. ! ywndow
1    ! ircol
1    ! itcol
1    ! idump
axepar (axes parameters)...
0.14192   ! xmax
0.14192   ! xmm
0.020     ! zmax
0.020     ! zmm
10.       ! tmax
10.       ! tmm
3.5       ! albht
15.       ! orig
10.       ! sep
ray-tracing parameters...
1        ! imodf
0        ! ibsmth
0        ! i2pt
97      ! number of entries in ishot
1        ! ishot(1)
1        ! ishot(2)
1        ! ishot(3)
1        ! ishot(4)
1        ! ishot(5)
1        ! ishot(6)
1        ! ishot(7)
1        ! ishot(8)
1        ! ishot(9)
1        ! ishot(10)
1        ! ishot(11)
1        ! ishot(12)
1        ! ishot(13)
1        ! ishot(14)
1        ! ishot(15)
1        ! ishot(16)
1        ! ishot(17)
1        ! ishot(18)
1        ! ishot(19)
1        ! ishot(20)

```

```
1      ! ishot(21)
1      ! ishot(22)
1      ! ishot(23)
1      ! ishot(24)
1      ! ishot(25)
1      ! ishot(26)
1      ! ishot(27)
1      ! ishot(28)
1      ! ishot(29)
1      ! ishot(30)
1      ! ishot(31)
1      ! ishot(32)
1      ! ishot(33)
1      ! ishot(34)
1      ! ishot(35)
1      ! ishot(36)
1      ! ishot(37)
1      ! ishot(38)
1      ! ishot(39)
1      ! ishot(40)
1      ! ishot(41)
1      ! ishot(42)
1      ! ishot(43)
1      ! ishot(44)
1      ! ishot(45)
1      ! ishot(46)
1      ! ishot(47)
1      ! ishot(48)
-1      ! ishot(49)
-1      ! ishot(50)
-1      ! ishot(51)
-1      ! ishot(52)
-1      ! ishot(53)
-1      ! ishot(54)
-1      ! ishot(55)
-1      ! ishot(56)
-1      ! ishot(57)
-1      ! ishot(58)
-1      ! ishot(59)
-1      ! ishot(60)
-1      ! ishot(61)
-1      ! ishot(62)
-1      ! ishot(63)
-1      ! ishot(64)
-1      ! ishot(65)
-1      ! ishot(66)
-1      ! ishot(67)
-1      ! ishot(68)
-1      ! ishot(69)
-1      ! ishot(70)
-1      ! ishot(71)
-1      ! ishot(72)
-1      ! ishot(73)
-1      ! ishot(74)
```

```
-1      ! ishot(75)
-1      ! ishot(76)
-1      ! ishot(77)
-1      ! ishot(78)
-1      ! ishot(79)
-1      ! ishot(80)
-1      ! ishot(81)
-1      ! ishot(82)
-1      ! ishot(83)
-1      ! ishot(84)
-1      ! ishot(85)
-1      ! ishot(86)
-1      ! ishot(87)
-1      ! ishot(88)
-1      ! ishot(89)
-1      ! ishot(90)
-1      ! ishot(91)
-1      ! ishot(92)
-1      ! ishot(93)
-1      ! ishot(94)
-1      ! ishot(95)
-1      ! ishot(96)
-1      ! ishot(97)
97      ! number of entries in xshot
0.00000  ! xshot(1)
0.00204  ! xshot(2)
0.00407  ! xshot(3)
0.00593  ! xshot(4)
0.00801  ! xshot(5)
0.00996  ! xshot(6)
0.01179  ! xshot(7)
0.01410  ! xshot(8)
0.01594  ! xshot(9)
0.01797  ! xshot(10)
0.01994  ! xshot(11)
0.02187  ! xshot(12)
0.02387  ! xshot(13)
0.02590  ! xshot(14)
0.02797  ! xshot(15)
0.02997  ! xshot(16)
0.03199  ! xshot(17)
0.03397  ! xshot(18)
0.03598  ! xshot(19)
0.03792  ! xshot(20)
0.04002  ! xshot(21)
0.04196  ! xshot(22)
0.04390  ! xshot(23)
0.04582  ! xshot(24)
0.04789  ! xshot(25)
0.04990  ! xshot(26)
0.05182  ! xshot(27)
0.05383  ! xshot(28)
0.05583  ! xshot(29)
0.05790  ! xshot(30)
```

0.05995 ! xshot(31)
0.06192 ! xshot(32)
0.06384 ! xshot(33)
0.06590 ! xshot(34)
0.06792 ! xshot(35)
0.06985 ! xshot(36)
0.07193 ! xshot(37)
0.07394 ! xshot(38)
0.07588 ! xshot(39)
0.07785 ! xshot(40)
0.08000 ! xshot(41)
0.08188 ! xshot(42)
0.08387 ! xshot(43)
0.08590 ! xshot(44)
0.08787 ! xshot(45)
0.08990 ! xshot(46)
0.09183 ! xshot(47)
0.09385 ! xshot(48)
0.14192 ! xshot(49)
0.13991 ! xshot(50)
0.13790 ! xshot(51)
0.13588 ! xshot(52)
0.13390 ! xshot(53)
0.13195 ! xshot(54)
0.12989 ! xshot(55)
0.12795 ! xshot(56)
0.12589 ! xshot(57)
0.12393 ! xshot(58)
0.12191 ! xshot(59)
0.11990 ! xshot(60)
0.11788 ! xshot(61)
0.11586 ! xshot(62)
0.11393 ! xshot(63)
0.11196 ! xshot(64)
0.10991 ! xshot(65)
0.10791 ! xshot(66)
0.10594 ! xshot(67)
0.10391 ! xshot(68)
0.10195 ! xshot(69)
0.09990 ! xshot(70)
0.09787 ! xshot(71)
0.09585 ! xshot(72)
0.09385 ! xshot(73)
0.09183 ! xshot(74)
0.08990 ! xshot(75)
0.08787 ! xshot(76)
0.08590 ! xshot(77)
0.08387 ! xshot(78)
0.08188 ! xshot(79)
0.08000 ! xshot(80)
0.07785 ! xshot(81)
0.07588 ! xshot(82)
0.07394 ! xshot(83)
0.07193 ! xshot(84)

```
0.06985      ! xshot(85)
0.06792      ! xshot(86)
0.06590      ! xshot(87)
0.06384      ! xshot(88)
0.06192      ! xshot(89)
0.05995      ! xshot(90)
0.05790      ! xshot(91)
0.05583      ! xshot(92)
0.05383      ! xshot(93)
0.05182      ! xshot(94)
0.04990      ! xshot(95)
0.04789      ! xshot(96)
0.04582      ! xshot(97)
97          ! number of entries in zshot
0.00151      ! zshot(1)
0.00155      ! zshot(2)
0.00151      ! zshot(3)
0.00150      ! zshot(4)
0.00151      ! zshot(5)
0.00146      ! zshot(6)
0.00140      ! zshot(7)
0.00140      ! zshot(8)
0.00141      ! zshot(9)
0.00144      ! zshot(10)
0.00143      ! zshot(11)
0.00147      ! zshot(12)
0.00146      ! zshot(13)
0.00150      ! zshot(14)
0.00149      ! zshot(15)
0.00145      ! zshot(16)
0.00147      ! zshot(17)
0.00146      ! zshot(18)
0.00143      ! zshot(19)
0.00140      ! zshot(20)
0.00135      ! zshot(21)
0.00135      ! zshot(22)
0.00141      ! zshot(23)
0.00146      ! zshot(24)
0.00151      ! zshot(25)
0.00150      ! zshot(26)
0.00154      ! zshot(27)
0.00155      ! zshot(28)
0.00153      ! zshot(29)
0.00151      ! zshot(30)
0.00152      ! zshot(31)
0.00157      ! zshot(32)
0.00155      ! zshot(33)
0.00156      ! zshot(34)
0.00154      ! zshot(35)
0.00158      ! zshot(36)
0.00159      ! zshot(37)
0.00156      ! zshot(38)
0.00158      ! zshot(39)
0.00163      ! zshot(40)
```

```
0.00166 ! zshot(41)
0.00166 ! zshot(42)
0.00170 ! zshot(43)
0.00170 ! zshot(44)
0.00171 ! zshot(45)
0.00167 ! zshot(46)
0.00172 ! zshot(47)
0.00170 ! zshot(48)
0.00219 ! zshot(49)
0.00215 ! zshot(50)
0.00216 ! zshot(51)
0.00216 ! zshot(52)
0.00215 ! zshot(53)
0.00215 ! zshot(54)
0.00217 ! zshot(55)
0.00214 ! zshot(56)
0.00219 ! zshot(57)
0.00216 ! zshot(58)
0.00215 ! zshot(59)
0.00214 ! zshot(60)
0.00206 ! zshot(61)
0.00203 ! zshot(62)
0.00199 ! zshot(63)
0.00199 ! zshot(64)
0.00189 ! zshot(65)
0.00195 ! zshot(66)
0.00192 ! zshot(67)
0.00188 ! zshot(68)
0.00185 ! zshot(69)
0.00182 ! zshot(70)
0.00181 ! zshot(71)
0.00175 ! zshot(72)
0.00170 ! zshot(73)
0.00172 ! zshot(74)
0.00167 ! zshot(75)
0.00171 ! zshot(76)
0.00170 ! zshot(77)
0.00170 ! zshot(78)
0.00166 ! zshot(79)
0.00166 ! zshot(80)
0.00163 ! zshot(81)
0.00158 ! zshot(82)
0.00156 ! zshot(83)
0.00159 ! zshot(84)
0.00158 ! zshot(85)
0.00154 ! zshot(86)
0.00156 ! zshot(87)
0.00155 ! zshot(88)
0.00157 ! zshot(89)
0.00152 ! zshot(90)
0.00151 ! zshot(91)
0.00153 ! zshot(92)
0.00155 ! zshot(93)
0.00154 ! zshot(94)
```

```
0.00150      ! zshot(95)
0.00151      ! zshot(96)
0.00146      ! zshot(97)
2           ! number of entries in ray
1.3         ! ray(1)
2.3         ! ray(2)
2           ! number of entries in nsmax
25          ! nsmax(1)
25          ! nsmax(2)
2           ! number of entries in nray
50          ! nray(1)
50          ! nray(2)
1           ! number of entries in space
1.          ! space(1)
0.25        ! aamin
75.        ! aamax
inversion parameters
1           ! invr
2           ! number of entries in ivray
13         ! ivray(1)
23         ! ivray(2)
```

tx.IN File:

0.00000	1.00000	0.00000	0
0.01797	0.03193	0.00100	13
0.01994	0.03361	0.00100	13
0.02187	0.03529	0.00100	13
0.02387	0.03697	0.00100	13
0.02997	0.03908	0.00100	13
0.03199	0.04076	0.00100	13
0.04196	0.04622	0.00100	13
0.04390	0.04706	0.00100	13
0.00204	1.00000	0.00000	0
0.01797	0.03193	0.00100	13
0.02187	0.03445	0.00100	13
0.02387	0.03529	0.00100	13
0.02797	0.03782	0.00100	13
0.03199	0.04034	0.00100	13
0.03397	0.04076	0.00100	13
0.04390	0.04622	0.00100	13
0.04582	0.04790	0.00100	13
0.00407	1.00000	0.00000	0
0.01994	0.03277	0.00100	13
0.02387	0.03529	0.00100	13
0.02590	0.03655	0.00100	13
0.03199	0.03950	0.00100	13
0.03397	0.04034	0.00100	13
0.04582	0.04706	0.00100	13
0.04789	0.04790	0.00100	13
0.04990	0.04916	0.00100	13
0.00593	1.00000	0.00000	0
0.02997	0.03697	0.00100	13
0.03199	0.03908	0.00100	13
0.03397	0.03950	0.00100	13
0.03792	0.04034	0.00100	13
0.04002	0.04286	0.00100	13
0.04196	0.04412	0.00100	13
0.04582	0.04622	0.00100	13
0.04789	0.04706	0.00100	13
0.00996	1.00000	0.00000	0
0.02797	0.03277	0.00100	13
0.02997	0.03361	0.00100	13
0.03199	0.03529	0.00100	13
0.03598	0.03697	0.00100	13
0.04002	0.03992	0.00100	13
0.04196	0.04118	0.00100	13
0.04582	0.04328	0.00100	13
0.04789	0.04454	0.00100	13
0.01410	1.00000	0.00000	0
0.03199	0.03277	0.00100	13
0.03598	0.03487	0.00100	13
0.03792	0.03529	0.00100	13
0.04002	0.03697	0.00100	13
0.04196	0.03782	0.00100	13

0.04789	0.04034	0.00100	13
0.04990	0.04286	0.00100	13
0.05383	0.04370	0.00100	13
0.01797	1.00000	0.00000	0
0.03397	0.03235	0.00100	13
0.03598	0.03361	0.00100	13
0.03792	0.03445	0.00100	13
0.04196	0.03697	0.00100	13
0.04582	0.03866	0.00100	13
0.04990	0.04034	0.00100	13
0.05383	0.04202	0.00100	13
0.05583	0.04370	0.00100	13
0.02187	1.00000	0.00000	0
0.03792	0.03319	0.00100	13
0.04002	0.03529	0.00100	13
0.04390	0.03697	0.00100	13
0.04582	0.03824	0.00100	13
0.04789	0.03950	0.00100	13
0.05182	0.04118	0.00100	13
0.05583	0.04370	0.00100	13
0.05790	0.04370	0.00100	13
0.02590	1.00000	0.00000	0
0.04390	0.03487	0.00100	13
0.04582	0.03613	0.00100	13
0.04789	0.03782	0.00100	13
0.05182	0.04034	0.00100	13
0.05383	0.04202	0.00100	13
0.05790	0.04244	0.00100	13
0.06792	0.04790	0.00100	13
0.06985	0.04874	0.00100	13
0.02997	1.00000	0.00000	0
0.04582	0.03361	0.00100	13
0.04789	0.03445	0.00100	13
0.04990	0.03613	0.00100	13
0.05182	0.03655	0.00100	13
0.05383	0.03739	0.00100	13
0.05790	0.03866	0.00100	13
0.06192	0.04118	0.00100	13
0.06590	0.04328	0.00100	13
0.03397	1.00000	0.00000	0
0.04990	0.03403	0.00100	13
0.05383	0.03487	0.00100	13
0.05790	0.03739	0.00100	13
0.05995	0.03866	0.00100	13
0.06384	0.04076	0.00100	13
0.06792	0.04244	0.00100	13
0.06985	0.04286	0.00100	13
0.07193	0.04412	0.00100	13
0.04002	1.00000	0.00000	0
0.05583	0.03361	0.00100	13
0.05790	0.03403	0.00100	13
0.05995	0.03529	0.00100	13
0.06192	0.03613	0.00100	13
0.06590	0.03866	0.00100	13

0.06985	0.03992	0.00100	13
0.07394	0.04286	0.00100	13
0.07785	0.04370	0.00100	13
0.04196	1.00000	0.00000	0
0.05790	0.03319	0.00100	13
0.05995	0.03445	0.00100	13
0.06384	0.03697	0.00100	13
0.06590	0.03782	0.00100	13
0.06985	0.03866	0.00100	13
0.07193	0.04034	0.00100	13
0.07394	0.04202	0.00100	13
0.07785	0.04286	0.00100	13
0.04390	1.00000	0.00000	0
0.06192	0.03361	0.00100	13
0.06384	0.03529	0.00100	13
0.06590	0.03613	0.00100	13
0.06985	0.03697	0.00100	13
0.07193	0.03866	0.00100	13
0.07394	0.04034	0.00100	13
0.07785	0.04160	0.00100	13
0.08188	0.04412	0.00100	13
0.04582	1.00000	0.00000	0
0.06384	0.03445	0.00100	13
0.06590	0.03529	0.00100	13
0.06792	0.03613	0.00100	13
0.07193	0.03782	0.00100	13
0.07394	0.03950	0.00100	13
0.07785	0.04118	0.00100	13
0.08787	0.04664	0.00100	13
0.08990	0.04580	0.00100	13
0.04990	1.00000	0.00000	0
0.06792	0.03361	0.00100	13
0.07193	0.03613	0.00100	13
0.07394	0.03782	0.00100	13
0.07785	0.03992	0.00100	13
0.08188	0.04118	0.00100	13
0.08387	0.04202	0.00100	13
0.08590	0.04286	0.00100	13
0.08990	0.04454	0.00100	13
0.05383	1.00000	0.00000	0
0.06985	0.03235	0.00100	13
0.07193	0.03361	0.00100	13
0.07394	0.03529	0.00100	13
0.07588	0.03571	0.00100	13
0.07785	0.03697	0.00100	13
0.08188	0.03950	0.00100	13
0.08590	0.04118	0.00100	13
0.08990	0.04286	0.00100	13
0.05583	1.00000	0.00000	0
0.07193	0.03235	0.00100	13
0.07394	0.03445	0.00100	13
0.07785	0.03571	0.00100	13
0.08000	0.03655	0.00100	13
0.08387	0.03908	0.00100	13

0.08590	0.04118	0.00100	13
0.08990	0.04160	0.00100	13
0.09183	0.04286	0.00100	13
0.05995	1.00000	0.00000	0
0.07588	0.03277	0.00100	13
0.07785	0.03445	0.00100	13
0.08000	0.03571	0.00100	13
0.08387	0.03782	0.00100	13
0.08590	0.03950	0.00100	13
0.08787	0.04034	0.00100	13
0.09183	0.04118	0.00100	13
0.06384	1.00000	0.00000	0
0.08000	0.03403	0.00100	13
0.08387	0.03571	0.00100	13
0.08590	0.03697	0.00100	13
0.08787	0.03782	0.00100	13
0.08990	0.03866	0.00100	13
0.09385	0.04034	0.00100	13
0.06792	1.00000	0.00000	0
0.08387	0.03277	0.00100	13
0.08590	0.03319	0.00100	13
0.08787	0.03445	0.00100	13
0.08990	0.03487	0.00100	13
0.09183	0.03571	0.00100	13
0.09385	0.03613	0.00100	13
0.14192	-1.00000	0.00000	0
0.12393	0.03403	0.00100	13
0.12191	0.03613	0.00100	13
0.11990	0.03613	0.00100	13
0.11586	0.03950	0.00100	13
0.11196	0.04034	0.00100	13
0.10391	0.04454	0.00100	13
0.10195	0.04538	0.00100	13
0.09990	0.04622	0.00100	13
0.13588	-1.00000	0.00000	0
0.11788	0.03361	0.00100	13
0.11586	0.03529	0.00100	13
0.11393	0.03613	0.00100	13
0.10991	0.03739	0.00100	13
0.10594	0.03908	0.00100	13
0.10195	0.04118	0.00100	13
0.09585	0.04370	0.00100	13
0.09385	0.04454	0.00100	13
0.12795	-1.00000	0.00000	0
0.10791	0.03487	0.00100	13
0.10594	0.03529	0.00100	13
0.10195	0.03739	0.00100	13
0.09990	0.03866	0.00100	13
0.09385	0.04034	0.00100	13
0.08787	0.04412	0.00100	13
0.08590	0.04454	0.00100	13
0.08387	0.04664	0.00100	13
0.12191	-1.00000	0.00000	0
0.10594	0.03361	0.00100	13

0.10391	0.03445	0.00100	13
0.10195	0.03529	0.00100	13
0.09990	0.03697	0.00100	13
0.09585	0.03866	0.00100	13
0.09183	0.03908	0.00100	13
0.08990	0.03950	0.00100	13
0.08787	0.04202	0.00100	13
0.11586	-1.00000	0.00000	0
0.09990	0.03402	0.00100	13
0.09385	0.03571	0.00100	13
0.09183	0.03697	0.00100	13
0.08990	0.03782	0.00100	13
0.08590	0.04076	0.00100	13
0.07588	0.04412	0.00100	13
0.07394	0.04664	0.00100	13
0.07193	0.04790	0.00100	13
0.10991	-1.00000	0.00000	0
0.09183	0.03361	0.00100	13
0.08990	0.03529	0.00100	13
0.08787	0.03655	0.00100	13
0.08387	0.03824	0.00100	13
0.08000	0.03950	0.00100	13
0.06985	0.04370	0.00100	13
0.06792	0.04580	0.00100	13
0.06590	0.04622	0.00100	13
0.10594	-1.00000	0.00000	0
0.08990	0.03151	0.00100	13
0.08590	0.03571	0.00100	13
0.08387	0.03613	0.00100	13
0.08000	0.03782	0.00100	13
0.07785	0.03824	0.00100	13
0.07588	0.03908	0.00100	13
0.07193	0.04118	0.00100	13
0.06792	0.04244	0.00100	13
0.10195	-1.00000	0.00000	0
0.08387	0.03361	0.00100	13
0.08188	0.03613	0.00100	13
0.08000	0.03529	0.00100	13
0.08387	0.03361	0.00100	13
0.07193	0.03908	0.00100	13
0.06192	0.04538	0.00100	13
0.05995	0.04664	0.00100	13
0.05790	0.04706	0.00100	13
0.09787	-1.00000	0.00000	0
0.08188	0.03277	0.00100	13
0.07785	0.03445	0.00100	13
0.07588	0.03529	0.00100	13
0.07394	0.03697	0.00100	13
0.06985	0.03782	0.00100	13
0.06792	0.03950	0.00100	13
0.06384	0.04244	0.00100	13
0.06192	0.04370	0.00100	13
0.09385	-1.00000	0.00000	0
0.07588	0.03235	0.00100	13

0.07394	0.03445	0.00100	13
0.07193	0.03445	0.00100	13
0.06792	0.03655	0.00100	13
0.06384	0.03950	0.00100	13
0.05383	0.04454	0.00100	13
0.05182	0.04622	0.00100	13
0.04990	0.04706	0.00100	13
0.08787	-1.00000	0.00000	0
0.07193	0.03193	0.00100	13
0.06985	0.03277	0.00100	13
0.06792	0.03445	0.00100	13
0.06384	0.03697	0.00100	13
0.05995	0.03866	0.00100	13
0.05790	0.03950	0.00100	13
0.05383	0.04286	0.00100	13
0.04990	0.04538	0.00100	13
0.08188	-1.00000	0.00000	0
0.06792	0.03100	0.00100	13
0.06384	0.03361	0.00100	13
0.06192	0.03487	0.00100	13
0.05995	0.03613	0.00100	13
0.05583	0.03782	0.00100	13
0.05383	0.03908	0.00100	13
0.05182	0.04034	0.00100	13
0.04582	0.04286	0.00100	13
0.07785	-1.00000	0.00000	0
0.06384	0.03100	0.00100	13
0.05995	0.03277	0.00100	13
0.05790	0.03361	0.00100	13
0.05583	0.03487	0.00100	13
0.05383	0.03571	0.00100	13
0.05182	0.03697	0.00100	13
0.04990	0.03824	0.00100	13
0.04789	0.03866	0.00100	13
0.07588	-1.00000	0.00000	0
0.06192	0.03100	0.00100	13
0.05995	0.03193	0.00100	13
0.05790	0.03277	0.00100	13
0.05583	0.03445	0.00100	13
0.05383	0.03529	0.00100	13
0.05182	0.03655	0.00100	13
0.04990	0.03782	0.00100	13
0.04789	0.03824	0.00100	13
0.07193	-1.00000	0.00000	0
0.05583	0.03277	0.00100	13
0.05383	0.03361	0.00100	13
0.05182	0.03697	0.00100	13
0.04990	0.03697	0.00100	13
0.04582	0.03824	0.00100	13
0.00000	0.00000	0.00000	-1

v.IN File:

1 .01994 .02187 .02387 .02590 .02797 .02997 .03199 .03397 .03598
 .03792
 1 0.3640 0.3640 0.3640 0.3640 0.3640 0.3640 0.3640 0.3640 0.3640
 0.3640
 0 0 0 0 0 0 0 0 0 0
 0
 1 .04002 .04196 .04390 .04582 .04789 .04990 .05182 .05383 .05583
 .05790
 1 0.3640 0.3640 0.3640 0.3640 0.3640 0.3640 0.3640 0.3640 0.3640
 0.3640
 0 0 0 0 0 0 0 0 0 0
 0
 1 .05995 .06192 .06384 .06590 .06792 .06985 .07193 .07394 .07588
 .07785
 1 0.3640 0.3640 0.3640 0.3640 0.3640 0.3640 0.3640 0.3640 0.3640
 0.3640
 0 0 0 0 0 0 0 0 0 0
 0
 1 .08000 .08188 .08387 .08590 .08787 .08990 .09183 .09385 .09585
 .09787
 1 0.3640 0.3640 0.3640 0.3640 0.3640 0.3640 0.3640 0.3640 0.3640
 0.3640
 0 0 0 0 0 0 0 0 0 0
 0
 1 .09990 .10195 .10391 .10594 .10791 .10991 .11196 .11393 .11586
 .11788
 1 0.3640 0.3640 0.3640 0.3640 0.3640 0.3640 0.3640 0.3640 0.3640
 0.3640
 0 0 0 0 0 0 0 0 0 0
 0
 1 .11990 .12191 .12393 .12589 .12795 .12989 .13195 .13390 .13588
 .13790
 1 0.3640 0.3640 0.3640 0.3640 0.3640 0.3640 0.3640 0.3640 0.3640
 0.3640
 0 0 0 0 0 0 0 0 0 0
 0
 1 .13991 .14192
 0 0.3640 0.3640
 0 0
 1 .00000 .00204 .00407 .00593 .00801 .00996 .01179 .01410 .01594
 .01797
 1 0.3640 0.3640 0.3640 0.3640 0.3640 0.3640 0.3640 0.3640 0.3640
 0.3640
 0 0 0 0 0 0 0 0 0 0
 0
 1 .01994 .02187 .02387 .02590 .02797 .02997 .03199 .03397 .03598
 .03792
 1 0.3640 0.3640 0.3640 0.3640 0.3640 0.3640 0.3640 0.3640 0.3640
 0.3640
 0 0 0 0 0 0 0 0 0 0
 0
 1 .04002 .04196 .04390 .04582 .04789 .04990 .05182 .05383 .05583
 .05790

```

1 0.3640 0.3640 0.3640 0.3640 0.3640 0.3640 0.3640 0.3640 0.3640 0.3640 0.3640 0.3640
0.3640
0 0 0 0 0 0 0 0 0 0 0 0
1 .05995 .06192 .06384 .06590 .06792 .06985 .07193 .07394 .07588
.07785
1 0.3640 0.3640 0.3640 0.3640 0.3640 0.3640 0.3640 0.3640 0.3640 0.3640 0.3640 0.3640
0.3640
0 0 0 0 0 0 0 0 0 0 0 0
0
1 .08000 .08188 .08387 .08590 .08787 .08990 .09183 .09385 .09585
.09787
1 0.3640 0.3640 0.3640 0.3640 0.3640 0.3640 0.3640 0.3640 0.3640 0.3640 0.3640 0.3640
0.3640
0 0 0 0 0 0 0 0 0 0 0 0
0
1 .09990 .10195 .10391 .10594 .10791 .10991 .11196 .11393 .11586
.11788
1 0.3640 0.3640 0.3640 0.3640 0.3640 0.3640 0.3640 0.3640 0.3640 0.3640 0.3640 0.3640
0.3640
0 0 0 0 0 0 0 0 0 0 0 0
0
1 .11990 .12191 .12393 .12589 .12795 .12989 .13195 .13390 .13588
.13790
1 0.3640 0.3640 0.3640 0.3640 0.3640 0.3640 0.3640 0.3640 0.3640 0.3640 0.3640 0.3640
0.3640
0 0 0 0 0 0 0 0 0 0 0 0
0
1 .13991 .14192
0 0.3640 0.3640
0 0
2 .00000 .00204 .00407 .00593 .00801 .00996 .01179 .01410 .01594
.01797
1 .00600 .00600 .00600 .00600 .00600 .00600 .00600 .00600 .00600
.00600
1 1 1 1 1 1 1 1 1 1 1
1
2 .01994 .02187 .02387 .02590 .02797 .02997 .03199 .03397 .03598
.03792
1 .00600 .00600 .00600 .00600 .00600 .00600 .00600 .00600 .00600
.00600
1 1 1 1 1 1 1 1 1 1
1
2 .04002 .04196 .04390 .04582 .04789 .04990 .05182 .05383 .05583
.05790
1 .00600 .00600 .00600 .00600 .00600 .00600 .00600 .00600 .00600
.00600
1 1 1 1 1 1 1 1 1 1
1
2 .05995 .06192 .06384 .06590 .06792 .06985 .07193 .07394 .07588
.07785
1 .00600 .00600 .00600 .00600 .00600 .00600 .00600 .00600 .00600
.00600

```


2 .09990 .10195 .10391 .10594 .10791 .10991 .11196 .11393 .11586
 .11788
 1 1.8000 1.8000 1.8000 1.8000 1.8000 1.8000 1.8000 1.8000 1.8000
 1.8000
 0 0 0 0 0 0 0 0 0 0
 0
 2 .11990 .12191 .12393 .12589 .12795 .12989 .13195 .13390 .13588
 .13790
 1 1.8000 1.8000 1.8000 1.8000 1.8000 1.8000 1.8000 1.8000 1.8000
 1.8000
 0 0 0 0 0 0 0 0 0 0
 0
 2 .13991 .14192
 0 1.8000 1.8000
 0 0
 2 .00000 .00204 .00407 .00593 .00801 .00996 .01179 .01410 .01594
 .01797
 1 1.8000 1.8000 1.8000 1.8000 1.8000 1.8000 1.8000 1.8000 1.8000
 1.8000
 0 0 0 0 0 0 0 0 0 0
 0
 2 .01994 .02187 .02387 .02590 .02797 .02997 .03199 .03397 .03598
 .03792
 1 1.8000 1.8000 1.8000 1.8000 1.8000 1.8000 1.8000 1.8000 1.8000
 1.8000
 0 0 0 0 0 0 0 0 0 0
 0
 2 .04002 .04196 .04390 .04582 .04789 .04990 .05182 .05383 .05583
 .05790
 1 1.8000 1.8000 1.8000 1.8000 1.8000 1.8000 1.8000 1.8000 1.8000
 1.8000
 0 0 0 0 0 0 0 0 0 0
 0
 2 .05995 .06192 .06384 .06590 .06792 .06985 .07193 .07394 .07588
 .07785
 1 1.8000 1.8000 1.8000 1.8000 1.8000 1.8000 1.8000 1.8000 1.8000
 1.8000
 0 0 0 0 0 0 0 0 0 0
 0
 2 .08000 .08188 .08387 .08590 .08787 .08990 .09183 .09385 .09585
 .09787
 1 1.8000 1.8000 1.8000 1.8000 1.8000 1.8000 1.8000 1.8000 1.8000
 1.8000
 0 0 0 0 0 0 0 0 0 0
 0
 2 .09990 .10195 .10391 .10594 .10791 .10991 .11196 .11393 .11586
 .11788
 1 1.8000 1.8000 1.8000 1.8000 1.8000 1.8000 1.8000 1.8000 1.8000
 1.8000
 0 0 0 0 0 0 0 0 0 0
 0
 2 .11990 .12191 .12393 .12589 .12795 .12989 .13195 .13390 .13588
 .13790


```

          0     0     0     0     0     0     0     0     0     0
0
3   .04002  .04196  .04390  .04582  .04789  .04990  .05182  .05383  .05583
.05790
1   2.2000  2.2000  2.2000  2.2000  2.2000  2.2000  2.2000  2.2000  2.2000
2.2000
          0     0     0     0     0     0     0     0     0     0
0
3   .05995  .06192  .06384  .06590  .06792  .06985  .07193  .07394  .07588
.07785
1   2.2000  2.2000  2.2000  2.2000  2.2000  2.2000  2.2000  2.2000  2.2000
2.2000
          0     0     0     0     0     0     0     0     0     0
0
3   .08000  .08188  .08387  .08590  .08787  .08990  .09183  .09385  .09585
.09787
1   2.2000  2.2000  2.2000  2.2000  2.2000  2.2000  2.2000  2.2000  2.2000
2.2000
          0     0     0     0     0     0     0     0     0     0
0
3   .09990  .10195  .10391  .10594  .10791  .10991  .11196  .11393  .11586
.11788
1   2.2000  2.2000  2.2000  2.2000  2.2000  2.2000  2.2000  2.2000  2.2000
2.2000
          0     0     0     0     0     0     0     0     0     0
0
3   .11990  .12191  .12393  .12589  .12795  .12989  .13195  .13390  .13588
.13790
1   2.2000  2.2000  2.2000  2.2000  2.2000  2.2000  2.2000  2.2000  2.2000
2.2000
          0     0     0     0     0     0     0     0     0     0
0
3   .13991  .14192
0   2.2000  2.2000
          0     0
4   .00000  .14192
0   .01200  .01200

```

d.IN File:

```

0.14192      ! xmax
0.050        ! damping factor
0.001        ! velocity uncertainty [km/s]
0.00001      ! depth-to-boundary uncertainty [km]

```

APPENDIX C
TABULATED TOPOGRAPHIC DATA

Line 1	Z in km	Line 2	Z in km	Line 3	Z in km
0	-0.00126309	0	-0.001643482	0	-0.001508150
0.0018989	-0.0012509	0.0019274	-0.001702918	0.0020434	-0.001550822
0.0039619	-0.00127986	0.0039156	-0.001780642	0.0040666	-0.001512722
0.0058832	-0.00129662	0.0060182	-0.001747114	0.0059273	-0.001497482
0.0078542	-0.00131491	0.0079606	-0.001794358	0.0080081	-0.001511198
0.0098539	-0.0012829	0.0099486	-0.001751686	0.0099595	-0.001459382
0.0119124	-0.0014094	0.0119279	-0.001771498	0.0117865	-0.001396898
0.0139186	-0.0014734	0.0139172	-0.001805026	0.0141020	-0.001398422
0.015810	-0.00163647	0.015880	-0.001800454	0.0159367	-0.001407566
0.0178275	-0.00177668	0.0179136	-0.001809598	0.0179680	-0.001442618
0.0198141	-0.00178582	0.0199095	-0.001833982	0.0199357	-0.001428902
0.0218055	-0.00184374	0.0219264	-0.001856842	0.0218744	-0.001471574
0.0238481	-0.00191689	0.0239325	-0.001882750	0.0238712	-0.001457858
0.0258164	-0.00198547	0.0258845	-0.001884274	0.0259009	-0.001495958
0.0277578	-0.00205252	0.027874	-0.001855318	0.0279682	-0.001491386
0.0298741	-0.00204948	0.0299343	-0.001916278	0.0299738	-0.001451762
0.031820	-0.0020571	0.0319035	-0.001951330	0.0319909	-0.001468526
0.0338429	-0.00202052	0.0339316	-0.001939138	0.0339691	-0.001463954
0.035830	-0.00196566	0.0359311	-0.001971142	0.0359836	-0.001431950
0.037842	-0.00218206	0.0378725	-0.001981810	0.0379158	-0.001399946
0.0397412	-0.00246248	0.0398982	-0.001977238	0.0400156	-0.001349654
0.0417349	-0.00281452	0.0418946	-0.001987906	0.0419647	-0.001351178
0.0436906	-0.00321991	0.0439277	-0.002077822	0.0439000	-0.001409090
0.0456188	-0.00351556	0.0458863	-0.002109826	0.0458228	-0.001460906
0.0475406	-0.00385237	0.0478812	-0.002143354	0.0478865	-0.001514246
0.0494479	-0.0041526	0.0498819	-0.002141830	0.0499049	-0.001497482
0.0514877	-0.00449854	0.051820	-0.002140306	0.0518160	-0.001535582
0.0534679	-0.00486583	0.0538421	-0.002170786	0.0538332	-0.001552346
0.0554132	-0.00514015	0.0558482	-0.002147926	0.0558293	-0.001531010
0.0573918	-0.00538246	0.0578127	-0.002167738	0.0578988	-0.001508150
0.0593663	-0.00562021	0.0598106	-0.002195170	0.0599531	-0.001515770
0.061320	-0.00585186	0.0617745	-0.002234794	0.0619184	-0.001566062
0.0633371	-0.00602559	0.0638359	-0.002272894	0.0638430	-0.001546250
0.0653632	-0.00638373	0.0657858	-0.002327758	0.0659015	-0.001555394
0.067290	-0.00674035	0.0678468	-0.002376526	0.0679221	-0.001541678
0.0691939	-0.00705582	0.0697931	-0.002451202	0.0698503	-0.001575206
0.0712472	-0.00723565	0.0717969	-0.002533498	0.0719308	-0.001591970
0.073198	-0.00750844	0.0737835	-0.002600554	0.0739404	-0.001563014
0.0752776	-0.00778124	0.0757544	-0.002698090	0.0758836	-0.001576730

0.0772308	-0.00798606	0.0777623	-0.002781910	0.0778539	-0.001631594
0.079280	-0.00810494	0.0798155	-0.002839822	0.0800010	-0.001657502
0.0813284	-0.00856397	0.0817416	-0.002908402	0.0818806	-0.001655978
0.0831663	-0.00834908	0.0837785	-0.002963266	0.0838655	-0.001695602
0.0849495	-0.00806257	0.0857371	-0.002998318	0.0859028	-0.001701698
0.0871362	-0.00785988	0.087740	-0.003045562	0.0878662	-0.001710842
0.0888873	-0.00750296	0.0897534	-0.003060802	0.0899037	-0.001671218
0.0908411	-0.00707319	0.0917328	-0.003164434	0.0918327	-0.001716938
0.0928059	-0.00691469	0.0937381	-0.003275686	0.0938523	-0.001704746
0.0949607	-0.00659618	0.0956972	-0.003356458	0.0958483	-0.001748942
0.0970289	-0.0062487	0.0977168	-0.003437230	0.0978684	-0.001808378
0.0989964	-0.00578632	0.0997043	-0.003476854	0.0998989	-0.001823618
0.1008829	-0.00553182	0.101710	-0.003521050	0.1019546	-0.001848002
0.102870	-0.00522092	0.103665	-0.003655162	0.1039125	-0.001875434
0.1048067	-0.00486583	0.105670	-0.003807562	0.1059419	-0.001919630
0.1066846	-0.00449854	0.1076106	-0.003897478	0.1079065	-0.001945538
0.1086036	-0.00423946	0.1096354	-0.004055974	0.1099110	-0.001893722
0.110730	-0.00381274	0.1116462	-0.004187038	0.1119606	-0.001986686
0.112668	-0.00333268	0.1136184	-0.004404970	0.1139300	-0.001988210
0.1145713	-0.00284196	0.1155618	-0.004470502	0.1158648	-0.002026310
0.1165666	-0.00237561	0.1176078	-0.004580230	0.1178757	-0.002055266
0.1184911	-0.00235732	0.1195662	-0.004596994	0.1198998	-0.002143658
0.1205819	-0.00260269	0.121600	-0.004642714	0.1219086	-0.002149754
0.122455	-0.00249753	0.1235509	-0.004409542	0.1239342	-0.002157374
0.1244393	-0.00233599	0.125530	-0.004092550	0.1258940	-0.002190902
0.1265274	-0.00219578	0.127519	-0.003950818	0.1279506	-0.002137562
0.128460	-0.00213177			0.1298880	-0.002168042
0.1304746	-0.0020952			0.1319475	-0.002151278
0.1323782	-0.00204643			0.1338995	-0.002145182
0.1344388	-0.00199309			0.1358821	-0.002163470
0.1364268	-0.00187117			0.1379013	-0.002157374
0.1384374	-0.00175382			0.1399090	-0.002154326
0.1402888	-0.00170353			0.1419181	-0.002190902

APPENDIX D

TABULATED FIRST ARRIVAL TRAVEL TIMES

First Arrival Travel Times for Line 2 (seconds)

File	Shot #	Shot Location	Geophone Number																							
			1	2	3	4	5	6	7	8	9	10	11	12	13	14	15	16	17	18	19	20	21	22	23	24
1096	1	0 --	0.004202	99	0.015966	0.020168	0.02479	0.027731	--	0.030252	0.031513	0.032773	0.033613	0.034874	0.036134	0.036555	0.037815	0.038655	0.039076	0.040756	0.042017	0.042857	0.044118	0.044958	0.046218	
1097	2	0.0019274	--	--	0.011765	0.015966	0.021008	0.02521	0.027731	--	0.030252	0.031513	0.032773	0.033613	0.034454	0.035294	0.036134	0.037395	0.038235	0.039496	0.040336	0.042017	0.042857	0.044118	0.044538	0.046218
1098	3	0.0039156	--	0.005738	0.009016	0.015574	0.020082	0.02459	0.027459	--	0.029918	0.031148	0.032377	0.033197	0.033197	0.035246	0.036475	0.037705	0.039344	0.040164	0.041803	0.042623	0.043443	0.044262	0.045082	
1099	4	0.0060182	--	0.004508	0.008607	0.013934	0.019672	0.025	0.027049	--	0.029508	0.030738	0.031557	0.031967	0.033607	0.034016	0.035246	0.036885	0.037705	0.038934	0.040164	0.040984	0.041803	0.042213	0.043443	0.044262
1100	5	0.0079606	--	0.004508	0.009016	0.014754	0.020492	0.025	0.02623	--	0.028689	0.029918	0.030738	0.031967	0.032377	0.033607	0.035246	0.036066	0.036885	0.037705	0.039344	0.040164	0.040984	0.041803	0.043852	0.044262
1101	6	0.0099486	--	0.005738	0.011066	0.016393	0.021721	0.02541	0.027869	--	0.028689	0.029508	0.031148	0.031967	0.032787	0.034016	0.035246	0.036066	0.037295	0.038525	0.064344	0.040574	0.041803	0.042623	0.044672	0.044672
1102	7	0.0119279	--	0.004918	0.009016	0.016803	0.021311	0.02541	0.027049	--	0.028689	0.029918	0.030738	0.031557	0.032787	0.034016	0.035246	0.036066	0.037705	0.038525	0.039344	0.040164	0.041803	0.043443	0.044262	0.045082
1103	8	0.0139172	--	0.004098	0.009836	0.014754	0.020492	0.02541	0.026639	--	0.028689	0.029508	0.030328	0.031967	0.032787	0.034016	0.035246	0.036475	0.036885	0.038525	0.039344	0.040984	0.041803	0.042623	0.043852	0.045082
1104	9	0.0158804	--	0.004098	0.009836	0.015574	0.021311	0.02541	0.02623	--	0.028689	0.029508	0.030738	0.031967	0.032787	0.034016	0.035246	0.036066	0.036885	0.038115	0.039344	0.040164	0.040984	0.043443	0.043852	0.045082
1105	10	0.0179136	--	0.004098	0.007377	0.017213	0.020492	0.025	0.026639	--	0.028689	0.029918	0.030738	0.031967	0.032787	0.034426	0.035246	0.036475	0.036885	0.038934	0.040164	0.040164	0.042213	0.043033	0.042623	0.045082
1106	11	0.0199095	--	0.004098	0.011475	0.015574	0.021311	0.02459	0.02582	--	0.028279	0.029098	0.030328	0.031557	0.032787	0.033607	0.035246	0.036066	0.036885	0.038525	0.038525	0.040984	0.041803	0.043033	0.042623	0.043852
1107	12	0.0219264	--	0.005738	0.011475	0.016803	0.022951	0.025	0.02623	--	0.028689	0.029508	0.030738	0.031967	0.032787	0.034426	0.035246	0.036475	0.037705	0.038115	0.040164	0.040984	0.041803	0.042213	0.045082	
1108	13	0.0239325	--	0.004098	0.008197	0.015164	0.020492	0.02541	0.027049	--	0.028279	0.030328	0.031148	0.032787	0.033197	0.034426	0.036066	0.036885	0.037295	0.039344	0.040164	0.040984	0.041803	0.042623	0.043852	
1109	14	0.0258845	--	0.004098	0.008197	0.015574	0.021311	0.02459	0.02582	--	0.028279	0.029508	0.030328	0.031967	0.032787	0.034016	0.035656	0.036066	0.036885	0.038934	0.040164	0.041393	0.043033	0.043852	0.045082	
1110	15	0.027874	--	0.004098	0.007377	0.015574	0.021311	0.02459	0.02623	--	0.028689	0.029098	0.030328	0.031148	0.032787	0.034426	0.036066	0.037705	0.038525	0.039344	0.040984	0.041803	0.042623	0.044262	0.045082	
1111	16	0.0299343	--	0.003689	0.011066	0.016803	0.022131	0.02459	0.02623	--	0.027869	0.029098	0.030328	0.031967	0.033197	0.033607	0.035246	0.036885	0.037705	0.038525	0.039344	0.040164	0.041803	0.042213	0.043852	0.045082
1112	17	0.0319035	--	0.003279	0.009016	0.015574	0.020492	0.02377	0.02541	--	0.027049	0.027869	0.029918	0.031148	0.031967	0.033607	0.034426	0.035656	0.036475	0.037705	0.038525	0.039344	0.040164	0.040164	0.042623	--
1113	18	0.0339316	--	0.005738	0.010656	0.015574	0.021311	0.02377	0.025	--	0.027049	0.028689	0.030328	0.032377	0.033197	0.034426	0.035246	0.036066	0.036885	0.038115	0.038525	0.038525	0.039344	--	0.041803	0.042623
1114	19	0.0359311	--	0.004098	0.009016	0.015984	0.021721	0.02459	0.02623	--	0.028279	0.029508	0.030328	0.031967	0.032787	0.034426	0.035246	0.036475	0.036885	0.038525	0.038934	0.039754	--	0.041803	0.042623	0.042623
1115	20	0.0378725	--	0.004918	0.010656	0.016393	0.021311	0.02459	0.02541	--	0.028689	0.029508	0.031148	0.032377	0.033607	0.034016	0.035246	0.036066	0.037295	0.037705	0.038115	0.038934	--	0.040164	0.042623	0.042623
1116	21	0.0398982	--	0.004918	0.011885	0.015574	0.021311	0.02459	0.02623	--	0.028279	0.030328	0.031557	0.032787	0.033197	0.035656	0.035246	0.036475	0.037295	0.038115	--	0.040984	0.042623	0.043443	0.044262	
1117	22	0.0418946	--	0.004918	0.010246</																					

File	Shot #	Location	Geophone Number																							
			Shot																							
1151	14	0.1017103	--	0.004918	0.009016	0.013115	0.017213	0.022131	0.02377	--	0.02541	0.02623	0.027869	0.029508	0.031148	0.031148	0.032787	0.034016	0.035656	--	0.036885	0.037705	0.039754	0.040164	0.041803	0.041803
1152	15	0.0997043	--	0.005328	0.010656	0.014344	0.019262	0.022951	0.02377	--	0.02582	0.027869	0.028689	0.030738	0.030738	0.032377	0.032787	0.035246	--	0.036475	0.036885	0.038115	0.038934	0.040574	0.040984	0.041803
1153	16	0.0977168	--	0.005328	0.010246	0.014754	0.019672	0.022131	0.02377	--	0.02623	0.027869	0.029508	0.030328	0.031148	0.032787	0.033607	--	0.035246	0.036475	0.037705	0.039344	0.040164	0.039754	0.040984	0.040984
1154	17	0.0956972	--	0.004918	0.010656	0.015574	0.019672	0.022131	0.023361	--	0.02623	0.027869	0.028689	0.030328	0.031148	0.031967	--	0.034426	0.035246	0.036066	0.037705	0.039344	0.038525	0.039754	0.040164	0.040984
1155	18	0.0937381	--	0.005328	0.010656	0.016803	0.021311	0.022951	0.02459	--	0.027869	0.028689	0.029918	0.030738	0.031967	--	0.033607	0.034426	0.035656	0.036885	0.037705	0.038525	0.040164	0.040984	0.041393	
1156	19	0.0917328	--	0.005738	0.011475	0.017213	0.021721	0.02459	0.02582	--	0.028279	0.029508	0.030738	0.031148	--	0.033607	0.034426	0.035246	0.036885	0.038525	0.039344	0.039754	0.040574	0.041803	0.043443	
1157	20	0.0897534	--	0.005738	0.011475	0.017213	0.022131	0.02377	0.02582	--	0.027869	0.029098	0.030328	--	0.031967	0.033197	0.034426	0.035246	0.036475	0.036066	0.036475	0.038115	0.039344	0.039754	0.041803	0.043443
1158	21	0.0877397	--	0.005328	0.010656	0.016393	0.021311	0.023361	0.025	--	0.027869	0.029098	--	0.030738	0.031557	0.032787	0.033197	0.035246	0.034426	0.036066	0.036885	0.038525	0.039344	0.042623	0.043443	
1159	22	0.0857371	--	0.006967	0.012295	0.016393	0.020902	0.022951	0.025	--	0.027869	--	0.029508	0.030328	0.031148	0.031967	0.033607	0.033607	0.034426	0.035246	0.036066	0.036885	0.037705	0.040164	0.042623	0.043443
1160	23	0.0837785	--	0.005328	0.010656	0.016393	0.021311	0.02459	0.02623	--	--	0.029508	0.030328	0.031967	0.032787	0.033607	0.032787	0.034426	0.034836	0.036066	0.036885	0.038525	0.040164	0.041803	0.042623	0.042623
1161	24	0.0817416	--	0.005738	0.011475	0.016803	0.021311	0.02459	0.027049	--	0.028689	0.029508	0.030328	0.031967	0.033197	0.032377	0.033607	0.034426	0.035246	0.036885	0.037705	0.040574	0.041393	0.041803	0.042623	0.043443
1162	25	0.0798155	--	0.005738	0.010656	0.014754	0.018443	0.02459	--	--	0.027869	0.029508	0.030328	0.031967	0.031148	0.032787	0.032787	0.033607	0.035246	0.036475	0.038934	0.040164	0.040984	0.042623	0.042623	
1163	26	0.0777623	--	0.005738	0.010656	0.013934	0.019672	0.02541	0.027049	--	0.029098	0.030328	0.031557	0.031148	0.031967	0.032787	0.033607	0.034426	0.036066	0.038115	0.039344	0.040164	0.040574	0.041803	0.040984	0.044262
1164	27	0.0757544	--	0.005738	0.009016	0.014754	0.018033	0.02377	0.02541	--	0.027869	0.028689	0.028689	0.029508	0.030328	0.031148	0.032787	0.033607	0.035246	0.036475	0.037705	0.038525	0.040164	0.041803	0.043443	
1165	28	0.0737835	--	0.005738	0.010656	0.015574	0.022131	0.02459	0.02541	--	0.028279	0.027869	0.028689	0.029508	0.030328	0.031557	0.033197	0.035246	0.036066	0.036885	0.037295	0.038934	0.039344	0.040984	0.041803	0.042623
1166	29	0.0717969	--	0.005738	0.011475	0.016803	0.021311	0.02459	0.02582	--	0.02623	0.028689	0.029098	0.029918	0.031148	0.033197	0.034836	0.036066	0.037295	0.035656	--	0.040574	--	0.042623	0.044262	--
1167	30	0.0697931	--	--	0.011885	0.017213	0.022951	0.02582	0.027869	--	0.028689	0.028689	0.029918	0.031148	0.031967	0.034836	0.035246	0.036066	0.036885	0.037705	0.037705	0.041803	0.042623	0.044262	0.045902	
1168	31	0.0678468	--	0.005328	0.010656	0.016393	0.022131	0.026639	0.02623	--	0.028279	0.029098	0.030328	0.031148	0.033607	0.034426	0.035246	0.036066	0.037705	0.037705	0.038934	0.040164	0.041803	0.043033	0.044262	0.045082
1169	32	0.0657858	--	0.005738	0.011475	0.017213	0.022951	0.02541	0.027049	--	0.028689	0.029508	0.030328	0.032377	0.033607	0.034836	0.035656	0.036475	0.036885	0.038525	0.039344	0.040984	0.042213	0.043443	0.044262	0.045902
1170	33	0.0638359	--	0.004918	0.011475	0.017213	0.022131	0.02541	0.02623	--	0.027869	0.029508	0.031967	0.033197	0.034836	0.035246	0.035656	0.036885	0.037705	0.038525	0.040164	0.041803	0.043852	0.044262	0.046721	
1171	34	0.0617745	--	0.005738	0.011475	0.016393	0.022541	0.02541	0.02623	--	0.028689	0.031148	0.032377	0.033607	0.034426	0.035246	0.036885	0.038525	0.039344	0.040164	0.041393	0.042623	0.043852	0.044262	0.045082	
1172	35	0.0598106	--	0.005738	0.011475	0.017213	0.022951	0.025	0.02623	--	0.030328	0.031148	0.031967	0.032787	0.034426	0.035656	0.037295	0.037705	0.039344	0.040984	0.041393	0.041803	0.			

First Arrival Travel Times for Line 3 (seconds)

File Number	Shot #	Shot Location	Geophone Number																							
			1	2	3	4	5	6	7	8	9	10	11	12	13	14	15	16	17	18	19	20	21	22	23	24
1179	1	0	--	0.004622	0.010924	0.016387	0.022269	0.026891	0.028571	--	0.031092	0.031933	0.033613	0.035294	0.036975	0.037815	0.037815	0.039076	0.040756	0.041176	0.042437	0.042857	0.044118	0.046218	0.047059	0.048739
1180	2	0.00204	--	0.005882	0.011345	0.017227	0.022269	0.026891	0.029412	--	0.031933	0.033613	0.034454	0.035294	0.036975	0.037815	0.038655	0.040336	0.040756	0.042017	0.042857	0.044538	0.045378	0.046218	0.047899	0.048739
1181	3	0.00407	--	0.005882	0.011345	0.016807	0.021849	0.027311	0.029832	--	0.032773	0.034454	0.035294	0.036555	0.036555	0.037815	0.039496	0.040336	0.041176	0.042017	0.044538	0.044958	0.045798	0.047059	0.047899	0.04916
1182	4	0.00593	--	0.005042	0.011345	0.016807	0.022269	0.026891	0.029832	--	0.034034	0.035294	0.036134	0.036975	0.039076	0.039496	0.040336	0.040336	0.042857	0.044118	0.044538	0.046218	0.047059	0.047899	0.047899	0.048739
1183	5	0.00801	--	0.005882	0.012185	0.017647	0.022269	0.02563	0.029412	--	0.032773	0.034454	0.034454	0.035294	0.036975	0.037395	0.038655	0.039496	0.041176	0.041597	0.043277	0.044538	0.045378	0.047059	0.047899	0.048739
1184	6	0.00996	--	0.006723	0.012185	0.017647	0.021849	0.02521	0.029412	--	0.032773	0.032773	0.033613	0.035294	0.036975	0.037815	0.039916	0.041176	0.042017	0.043277	0.044538	0.045378	0.045378	0.047059	0.047479	0.047479
1185	7	0.01179	--	0.006723	0.013866	0.018487	0.022269	0.027311	0.029412	--	0.031092	0.032353	0.034454	0.034874	0.036134	0.036555	0.037815	0.038655	0.039916	0.041176	0.042857	0.044118	0.044538	0.046218	0.046218	0.047059
1186	8	0.01410	--	0.004622	0.010924	0.016807	0.021849	0.026891	0.029412	--	0.030672	0.032773	0.033613	0.034874	0.035294	0.036975	0.037815	0.038655	0.039496	0.040336	0.042857	0.043697	0.045378	0.046218	0.047059	0.047899
1187	9	0.01594	--	0.007143	0.011765	0.017227	0.022269	0.028571	0.029412	--	0.032773	0.033193	0.034454	0.035294	0.036975	0.037395	0.038655	0.039496	0.040336	0.042857	0.042857	0.043697	0.045378	0.046218	0.047899	0.048319
1188	10	0.01797	--	0.004202	0.012605	0.015966	0.023109	0.028571	0.029412	--	0.032353	0.033613	0.034454	0.036134	0.036975	0.037815	0.038655	0.039496	0.040336	0.041176	0.042017	0.043697	0.044958	0.046639	0.048739	0.048739
1189	11	0.01994	--	0.005882	0.011345	0.017227	0.023109	0.028571	0.031092	--	0.033613	0.034454	0.036134	0.036134	0.036975	0.037815	0.039916	0.040756	0.042017	0.042857	0.044118	0.045378	0.046218	0.047059	0.047899	0.05
1190	12	0.02187	--	0.005882	0.011765	0.016807	0.022269	0.028571	0.031092	--	0.033193	0.035294	0.036134	0.036975	0.038235	0.039496	0.041176	0.042437	0.043697	0.045378	0.046218	0.047899	0.048319	0.04958	0.04958	
1191	13	0.02387	--	0.004202	0.012605	0.018487	0.02437	0.029412	0.031092	--	0.034034	0.034454	0.035714	0.037395	0.038235	0.039496	0.040336	0.041176	0.042017	0.042857	0.044118	0.044958	0.045378	0.047059	0.048739	0.048739
1192	14	0.02590	--	0.006303	0.011765	0.017647	0.023109	0.028992	0.031092	--	0.033613	0.034874	0.036134	0.037815	0.039916	0.040336	0.042017	0.042437	0.043697	0.044118	0.045378	0.047059	0.047899	0.04958	0.04958	
1193	15	0.02797	--	0.005042	0.011765	0.016807	0.022269	0.028571	0.031092	--	0.033613	0.035294	0.036134	0.037815	0.038655	0.039496	0.040336	0.041176	0.042857	0.043697	0.045378	0.046218	0.046218	0.047899	0.05	
1194	16	0.02997	--	0.005882	0.011345	0.017227	0.022269	0.029412	0.031092	--	0.033613	0.034454	0.036134	0.036555	0.037395	0.038655	0.040336	0.041176	0.042437	0.043277	0.044538	0.045378	0.046218	0.047059	0.047899	0.047899
1195	17	0.03199	--	0.005042	0.011345	0.016807	0.022269	0.028151	0.031092	--	0.033613	0.035294	0.035714	0.036975	0.037815	0.038655	0.040336	0.041176	0.042437	0.043697	0.044538	0.045798	0.047899	0.047479	0.048739	
1196	18	0.03397	--	0.005882	0.011765	0.018487	0.022269	0.028571	0.031092	--	0.034034	0.034454	0.034874	0.036134	0.037395	0.038655	0.039496	0.040756	0.042017	0.042437	0.043277	0.044118	0.045798	0.046218	0.047899	0.047899
1197	19	0.03598	--	0.005882	0.012605	0.016807	0.022269	0.027731	0.031513	--	0.033613	0.034874	0.036134	0.036555	0.037815	0.038655	0.040336	0.041176	0.042017	0.042437	0.043277	0.044538	0.045378	0.046218	0.047899	0.047899
1198	20	0.03792	--	0.006723	0.010084	0.016807	0.022269	0.028151	0.031933	--	0.033613	0.034454	0.035294	0.036975	0.037395	0.039076	0.039916	0.040336	0.041176	0.042437	0.044118	0.044538	0.045378	0.046639	0.047479	0.048739
1199	21	0.04002	--	0.007563	0.011765	0.018487	0.023529	0.029412	0.030672	--	0.033613	0.034034	0.035294	0.036134	0.037815	0.038655	0.039496	0.039916	0.041176	0.042857	0.043697	0.044958	0.046639	0.047059	0.048739	

File Number	Shot #	Shot Location	Geophone Number																							
			0.12191	0.0021	0.005882	0.011345	0.016807	0.022689	0.028151	0.031933	0.0328	0.033613	0.034454	0.035294	0.036975	--	0.038655	0.039076	0.039496	--	0.042017	0.043277	0.043697	0.044538	0.045378	0.046218
1237	11	0.11990	0.00168	0.005882	0.010924	0.016807	0.022689	0.028151	0.031092	0.0319	0.033613	0.034454	0.035714	--	0.036975	0.036975	0.038235	0.039496	--	0.042017	0.043277	0.043697	0.045378	0.045378	0.045798	--
1238	12	0.11788	0.00126	0.006303	0.011765	0.017647	0.023529	0.028992	0.031092	0.0328	0.033193	0.034454	--	0.036134	0.035714	0.036975	0.037815	0.040336	--	0.041176	0.042857	0.043697	0.044538	0.045378	0.047059	--
1239	13	0.11586	0.0021	0.005882	0.011345	0.016807	0.022689	0.028571	0.032353	0.0324	0.034034	--	0.010924	0.035714	0.036975	0.037815	0.039496	0.040756	--	0.042857	0.043277	0.043697	0.044118	0.046639	0.047899	--
1240	14	0.11393	0.00252	0.005882	0.011765	0.017227	0.023109	0.028571	0.031513	0.0328	--	0.034034	0.034454	0.035714	0.036134	0.038235	0.039496	0.040756	--	0.042017	0.042857	0.043277	0.044538	0.043697	0.047059	--
1241	15	0.11196	0.00252	0.006723	0.011765	0.017227	0.023109	0.028571	0.031513	--	0.032773	0.033613	0.035294	0.035294	0.036975	0.037815	0.038655	0.040336	--	0.042017	0.042437	0.044118	0.044958	0.045378	0.047059	--
1242	16	0.10991	0.00168	0.005882	0.012185	0.016807	0.022689	0.028571	--	0.0324	0.032353	0.033613	0.035294	0.036555	0.037815	0.038235	0.039496	0.039496	--	0.041597	0.043697	0.043697	0.043697	0.045798	0.046218	--
1243	17	0.10791	0.00168	0.005882	0.011765	0.016807	0.022689	--	0.030672	0.0307	0.031933	0.032773	0.035714	0.035714	0.036975	0.037815	0.038655	0.039496	--	0.042017	0.042437	0.042857	0.044538	0.046218	0.047899	--
1244	18	0.10594	0.00168	0.005882	0.010924	0.016807	--	0.028571	0.029832	0.0311	0.031513	0.033613	0.035714	0.036134	0.036975	0.037815	0.038235	0.039076	--	0.041176	0.041176	0.042437	0.044118	0.047059	0.047059	--
1245	19	0.10391	0.00252	0.005462	0.011765	0.015966	0.022689	0.027731	0.029412	0.0307	0.031933	0.033613	0.034874	0.035294	0.036134	0.036975	0.037815	0.039496	--	0.040756	0.041176	0.042857	0.044958	0.045378	0.046218	--
1246	20	0.10195	0.00168	0.005882	--	0.017647	0.022689	0.028571	0.030252	0.0319	0.032773	0.033613	0.036134	0.035294	0.036134	0.036975	0.038655	0.039076	--	0.041176	0.042017	0.044118	0.045378	0.046639	0.047059	--
1247	21	0.09990	0.00252	0.006303	0.012185	0.016807	0.022689	0.026891	0.030252	0.0324	0.033613	0.034454	0.035294	0.036134	0.035714	0.038235	0.038655	0.039496	--	0.042017	0.043277	0.043697	0.045798	0.047059	0.047899	--
1248	22	0.09787	0.00336	0.006303	0.011345	0.016807	0.021008	0.02605	0.030252	0.0315	0.032773	0.033613	0.034454	0.035294	0.036975	0.037395	0.037815	0.039496	--	0.042437	0.043697	0.044118	0.044958	0.046218	0.047479	--
1249	23	0.09585	0.00252	0.005882	0.010924	0.015966	0.021008	0.02605	0.029832	0.0311	0.031513	0.032773	0.033613	0.035294	0.035714	0.037815	0.039076	--	0.042017	0.042857	0.043277	0.044538	0.045798	0.047899	--	
1250	24	0.09385	0.00168	0.005042	0.010924	0.016387	0.021429	0.026891	0.030252	0.0307	0.031092	0.032353	0.034454	0.034874	0.036555	0.037395	0.039496	--	0.041176	0.042017	0.043697	0.044538	0.046218	0.047059	--	
1251	25	0.09183	0.00126	0.006303	0.011765	0.016807	0.022269	0.027731	0.029832	0.0303	0.031513	0.033613	0.034034	0.034034	0.035294	0.036975	0.038655	0.039496	--	0.042017	0.043277	0.043697	0.045378	0.045378	0.047059	--
1252	26	0.08990	0.00084	0.005882	0.011345	0.016807	0.022269	0.027731	0.029412	0.0303	0.032773	0.032773	0.034454	0.034874	0.035714	0.037395	0.038235	0.039076	--	0.042017	0.042017	0.042857	0.044958	0.044958	0.046218	--
1253	27	0.08787	0.00084	0.005882	0.010924	0.016387	0.021849	0.027731	0.029412	0.0315	0.031933	0.032773	0.034454	0.035294	0.036975	0.037815	0.038655	0.039496	--	0.042857	0.043277	0.045378	0.045378	0.046639	0.047059	--
1254	28	0.08590	0.00168	0.006723	0.011765	0.016807	0.022689	0.028151	0.030672	0.0311	0.031933	0.033613	0.035294	0.036555	0.036975	0.037815	0.039496	0.040336	--	0.042857	0.043277	0.043697	0.046218	0.046218	0.047899	--
1255	29	0.08387	0.00168	0.005042	0.013025	0.017227	0.022689	0.028571	0.030252	0.0311	0.031933	0.033613	0.035294	0.036134	0.036975	0.037815	0.039496	0.040756	--	0.043277	0.043277	0.044118	0.044118	0.046218	0.048319	--
1256	30	0.08188	0.00042	0.007563	0.011765	0.017647	0.023109	0.028571	0.029412	0.0307	0.031933	0.033613	0.034874	0.036134	0.036555	0.037815	0.039076	0.040336	--	0.041597	0.042857	0.043697	0.045378	0.046639	0.047059	--
1257	31	0.08000	0.00126	0.005882	0.011765	0.017227	0.023109	0.028151	0.030252	0.0311	0.031933	0.033613														

VITA

Name: Joshua Smith Gowan

Address: Department of Geology and Geophysics,
MS 3115,
Texas A&M University,
College Station, TX 77843

Email Address: gowan_josh@hotmail.com

Education: B.A., Geology, Bates College, 2002
M.S., Geophysics, Texas A&M
University, 2012